Mitochondrial oxidative stress impairs contractile function but paradoxically increases muscle mass via fiber branching

Bumsoo Ahn[1], Rojina Ranjit[1], Pavithra Premkumar[1], Gavin Pharaoh[1,2], Katarzyna M. Piekarz[1,3], Satoshi Matsuzaki[1], Dennis R. Claflin[7], Kaitlyn Riddle[1], Jennifer Judge[6], Shylesh Bhaskaran[1], Kavithalakshmi Satara Natarajan[1], Erika Barboza[1], Benjamin Wronowski[2], Michael Kinter[1], Kenneth M. Humphries[1,2,5], Timothy M. Griffin[1,2,3,4,5], Willard M. Freeman[2,5], Arlan Richardson[2,4,5], Susan V. Brooks[6], Holly Van Remmen[1,2,4,5]

[1] Aging and Metabolism Research Program, Oklahoma Medical Research Foundation, Oklahoma City, OK 73104, USA
[2] Department of Physiology, University of Oklahoma Health Sciences Center, Oklahoma City, OK, USA
[3] Oklahoma Center for Neuroscience, University of Oklahoma Health Sciences Center, Oklahoma City, OK, USA
[4] Oklahoma City VA Medical Center, Oklahoma City, OK 73104, USA.
[5] Reynolds Oklahoma Center on Aging, University of Oklahoma Health Sciences Center, Oklahoma City, OK, USA
[6] Department of Molecular and Integrative Physiology, University of Michigan, Ann Arbor, Michigan
[7] Department of Surgery, Section of Plastic Surgery, University of Michigan, Ann Arbor, Michigan

Corresponding author:
Holly Van Remmen, Ph. D.
Aging and Metabolism Research Program

This is the author manuscript accepted for publication and has undergone full peer review but has not been through the copyediting, typesetting, pagination and proofreading process, which may lead to differences between this version and the Version of Record. Please cite this article as doi: 10.1002/jcsm.12375

Oklahoma Medical Research Foundation
825 NE 13th Street
Oklahoma City, OK 73104
Phone: 405-271-2520
Fax: 405-271-3470
Email:Holly-VanRemmen@omrf.org

ABSTRACT

Background Excess reactive oxygen species (ROS) and muscle weakness occur in parallel in multiple pathological conditions. However, the causative role of skeletal muscle mitochondrial ROS (mtROS) on neuromuscular junction (NMJ) morphology and function and muscle weakness has not been directly investigated.

Methods We generated mice lacking skeletal muscle-specific MnSOD (m*Sod2*KO) to increase mtROS using a cre-Lox approach driven by human skeletal actin. We determined primary functional parameters of skeletal muscle mitochondrial function (respiration, ROS and calcium retention capacity) using permeabilized muscle fibers and isolated muscle mitochondria. We assessed contractile properties of isolated skeletal muscle using *in situ* and *in vitro* preparations, and whole lumbrical muscles to elucidate the mechanisms of contractile dysfunction.

Results The m*Sod2*KO mice, contrary to our prediction, exhibit a 10-15% increase in muscle mass associated with an ~50% increase in central nuclei and ~35% increase in branched fibers ($p < 0.05$). Despite the increase in muscle mass of gastrocnemius and quadriceps, *in situ* sciatic nerve-stimulated isometric maximum specific force (N/cm^2), force per cross-sectional area, is impaired by ~60% and associated with increased NMJ fragmentation and size by ~40% ($p < 0.05$). Intrinsic alterations of components of the contractile machinery show elevated markers of oxidative stress, e.g., lipid peroxidation is increased by ~100%, oxidized glutathione is elevated by ~50%, and oxidative modifications of myofibrillar proteins are increased by ~30% ($p < 0.05$). We also find an approximate 20% decrease in the intracellular calcium transient that is associated with specific force deficit. Excess superoxide generation from the mitochondrial complexes causes a deficiency of succinate dehydrogenase and reduced complex-II mediated respiration and ATP generation rates leading to severe exercise intolerance (~10 mins vs ~2 hrs in WT, $p < 0.05$).

Conclusions Increased skeletal muscle mtROS is sufficient to elicit NMJ disruption and contractile abnormalities, but not muscle atrophy, suggesting new roles for mitochondrial oxidative stress in maintenance of muscle mass through increased fiber branching.

Keywords Skeletal muscle, mitochondria, MnSOD, reactive oxygen species, fiber branching, hyperplasia

Introduction

Oxidative stress, the imbalance between pro-oxidant generation and antioxidant defense, has been implicated in pathological conditions of skeletal muscle, including sarcopenia[1–3], denervation[4,5], and cancer cachexia[6]. Excess levels of reactive oxygen species (ROS) impair contractile function of skeletal muscle[7] and activate proteases that are associated with degradation of contractile machinery[2,8]. A primary source of oxidative stress is superoxide anions generated from a number of cellular sources, including the mitochondrial electron transport chain (ETC) and NADPH oxidase. Superoxide can be converted to other radical and non-radical species including hydroxyl radicals, peroxynitate, and hydrogen peroxide. Because superoxide and its derivatives can generate oxidative damage to cellular lipids, proteins, and DNA, controlling superoxide levels is a first and primary line of defense against oxidative stress and damage. Superoxide is primarily scavenged by copper zinc-superoxide dismutase (CuZnSOD) in the cytosol, and manganese-superoxide dismutase (MnSOD) in the mitochondrial matrix.

Our laboratory and others have provided insights into potential mechanisms of skeletal muscle weakness associated with oxidative stress during aging (i.e. sarcopenia) using mice lacking CuZnSOD (*Sod1*KO), the cytoplasmic superoxide scavenger[1,9,10]. *Sod1*KO mice reveal a number of phenotypes that mimic features of sarcopenia in old wildtype mice, including loss of innervation, mitochondrial dysfunction, and increased generation of mitochondrial ROS (mtROS)[2,11–13]. We have also shown that loss of innervation is associated with increased mtROS and downstream activation of muscle atrophy and weakness[4,11,14]. In this study, we asked whether increased skeletal muscle mtROS induced by skeletal muscle-specific deletion of the mitochondrial form of SOD (MnSOD), independent of loss of innervation, is sufficient to induce muscle atrophy and weakness.

Previous studies have shown that global deletion of the *Sod2* gene ($Sod2^{-/-}$) leads to neonatal lethality supporting the importance of controlling superoxide levels[15,16]. We demonstrated that heterozygous deletion of MnSOD ($Sod2^{+/-}$) does not affect survival but leads to mitochondrial dysfunction[17]. Muscle mass is not altered in heterozygous MnSOD knockout mice; however, skeletal muscle mitochondrial ATP production is reduced and hydrogen peroxide generation is significantly increased in skeletal muscle[18]. Using a model of *Sod2* deficiency targeted specifically to fast twitch (type IIB) skeletal muscle fibers, we reported an increase in ROS generation and oxidative modifications in fast twitch fibers that was not associated with skeletal muscle atrophy or contractile dysfunction in young and old mice[19,20]. The impact of skeletal muscle specific *Sod2* deletion on exercise intolerance has also been reported[21], but its role on NMJ disruption and skeletal muscle mass and contractile properties have not been directly tested.

Here we tested whether mitochondrial oxidative stress within skeletal muscle, in the absence of neuronal oxidative stress and denervation, contributes to muscle atrophy and weakness using a mouse model in which MnSOD (*Sod2)* is deleted specifically in skeletal muscle using a cre-Lox approach driven by human skeletal actin. Contrary to our expectation, m*Sod2*KO mice exhibit a significant increase in muscle mass associated with dramatic increases in central nuclei, hyperplasia and fiber branching. Despite the increase in muscle mass, contractile function is impaired due to NMJ fragmentation and intrinsic alterations within myofibers, presumably elicited by excess hydrogen peroxide in cytoplasm. Excess superoxide in

mitochondrial matrix induces a dramatic loss of succinate dehydrogenase (SDH) and severe functional defects of the mitochondria. Our findings demonstrate, for the first time, that mtROS from skeletal muscle is sufficient to induce NMJ disruption and contractile dysfunction. We also report our novel findings that elevated skeletal muscle mtROS leads to increases in muscle mass through hyperplasia and fiber branching.

Methods
Detailed methods are available in **Supporting Information** section at the end of the article.

Generation of Muscle-specific Sod2 Knockout (m*Sod2* KO) Mice
Tissue-specific *Sod2* KO ($Sod2^{fl/fl}$) mice were described previously and provided to Dr. Van Remmen by Dr. Takahiko Shimizu[19,22]. Briefly, $Sod2^{f/fl}$ mice were generated using mouse *Sod2* genomic DNA, in which the neomycin resistance gene and exon 3 were flanked by two loxP sites. $Sod2^{f/fl}$ mice were then bred to mice containing cre recombinase (Cre) driven by human skeletal actin (HSA) promotor (HSA Cre). PCR was used to identify mice carrying the Cre and Flox constructs by previously described primer sequences and methods[19].

Animals
Approximately 6-8 month old female and male m*Sod2*KO and wildtype (WT) mice were used for all experiments with an exception of mice used for calcium kinetics assays (these mice were 9-13 months). $Sod2^{fl/fl}$ mice were considered WT in the absence of HSA Cre and m*Sod2*KO in the presence of $Sod2^{fl/fl}$. All mice were housed under pathogen-free barrier conditions where water and foods were provided ad libitum. The Institutional Animal Care and Use Committee at Oklahoma Medical Research Foundation (Oklahoma City, OK, USA) approved all procedures.

Enzyme Activity
Activities of CuZnSOD and MnSOD were determined using native gels with negative staining as a method previously described[13]. For histological assessment of SDH activity in muscle sections, mid-belly of gastrocnemius was cut in cross-section and stained with a buffer containing, 50 mM sodium phosphate (pH7.4), 84 mM succinic acid, 0.2 mM phenazine methasulfate, 2 mg/ml nitroblue tetrazolium and 4.5 mM EDTA. For succinate dehydrogenase (SDH) activity in isolated mitochondria (see below for mitochondrial isolation), we diluted 0.25 mg/mL of mitochondria in a buffer containing 210 mM mannitol, 70 mM sucrose, 5.0 MM KH_2PO_4 and 10 mM MOPS, pH 7.4.

Isolation of Skeletal Muscle Mitochondria
Mitochondria were isolated from gastrocnemius muscle following a previously established method [18].

Rate of hydrogen peroxide generation, ATP production and calcium retention capacity
The rate of mitochondrial H_2O_2 production was measured using Amplex Red (77.8 µM), horseradish peroxidase (HRP, 1 U/ml) and SOD (37.5 U/ml) based on a previously described method with minor modifications[13]. Mitochondrial complex I was activated by glutamate (5 mM) and malate (5 mM), while complex II-specific activation was achieved by succinate (10 mM) and

rotenone (1 μM). Antimycin A (1 μM) was added to determine maximum rate of H_2O_2 generation. Fluorescence was measured at an excitation wavelength of 545 nm and emission wavelength of 590 nm. The slope of increase in fluorescence was converted to the rate of H_2O_2 generation using a standard curve. The rate of ATP synthesis was measured using the luciferin/luciferase assay following a previously described method[23]. Mitochondrial calcium retention capacity (CRC) was determined using the membrane impermeable dye, Calcium Green-5N, based on a previously described method with modifications[24].

Fiber Permeabilization

Preparation for skeletal muscle fiber permeabilization was previously described[25]. Briefly, a small piece (~3-5 mg) of red gastrocnemius muscle was carefully dissected, and we separated fibers along their striations using fine forceps in ice-cold *buffer X* containing (in mM) 7.23 K_2EGTA, 2.77 CaK_2EGTA, 20 imidazole, 0.5 DTT, 20 taurine, 5.7 ATP, 14.3 PCr, 6.56 $MgCl_2$-$6H_2O$, 50 K-MES (pH 7.1). The muscle bundle was permeabilized in saponin solution (30 μg/mL) for 30 minutes, followed by 3 x 5 minute washes in ice-cold wash buffer containing (in mM) 105 K-MES, 30 KCl, 10 K_2HPO_4, 5 $MgCl_2$-$6H_2O$, 0.5 mg/ml BSA, 0.1 EGTA (pH 7.1).

Measurement of Respiration and Hydrogen Peroxide Production

Oxygen consumption rate (OCR) and the rate of mitochondrial hydrogen peroxide production were measured using the Oxygraph-2k (O2k, OROBOROS Instruments, Innsbruck, Austria) by a previously described method [26] with minor modifications. OCR was determined using an oxygen probe, while rates of hydrogen peroxide generation were determined using O2k-Fluo LED2-Module Fluorescence-Sensor Green. Data for both OCR and rates of hydrogen peroxide generation were normalized by milligrams of muscle bundle wet weights.

Measurements of mitochondrial superoxide release

Mitochondrial superoxide release was determined by using electron paramagnetic resonance (EPR) spin-trap, 5-(2,2-dimethyl-1,3-propoxycyclophosphoryl)-5-methyl-1-pyrroline *N*-oxide (CYPMPO) by a previously described method with minor modifications[27].

Markers of Oxidative Modifications

Levels of F_2-isoprostanes in gastrocnemius were determined by a previously described method [28] with minor modifications. The levels of GSH and GSSG were determined using reverse-phase HPLC and electrochemical detection[29]. GSH and GSSG were extracted from tissue homogenate by treatment with 5% metaphosphoric acid. Myofibrillar (MF) proteins were isolated based on a previously reported method[30]. Abundance of carbonyl groups in muscle homogenate and MF proteins was determined by FTC based on a previously described method[31].

Energy Charge

Ratio of energy charge in gastrocnemius muscles was determined by using a previously published method[32]. All analytes were extracted from tissue homogenate by treatment with 150 mM potassium hydroxide. Concentrations of ATP, ADP, AMP, NAD+ and NADP+ were detected by absorption at 254 nm. Concentrations of NADH and NADPH were detected by fluorescence at excitation 340 nm and emission 430 nm. All analytes were quantified on the basis of the integrated area of standards.

Contractile Properties of Skeletal Muscle
Isometric contractile properties for *in situ* and *in vitro* gastrocnemius muscles were measured based on previously established methods[9].

Assessment of Calcium Kinetics using Skeletal Muscle
Experiments to determine the dynamic calcium responses to twitch stimuli were performed on lumbrical muscles from WT and m*Sod2*KO mice (age 9-13 months). Details on the techniques and apparatus used to measure lumbrical muscle contractile properties and fluorescence have been described previously[33,34].

SERCA activity
The measurement of SERCA ATPase activity was performed at 37°C by using a spectrophotometric assay as described elsewhere[35].

NMJ staining
Neuromuscular junctions were stained following a previously established method with minor modifications[36].

Histology
Gastrocnemius muscle tissues were frozen in liquid nitrogen-cooled isopentane. 10 μm cross sections were made using a microcryotome (-20°C), dried and used for immunohistochemistry staining.

Quantification of Myofiber Branching
Myofiber branching was determined based on a previously established method with modifications[37,38].

Quantification of Protein Abundances by Selected Reaction Monitoring
We used targeted quantitative mass spectrometry to measure protein abundance as previously described[39].

Determination of mtDNA Copy Number
Absolute copy number of mtDNA was quantified (copies per ng input DNA) by digital PCR based on a previously reported method[40,41].

Immunoblot and qPCR
Standard procedures were used for western blots and qPCR. Antibodies and primers used are detailed in Table S2.

Statistical analyses
Data were analyzed using unpaired two-tailed t tests. Levels of significance were set at $p < 0.05$ in all cases. Data are presented as mean ±SEM.

Results

Defects of Mitochondrial Respiration and Increased H_2O_2 Generation in mSod2KO Mice

To test the causality of excess mtROS on skeletal muscle weakness, we generated a muscle-specific *Sod2* knockout mouse line (m*Sod2*KO mice). We confirmed the extent and specificity of the MnSOD deletion by measuring the activity (Figures S1A) and protein abundance (Figures S1B) of MnSOD in gastrocnemius muscle and heart. Our PCR data also confirms *Sod2* deletion specifically in skeletal muscle (not in heart) of Acta cre positive $Sod2^{fl/fl}$ mice. Cre negative $Sod2^{fl/fl}$ mice show no deletion as expected (Figure S1C). CuZnSOD activity is not altered in response to the loss of MnSOD. We measured mitochondrial function using isolated skeletal muscle mitochondria. We found that mitochondrial H_2O_2 generation with complex I substrates is significantly higher in isolated skeletal muscle mitochondria from m*Sod2*KO compared to wildtype mitochondria while H_2O_2 generation is dramatically lower with complex II substrates. Antimycin A-induced H_2O_2 generation rate is significantly higher in mitochondria from the m*Sod2*KO mice (Figure 1A). The between-group differences in all conditions disappeared after catalase addition confirming that the signal is generated by H_2O_2 (data not shown). Consistent with the reduced H_2O_2 generation from complex II substrates, mitochondria from the m*Sod2*KO mice have a dramatically lower SDH activity than wildtype mitochondria (Figure S1D-F). The mRNA levels of complex II subunits A and B are not decreased in muscle from m*Sod2*KO (Figure S1G, H), suggesting that the decrease in complex II may be due to post-translational modifications and protein degradation, consistent with previous findings from our laboratory and others[19,42].

Excess mitochondrial ROS, in particular superoxide anions, have been shown to alter mitochondrial function[43]. In agreement with the observed decrease in SDH enzyme activity, complex II-induced ATP generation of m*Sod2*KO is dramatically decreased, while complex I induced ATP generation is not altered (Figure 1B). Consequently, the levels of ATP in gastrocnemius muscle are decreased by ~40 % in m*Sod2*KO compared to wildtype mice (Figure 1C). Mitochondria play an important role in cytoplasmic calcium homeostasis by absorbing calcium ions from cytoplasm[24]. To test mitochondrial calcium retention capacity (CRC), we challenged isolated mitochondria by adding 2μM calcium chloride ($CaCl_2$) per minute until the mitochondrial calcium release level overrides calcium uptake due to permeability transition pore opening. CRC in m*Sod2*KO mice is reduced by ~70% compared to WT (Figure 1D).

Preparation of isolated mitochondria can cause damage to the organelle altering mitochondrial morphology and function and induce selection bias during the centrifugation step[44]. Also, mitochondria *in vivo* have the added complexity of interactions with neighboring organelles and proteins. To address these potential limitations, we measured mitochondrial oxygen consumption (OCR) and H_2O_2 generation rates in permeabilized “red” gastrocnemius muscle fibers located in the lateral heads of the gastrocnemius. These fibers are visually more red in color than surrounding fibers. Consistent with our previous results in isolated mitochondria, we observed that complex II-induced OCR is selectively decreased in m*Sod2*KO mice (Figure 1E), and ROS generation is elevated (Figure 1H). The rates of mitochondrial H_2O_2 production are significantly elevated by ~4-5 fold at basal and during complex I and II-activated conditions in m*Sod2*KO mice. These observations are different from the findings in isolated mitochondria (Figure 1B) potentially due to presence of ADP in permeabilized fibers. Thus, we also measured ROS generation in the absence of ADP using permeabilized fibers (Figure 1I). In

muscle mitochondria from wildtype mice, we observed a steep rise in H_2O_2 generation in response to succinate, suggesting superoxide generation through reverse electron transfer[23]. The rise in H_2O_2 generation is substantially lower in m*Sod2*KO in response to succinate consistent with complex II deficiency.

To test mitochondrial function *in vivo*, we measured total running time to exhaustion for the mice on a treadmill, which shows a substantial reduction in m*Sod2*KO mice-10 mins compared with ~2 hrs in WT mice (Figure 1F). Voluntary cage activity of the m*Sod2*KO mice trended to decrease ($p < 0.07$) during the active (dark) phase (Figure S2A,B). Lactate build-up caused by decreased pyruvate utilization has been suggested to be the underlying cause of the exercise intolerance in m*Sod2*KO mice[19,42]. To test pyruvate utilization of skeletal muscle fibers from wildtype and m*Sod2*KO mice, we directly added pyruvate as a substrate in the permeabilized fibers while measuring mitochondrial respiration, indicated as red arrow in Figure 1G. Pyruvate effectively shuts down oxidative phosphorylation in m*Sod2*KO mice.

The rate of ROS generation in the isolated mitochondria or permeabilized fibers was determined using Amplex Red or Amplex UltraRed probes respectively, which detect H_2O_2, but not superoxide. Due to the deficiency of MnSOD in the matrix in m*Sod2*KO mice, the superoxide within the matrix will not be detected. To directly determine mitochondrial superoxide release, we used electron paramagnetic resonance (EPR) in conjunction with superoxide–targeted spin trap. Mitochondria isolated from gastrocnemius muscle were used for the measurements. Superoxide levels derived by EPR signals in m*Sod2*KO mice are significantly elevated for complex I- and II-linked substrates and the inhibitor Antimycin A (Figure 1J). Complex I and III inhibitors, rotenone and Antimycin A, increase superoxide generation from mitochondria for wildtype and m*Sod2*KO, but a greater increase is observed in mitochondria from m*Sod2*KO than from wildtype mice. Addition of exogenous CuZnSOD in the buffer effectively abolished the superoxide-derived EPR signals for complex I- and II-linked substrates (Figure S1I). These observations are consistent with previous data from our laboratory in which we measured an increase in superoxide generation in fast-twitch muscle specific deletion of *Sod2*KO mice[19].

Markers of Oxidative Stress and Redox Potential

To test whether a reduction in MnSOD leads to an increase in oxidative modifications, we assessed lipid peroxidation, protein carbonyls, and tyrosine nitration in gastrocnemius muscle. Lipid peroxidation was determined by F_2-isoprostane levels, which are stable products formed by free radical-catalyzed peroxidation of arachidonic acids. F_2-isoprostane levels are elevated by ~80% in the m*Sod2*KO mice (Figure 2A). To measure protein oxidation of skeletal muscles, we determined the level of carbonylation of proteins using muscle homogenate and observed a trend of increase ($p<0.1$) in the m*Sod2*KO mice (Figure 2E). Because skeletal muscle is a heterogeneous tissue and myofibrillar proteins are highly sensitive to oxidative damage, we isolated myofibrillar proteins and determined the levels of carbonylation, which are significantly elevated by ~30% in m*Sod2*KO mice (Figure 2F). Nitration of protein tyrosine residues represents another important post-translational modification caused by nitrosative and oxidative stress. The formation of 3-nitrotyrosine is the most commonly studied covalent modification of protein nitration, and elevated levels of this product are implicated in many oxidative stress-

associated pathologies, including aging[45]. We observed that protein nitration is elevated by ~60% in muscle from m*Sod2*KO mice (Figure 2C).

Changes in redox status have a major impact on cellular and physiological processes and may underlie many functional deficits associated with aging and oxidative stress[3,46]. Removal of H_2O_2 is catalyzed by the antioxidant enzymes catalase, glutathione peroxidase (Gpx), and peroxiredoxins (Prx). Gpx and Prx require oxidation of GSH and thioredoxin, respectively. The ratio of reduced and oxidized GSH (i.e., GSH:GSSG) is used as an index of redox potential[47]. We found a significant increase in the content of GSSG suggesting oxidative stress, although the GSH:GSSG ratio in m*Sod2*KO mice shows only a trend ($p < 0.07$) for a decrease in the ratio (Figure 2B). Reduction of GSH is catalyzed by glutathione reductase (GR), which requires oxidation of NADPH to $NADP^+$. Similarly, reduction of oxidized thioredoxin requires oxidation of NADH to NAD^+. Perhaps surprisingly, the muscle from m*Sod2*KO mice does not show a significant change in NAD^+, NADH or the NAD^+/NADH ratio (Figure 2D). Figure S5 illustrates the role of antioxidant enzymes and their co-factors in redox homeostasis.

Skeletal Muscle Myofibrils and Mitochondrial Proliferation

To evaluate the impact of mitochondrial oxidative stress on skeletal muscle ultrastructure, we obtained transmission electron micrograph (TEM) images of tibialis anterior (TA) muscles. In m*Sod2*KO, myofibrils are shorter and smaller and not as regularly organized as in wildtype skeletal muscle (Figure S6A). Myofilaments appear to be less tightly packed, I-bands around Z disks (shown as 'Z' in Figure S6A) are indistinct in many areas, and the M-lines (shown as 'M' in Figure S6A) are frequently out of alignment and faint. Mitochondria (shown as white arrow head in Figure S6A) in m*Sod2*KO exhibit localized accumulations between myofibrils and appear to be bigger than those of wildtype. The location of mitochondria in wildtype skeletal muscle is near Z-disks, but in m*Sod2*KO mice their cellular locations are irregular. We measured the protein content of isolated mitochondria in gastrocnemius muscle, and found ~30% increase in mitochondrial protein content in muscle from m*Sod2*KO mice compared to wildtype mice (data not shown). The mitochondrial proliferation is consistent with an increased level of mRNA levels of PGC 1-α (Figure 3A).

Mitochondrial proliferation was confirmed by measuring targeted mitochondrial protein abundance using Selected Reaction Monitoring (SRM). We observed that many TCA cycle enzymes are increased in *mSod2KO* with the notable exceptions of aconitase and SDH (Figure 3C), which are known to be highly sensitive to oxidative stress. Similarly, many enzymes in the fatty acid oxidation pathway are increased (Figure S4) consistent with mitochondrial proliferation. Proteins involved in glycolysis are largely unchanged (Table S1). We determined the abundance of antioxidant enzymes, and found that many of the antioxidant enzymes are significantly elevated in m*Sod2*KO except Sod1 and a few others (Figure S5). Upregulation of TCA cycle, fatty acid oxidation and antioxidant enzymes suggests a compensatory mechanism for decreased oxidative phosphorylation and excess oxidants.

Excess oxidants are known to cause oxidative damage to DNA and to increase mtDNA copy number in skeletal muscle[40] and potentially mtDNA sequence variants. Thus, we determined the copy number of mitochondrial and nuclear DNA using gastrocnemius muscles of wildtype and m*Sod2*KO mice. We found a significant increase in mtDNA copy number (Figure 3B) with no change in the copy number of nuclear DNA (data not shown). Our analyses of heteroplasmic

single nucleotide variant (SNV) frequency reveal no change in mtDNA mutational load (Figure S3A). A specific nucleotide, thymine, trends to show increased SNV frequency in m*Sod2*KO (Figure S3B), suggesting that thymine might be more subject to oxidative modifications. Interestingly, occurrence of SNVs higher than 1% frequency is increased in m*Sod2*KO (Figure S3C). These increases in SNVs are localized in D-Loop and Rnr1/2.

Contractile Dysfunction and Calcium Mishandling in mSod2KO Skeletal Muscle

Excess ROS is known to cause contractile dysfunction in skeletal muscles[9]. To test the impact of mitochondrial ROS on skeletal muscle from wildtype and m*Sod2*KO mice, we measured *in situ* and *in vitro* contractile function of skeletal muscle. The *in vitro* contractile properties of soleus and extensor digitorum longus (EDL) muscles reveal a significant decrease in maximum isometric specific force (N/cm^2) for muscles of m*Sod2*KO compared with wild type mice (Figure S6B,C) with unchanged fatiguability (Figures S6D,E). Our *in situ* experiments using direct stimulation on the gastrocnemius similarly demonstrates a ~40% decrease in specific force for m*Sod2*KO. The force deficit is exacerbated in sciatic nerve-stimulated force generation (Figure 4A,B), suggesting disruption and abnormalities of the neuromuscular junction (NMJ). Intrinsic force deficit is highly associated with calcium mishandling, including intracellular calcium transient (ICT), sensitivity, and uptake kinetics[48]. We find a significant reduction in ICT measured in m*Sod2*KO lumbrical muscles (Figure 4C), while specific force and intracellular calcium fall time are unchanged (Figure 4D,E). The drop in peak intracellular free calcium may be affected by a decrease in calcium release, enhanced calcium buffering, or faster calcium uptake in m*Sod2*KO. Arguing against the latter, we find severe defects in mitochondrial buffering (Figure 1D) and sarcoplasmic/endoplasmic reticulum calcium ATPase (SERCA) pump (Figure 4F).

NMJ Disruption and Fragmentation of mSod2KO Skeletal Muscle

Because our contraction data suggest NMJ abnormalities may exist in the muscle from m*Sod2*KO mice, we asked whether the loss of MnSOD and increased mitochondrial ROS alters the mRNA and protein levels of the acetylcholine receptor (AchR). We found ~2-fold increase in the mRNA level for the AchRα-isoform (Figure 5A). Despite the increase in the mRNA level, the protein abundance of AchR is decreased by ~50% in m*Sod2*KO (Figure 5B), which may be due to an increase in protein degradation. To further determine morphological alterations by excess mtROS, we measured the size of NMJ and the number of fragments and found significant increases in m*Sod2*KO (Figure 5C-E), which are typical of denervation and sarcopenia phenotypes[2]. Note that scoring of the percentage of denervated NMJ reveals no effect of MnSOD deficiency (Figure 5F).

Mitochondrial Oxidative Stress Increases Muscle Mass via Hyperplasia

Contrary to our expected results, m*Sod2*KO mice do not exhibit a loss in muscle mass (Figure 6A). Indeed, in gastrocnemius and quadriceps muscles there are ~10-15% increases in muscle mass, while no changes were observed in smaller muscles. The increase in muscle mass observed in female mice is also evident in male mice (Figure S6A). We find that isolated skeletal muscles from m*Sod2*KO are more red in color than wildtype muscles (Figure S1J) as reported previously[42]. To test a potential shift in muscle fiber type, we performed

immunohistochemistry using isoform specific antibodies on cross-sections and found a significant increase in Type 2x fibers in m*Sod2*KO gastrocnemius (Figure 6B). We postulate that accumulation of mitochondria is the underlying cause of red pigment of the skeletal muscle. In line with the idea, our m*Sod2*KO mice demonstrated mitochondrial proliferation (Figure 3A-C). An animal model leading to a significant mitochondrial dysfunction (ANT1KO) and compensatory proliferation exhibits redness of the muscle[49]. Another animal model with PGC1-α overexpression demonstrates increased pigment in skeletal muscle tissues[50]. Increase in muscle mass in gastrocnemius is not caused by a change in fiber size (i.e. hypertrophy), but rather by an increase in the number of fibers by ~60% (hyperplasia) (Figure 6C-E). Furthermore, ~50% of the fibers contain central nuclei in m*Sod2*KO (Figure 6F,G), suggesting generation of new fibers. Regardless of the dramatic increase in central nuclei, embryonic myosin heavy chain (eMHC) expression is not increased in m*Sod2*KO mice (Figure 6H). Histogram analysis of fiber area in m*Sod2*KO reveals highly variable and distorted bell-shape distributions, as opposed to normally distributed wildtype gastrocnemius (Figure 6I).

Fiber Branching as a Mechanism of an Increase in Muscle Mass in mSod2KO

To directly test the mechanism responsible for hyperplasia, we teased out single fibers from gastrocnemius muscles and determined the number of fibers with or without branches (Figure 7A). We find that ~35% of the fibers contain fiber branches in muscle from the m*Sod2*KO mice, while no fibers exhibit branches in muscle from wildtype mice (Figure 7B). In addition to fiber branching, we examined changes of a calcium-mediated protein degradation pathway calpain, a muscle protease. We find protein expression of calpain-1 significantly lower in m*Sod2*KO mice (Figure 7C). To measure the activity of calpain, we determined the abundance of breakdown products from α-II spectrin at ~150 kDa[51], which is significantly decreased in m*Sod2*KO mice (Figure 7D).

Discussion

The goal of this study is to determine whether compromised function of skeletal muscle mitochondria and elevated mtROS generation are sufficient to cause muscle atrophy independent of loss of muscle innervation. Contrary to our prediction, elevated mitochondrial oxidative stress leads to increases in muscle mass and hyperplasia via fiber branching. Despite the compensatory increase in muscle mass, contractile function is impaired associated with NMJ disruption and possibly due to a calcium mishandling within myofibers. Excess superoxide in mitochondrial matrix leads to dramatic loss of SDH and severe exercise intolerance as reported in animals and patients with SDH deficiency[52,53]. Our findings demonstrate, for the first time, that mtROS from skeletal muscle is sufficient to induce NMJ disruption but not denervation. We also report our novel findings that ROS from skeletal muscle mitochondria increase muscle mass through fiber branching.

MnSOD is localized in the mitochondrial matrix where it is poised to protect the ETC subunits and other matrix proteins from oxidative insult induced by ETC generation of superoxide. In the absence of MnSOD, superoxide is unchecked and the mitochondria are susceptible to oxidative damage that can impair function. We measured a number of indicators of mitochondrial function in muscle from m*Sod2*KO mice. One of the most dramatic changes is the substantial decrease in the level of complex II (SDH) protein subunits despite upregulation of the mRNA levels. The

mechanisms by which increased superoxide causes SDH-specific deficiency are unclear, but potential causes include deficiency or dysfunction of SDH import proteins, assembly factors, or activation of mitochondrial proteases, including Lon protease[54]. Previous studies have shown that loss of SDH contributes to substantial reductions in ETC activity and ATP generation rate, leading to severe exercise intolerance in animals[19,21] and in patients[52,53]. Mitochondrial respiration in response to complex II substrate is also significantly lower in mitochondria from m*Sod2*KO mice compared to wildtype mice. Complex I activity is partially reduced, but the loss of SDH is much more substantial than other complexes of ETC in agreement with previous reports in mice lacking MnSOD in skeletal and cardiac muscles[21,55]. We confirmed the impaired mitochondrial function *in vivo* using treadmill running time. The m*Sod2*KO mice are more susceptible to exhaustion during treadmill running. Although our data exhibit ETC activity only, mitochondria are also responsible for fatty acid oxidation, defects in which are likely to contribute to exercise intolerance as shown before[56]. Overall, our results confirm that mitochondrial function is significantly compromised by the loss of MnSOD.

In addition to severe defects in respiration, mitochondria from m*Sod2*KO mice have increased generation of ROS. Excess ROS are known to impair contractile function of skeletal muscle[9]. Isolated skeletal muscle incubated with varying hydrogen peroxide concentrations has demonstrated dose-dependent effects on maximum force generation[7,57]. Increased hydrogen peroxide is known to induce lipid peroxidation in the sarcolemma, which was supported by our data (Figure 2A). Excess oxidants also induce oxidative modifications in proteins associated with the contractile machinery (i.e. thiol oxidation). To test this idea, we isolated myofibrillar proteins using previously established methods[30], and found that carbonylated proteins were significantly elevated in *mSod2*KO mice. These data support the concept that multiple factors can contribute to muscle weakness, including altered signal transmission through the neuromuscular junction and intrinsic changes to the proteins response for carrying out contractile force generation.

Alterations in the NMJ are a critical contributor to sarcopenia[46], but it is not clear whether defective mitochondrial function precede or follow changes in NMJ and skeletal muscle atrophy and contractile dysfunction[58]. Our laboratory and others previously demonstrated that denervation plays a causal role in AchR fragmentation and degeneration, leading to skeletal muscle atrophy[12]. Furthermore, recent studies support an association between skeletal muscle mtROS and NMJ disruption in multiple pathological conditions, including aging and denervation[36,56,58,59]. In this study, we were interested in determining whether the increased mtROS and mitochondrial dysfunction in the skeletal muscle of m*Sod2*KO mice compromises the NMJ in a feedback manner to potentially initiate muscle atrophy. Our results are consistent with alterations in the NMJ in gastrocnemius muscle of the m*Sod2*KO mice. For example, our *in situ* contractile function data reveal that the maximum isometric specific force of the gastrocnemius is decreased by ~40% with stimulation directly on the muscle, but force generation through sciatic nerve stimulation shows a greater reduction (~60%). This result suggests compromised signaling through the neuromuscular junction in the m*Sod2*KO mice. Consistent with these findings, the expression of the acetylcholine receptor alpha subunit (AchR-α) is decreased in gastrocnemius muscle from the m*Sod2*KO despite an upregulation of AchR-α mRNA levels[59]. Further analyses of NMJ morphology reveals that fragmentation and size of the NMJ area are increased in m*Sod2* KO. Together, these changes suggest that

elevated mitochondrial ROS and oxidative stress induce morphological changes in the acetylcholine receptor, including a potentially increased degradation of AchR-α or reduced stability of the AchR complex. Notably, however, we did not find any evidence of loss of innervation in gastrocnemius muscle from the m*Sod2*KO mice. Thus, for the first time, we demonstrate a causal role of excess ROS from skeletal muscle mitochondria on NMJ disruption and muscle weakness, supporting a retrograde effect of muscle mtROS *in vivo*[60].

Contrary to our expected results, significant damage to the mitochondria and excess ROS do not cause atrophy in skeletal muscle. Rather, we find an increase in muscle mass in gastrocnemius and quadriceps. Our findings differ from an existing report, which found no change in skeletal muscle mass in m*Sod2*KO mice[21]. Our study includes data collected from 30-35 female mice/group compared with 5 mice/group in the study that did not see a difference in mass. Our findings in female mice were confirmed in male mice (Figure S7A,B). Notably, the impact of mitochondrial oxidative stress causing hypertrophy on large muscle groups (gastrocnemius and quadriceps), but not in small muscles (TA, EDL and soleus), remains unclear. Another redox-dependent pathological condition, Duchenne Muscular Dystrophy, also preferentially affects muscle groups as reported[61–63]. We predict that the preferential calf hypertrophy results from overuse while functioning to stabilize the body against gravity. A case report of a patient with familiar mitochondrial myopathy, who demonstrated deficiencies in SDH and aconitase with lifelong exercise intolerance, reported calf hypertrophy consistent with our report[52,53]. We also previously found a similar increase in muscle mass in mice with a muscle specific deletion of CuZnSOD[13]. Together these data point to a modulation of muscle mass by oxidative stress that leads to increased muscle mass, but not atrophy.

The increase in muscle mass in the m*Sod2*KO mice is associated with increased central nuclei[21] and a dramatic increase in the number of fibers appearing in a cross section. The increase in fiber number results from fiber branches rather than independently separated fibers. The cause of fiber branching is unknown, but one explanation is incomplete lateral fusion of myotubes during regeneration elicited by injury-induced necrosis[64], which is dramatically elevated in m*Sod2*KO mice[21]. The increased fiber branching has previously been shown in EDL muscle from old compared to young rats[65]. Fiber branching is also the basis for the increase in fiber numbers in *mdx* mice, where there is also an increase in oxidative stress leading to skeletal muscle hypertrophy and decreased specific force[37] as in m*Sod2*KO skeletal muscle. Although branched fibers compensate for skeletal muscle cell death via necrosis in m*Sod2*KO mice[21], excitation-contraction coupling is disturbed in the branched myofibers[37], and calcium-activated force production has been shown to be reduced[66]. The *mdx* mice have shown an increase in muscle mass, but exhibited decreases in calcium transients in branched fibers compared with unbranched fibers[67]. The calcium transient is indeed decreased in m*Sod2*KO skeletal muscle. Considering that there is no matching increase in synapse number with fiber branching[37], branched fibers may also contribute to neuromuscular dysfunction.

Conclusions

In summary, our results demonstrate that loss of MnSOD increases superoxide in mitochondrial matrix, leading to SDH deficiency, mitochondrial defects, and severe exercise intolerance. Excess hydrogen peroxide produced from the mitochondria induces NMJ alterations through a retrograde effect on neuromuscular junction proteins, contributing to

neuromuscular dysfunction-induced skeletal muscle weakness. Despite reports of neurogenic atrophy in multiple pathological conditions (i.e. aging, inactivity, chronic inflammatory diseases), skeletal muscle mass of large muscle groups, including gastrocnemius and quadriceps, is increased due to hyperplasia via fiber branching that may also contribute to NMJ dysfunction.

ACKNOWLEDGEMENTS
This work was supported by the National Institute of Health and National Institute of Aging [P01AG051442, R01-AG047879, R01-AG055395, P30AG050911, T32AG052363], National Institute of General Medical Sciences [5P30GM114731], and the United States Department of Veterans Affairs. The authors would like to thank the Targeted DNA Methylation & Mitochondrial Heteroplasmy, Integrative Redox Biology and Multiplex Protein Quantification Cores at Nathan Shock Center for sharing their expertise. The authors certify that they comply with the ethical guidelines for authorship and publishing of the *Journal of Cachexia, Sarcopenia and Muscle* [68].

ONLINE SUPPLEMENTARY MATERIAL
Additional Supporting Information may be found online in the Supporting Information section.

Supplemental Figure 1. The m*Sod2*KO mice exhibit skeletal muscle specific loss of MnSOD activity and dramatic loss of complex II activity in electron transport chain (ETC). (A) A representative image showing activities of MnSOD and CuZnSOD in skeletal and cardiac muscle homogenates. (B) Immunoblot analysis using gastrocnemius muscle homogenates shows protein abundance of MnSOD in WT, but not in m*Sod2*KO (n = 7-8/group). (C) A representative PCR results showing deletion of floxed site by human skeletal actin (HAS) cre recombinase. (D) Representative SDH activity performed on sections of gastrocnemius muscle. (E) Representative profile of spectrophotometric SDH activity using isolated mitochondria (25 µg/mL) from gastrocnemius. Activation of the SDH enzyme was achieved by 2 min incubation with succinate. (F) Quantification of the succinate consumption rate at active conditions (n = 2). (G) mRNA levels of SDH subunits (n = 7-8). (H) Protein expression of SDH subunits determined by mass spectrometry (n = 6). (I) Representative EPR spectra for measurement of mitochondrial superoxide release rate using isolated skeletal muscle mitochondria with or without superoxide dismutase. Abbreviations (concentrations): glu, glutamate (25 mM); mal, malate (2.5 mM); suc, succinate (25 mM); rot, rotenone (1 µM); SOD, superoxide dismutase (250U/mL). (J) Representative images of isolated gastrocnemius (top) and TA (bottom) muscles that demonstrate redness of the m*Sod2*KO muscle. Values are mean ±SEM. *$p < 0.05$.

Supplemental Figure S2. Spontaneous home cage activity. Mice were individually housed in cages with motion and activity detector units. (A) Hourly activity during 24 hours divided by lights on or off. (B) Average hourly activity during Light Phase and Dark Phase. n = 6. Values are mean ±SEM.

Supplemental Figure S3. Mitochondrial DNA variants. (A) Total frequency of mitochondrial DNA variants from gastrocnemius (n = 8-9). (B) Nucleotide-specific variant frequencies of mitochondrial DNA (n = 4-9). (C) A circos plot image demonstrating single nucleotide variants higher than 1% from WT (black) and m*Sod2*KO (red).

Supplemental Figure S4. Isoform and subunit expression of the enzymes involved in beta-oxidation. Gastrocnemius muscle homogenate was used to determine protein abundance (n = 6). Data are shown as pmol per 100 µg protein. Values are mean ±SEM. *p < 0.05. Abbreviation: Cpt, carnitine palmitoyltransferase. See Table 2 for gene id and protein names.

Supplemental Figure S5. Isoform and subunit expression of antioxidant enzymes. Gastrocnemius muscle homogenate was used for the data (n = 6). Data are shown as pmol per 100 µg protein. Values are mean ±SEM. *p < 0.05. Abbreviations: Sod, superoxide dismutase; Prx, peroxiredoxin; Trx, thioredoxin; TR, thioredoxin reductase; GSH, glutathione; Gpx, glutathione peroxidase; GR, glutathione reductase; Cat, catalase. See Table 2 for gene id and protein names.

Supplemental Figure S6. *In vitro* contractile properties of isolated fast (EDL) and slow (soleus) twitch muscles. (A) Transmission electron microscopic (TEM) images showing sarcomeric proteins and two subpopulations of mitochondria, subsarcollemal (SS) and intermyofibrillar (IMF) mitochondria. M; M-line, Z; Z-disk. White arrow heads, mitochondria. Isometric maximum specific force (sFo, N/cm^2), force per cross-sectional area in EDL (B) and soleus (C). Relative force (percent of initial) during fatigue protocol in EDL (C) and soleus (D). n = 6. Values are mean ±SEM. *p < 0.05.

Supplemental Figure S7. Muscle mass and mitochondrial ATP generation rate in 6-8 months old male mice. (A) Isolated skeletal muscle mass. Abbreviations: Gast, gastrocnemius; Sol, soleus; TA, tibialis anterior; EDL, extensor digitorum longus; Quad, quadriceps. (B) Rate of ATP generation from isolated skeletal muscle mitochondria from male mice (n = 3). Values are mean ±SEM. *p < 0.05. Abbreviations: GM, glutamate and malate; Suc, succinate; Rot, Rotenone.

Table S1. Enzymes in glycolysis and gluconeogenesis. Gastrocnemius muscle homogenate was used determine protein abundance (n = 6). Data are shown as pmol per 100 µg protein. Values are mean ±SEM. *p < 0.05. See Table 2 for gene id and protein names.

Table S2. Gene IDs and protein names in TCA cycle (A), beta-oxidation (B), antioxidant enzymes (C) and glucose metabolism (D).

Table S3. List of antibody catalog numbers and qRT-PCR primer sequences.

CONFLICT OF INTEREST

Bumsoo Ahn, Rojina Ranjit, Pavithra Premkumar, Gavin Pharaoh, Katarzyna M. Piekarz, Satoshi Matsuzaki, Dennis R. Claflin, Kaitlyn Riddle, Jennifer Judge, Shylesh Bhaskaran, Kavithalakshmi Satara Natarajan, Erika Barboza, Benjamin Wronowski, Mike Kinter, Kenneth M. Humphries, Timothy M. Griffin, Willard M. Freeman, Arlan Richardson, Susan V. Brooks, Holly Van Remmen declare that they have no conflict of interest.

FIGURE LEGENDS.

Figure 1. Defects of Mitochondrial Respiration and Increased H_2O_2 Generation in m*Sod2*KO Mice. (A) Rates of hydrogen peroxide generation determined in isolated mitochondria from gastrocnemius muscle using Amplex Red (n = 3-6). Substrates and inhibitors were added to determine ROS generation in response to substrates and inhibitors of mitochondrial ETC. (B) Rates of ATP production determined in isolated mitochondria from complex I and II (n = 4-5). (C) Contents of cellular nucleotides determined in gastrocnemius tissue homogenate (n = 7-8). (D) Left: A sample observation of calcium retention capacity (CRC) of isolated mitochondria (WT vs. m*Sod2* KO). Calcium levels were determined using membrane-impermeable calcium indicator, Calcium-Green 5N. Right: Quantified calcium retention capacity (n = 4-5). (E) Mitochondrial oxygen consumption rate (OCR) in response to sequential addition of substrates and inhibitors in permeabilized gastrocnemius fibers (n = 4-5). (F) Running time on a treadmill (n = 6). (G) Mitochondrial oxygen consumption rate (OCR) in response to sequential addition of substrates and inhibitors in permeabilized gastrocnemius fibers-testing the impact of pyruvate on mitochondrial OCR (n = 3). (H) Rate of hydrogen peroxide generation determined in response to sequential addition of substrates and inhibitors in permeabilized gastrocnemius fibers using Amplex UltraRed (n = 4-5). (I) Hydrogen peroxide generation rate assessed from permeabilized gastrocnemius fibers in the absence of ADP (n = 4). (J) Mitochondrial superoxide release measured by spin trap CYPMPO using isolated mitochondria. Data are quantification of EPR spectra (n = 5). Values are mean ±SEM. *$p < 0.05$. Abbreviations. ETC, electron transport chain; GM, glutamate and malate; Suc, succinate; Rot, Rotenone; AA, Antimycin A; Asc, Ascorbate; TMPD, N,N,N',N'-tetramethyl-p-phenylenediamine.

Figure 2. Markers of Oxidative Stress and Redox Potential. (A) Lipid peroxidation determined by F_2-isoprostane in gastrocnemius muscles. Values are ng F_2-isoprostane/g muscle tissue (n = 7-8). (B) Reduced GSH, oxidized GSH (GSSG), and the ratio (GSH: GSSG) in gastrocnemius muscles (n = 8-9). (C) Immunoblot images and quantified data showing the proteins conjugated with tyrosine nitration from WT and m*Sod2* KO (n = 7). (D) NAD^+, NADH, and the ratio (NAD^+/NADH) was determined using HPLC in gastrocnemius muscles (n = 9-10). (E) Left: Quantified data for carbonylated proteins from total gastrocnemius homogenate (n = 4-5). Right: Representative images showing carbonylated proteins (Top) and Coomassie-stained total proteins (Bottom). (F) Left: Quantified data for carbonylated proteins from isolated myofibrillar (MF) proteins (n = 4). Right: Representative images showing carbonylated MF proteins (Top) and Coomassie-stained total MF proteins (Bottom). Values are mean ±SEM. *$p < 0.05$.

Figure 3. Skeletal Muscle Myofibrils and Mitochondrial Proliferation. (A) Levels of PGC1-α mRNA in WT and m*Sod2*KO mice (n = 7-8). (B) Mitochondrial DNA (mtDNA) copy numbers per ng genomic DNA (gDNA) from gastrocnemius muscle (n = 9-10). (C) Protein expression of isoforms and subunits in Krebs cycle enzymes (n = 6). Values are mean ±SEM. *$p < 0.05$.

Figure 4. Contractile Dysfunction and Calcium Mishandling in *mSod2KO* Skeletal Muscle. (A) Isometric contractile function of gastrocnemius muscles were determined using *in situ* preparation. Maximum isometric specific force (sFo), force per cross-sectional area (n = 5-7). (B) Force deficit induced by muscle- or nerve-stimulation (n = 5-7). (C) Intracellular calcium transient (ICT, n = 6). (D) Specific force generation (kPa) (n = 6-7), (E) ICT fall time (n = 6). Isolated lumbrical muscles are used for C-E. (F) Activity of sarcoplasmic/endoplasmic reticulum calcium ATPase (SERCA pump) in response to varying calcium concentrations from gastrocnemius (n = 6). Values are mean ±SEM. *$p < 0.05$.

Figure 5. NMJ Disruption and Fragmentation of m*Sod2*KO Skeletal Muscle. (A) Levels of acetylcholine receptors (AchR) mRNAs. mRNA levels of three AchR isoforms (α, δ, and ε) were determined by qRT-PCR using gastrocnemius muscles (n = 7-8). (B) Protein abundance of AchR-α was determined using immunoblot analysis (n = 8). (C) Representative neuromuscular junction (NMJ) immunofluorescence images from gastrocnemius muscle from WT (Left) and m*Sod2* KO (Right). Acetylcholine receptors (AchR) are stained with Alexa-488 conjugated α-bungarotoxin (n = 5). (D) Quantification of NMJ area. (E) Categorization of NMJs by the number of fragments. (F) Percent of denervated NMJ. Averages of 30-50 NMJs were used as each data point from each mouse. Values are mean ±SEM. *$p < 0.05$.

Figure 6. Mitochondrial Oxidative Stress Increases Muscle Mass via Hyperplasia. (A) Relative muscle weights were determined by skeletal muscle mass (mg) normalized by body weight (g) (n = 30-35). (B) Left: Representative images of fiber typing from WT (top) and m*Sod2*KO (bottom). Type 1 fibers were peuso-colored blue, type 2a fibers red, type 2b fibers green, and extracellular matrix was colored white. Right: Quantified fiber type distribution by percent of total. (C) Mean fiber cross-sectional area (CSA), (D) Total number of fibers, (E) Gross area of gastrocnemius muscle (n = 3), (F) H&E-stained cross-sectional images of gastrocnemius from WT (top) and mSod2 KO (bottom). Dark brown dots indicate nuclei. (G) Percent of fibers with central nuclei (n = 5). (H) Immuno-fluorescent images showing expression of eMHC by barium chrolide injection (Right), but not in WT and m*Sod2*KO gastrocnemius (Left, Middle). (I) A histogram demonstrating fiber sizes from WT and m*Sod2*KO gastrocnemius (~80-100 fibers / mouse) were used for size measurements (n = 5). Values are mean ±SEM. *$p < 0.05$.

Figure 7. Fiber Branching as a Mechanism for an Increase in Muscle Mass in m*Sod2*KO. (A) Representative images of gastrocnemius single fibers that are unbranched (left) and branched (right). (B) Quantifications by percent of branched fibers from WT and m*Sod2* KO mice. (C) Protein contents of calpain-1 determined by immunoblot (n = 4-7). (D) Calpain-cleaved products of αII-spectrin at ~145 kDa (n = 6-7).

REFERENCES

1. Muller FL, Song W, Liu Y, Chaudhuri A, Pieke-Dahl S, Strong R *et al.* Absence of CuZn superoxide dismutase leads to elevated oxidative stress and acceleration of age-dependent skeletal muscle atrophy. *Free Radic Biol Med* 2006;**40**:1993–2004.

2. Jang YC, Lustgarten MS, Liu Y, Muller FL, Bhattacharya A, Liang H *et al.* Increased superoxide in vivo accelerates age-associated muscle atrophy through mitochondrial dysfunction and neuromuscular junction degeneration. *FASEB J* 2010;**24**:1376–1390.

3. Boengler K, Kosiol M, Mayr M, Schulz R, Rohrbach S. Mitochondria and ageing: role in heart, skeletal muscle and adipose tissue. *J Cachexia Sarcopenia Muscle* 2017;**8**:349–369.

4. Muller FL, Song W, Jang YC, Liu Y, Sabia M, Richardson A *et al.* Denervation-induced skeletal muscle atrophy is associated with increased mitochondrial ROS production. *Am J Physiol Regul Integr Comp Physiol* 2007;**293**:R1159-1168.

5. Csukly K, Ascah A, Matas J, Gardiner PF, Fontaine E, Burelle Y. Muscle denervation promotes opening of the permeability transition pore and increases the expression of cyclophilin D. *J Physiol (Lond)* 2006;**574**:319–327.

6. Brown JL, Rosa-Caldwell ME, Lee DE, Blackwell TA, Brown LA, Perry RA *et al.* Mitochondrial degeneration precedes the development of muscle atrophy in progression of cancer cachexia in tumour-bearing mice. *J Cachexia Sarcopenia Muscle* 2017;**8**:926–938.

7. Plant DR, Gregorevic P, Williams DA, Lynch GS. Redox modulation of maximum force production of fast-and slow-twitch skeletal muscles of rats and mice. *J Appl Physiol* 2001;**90**:832–838.

8. McClung JM, Judge AR, Talbert EE, Powers SK. Calpain-1 is required for hydrogen peroxide-induced myotube atrophy. *Am J Physiol, Cell Physiol* 2009;**296**:C363-371.

9. Larkin LM, Davis CS, Sims-Robinson C, Kostrominova TY, Van Remmen H, Richardson A *et al.* Skeletal muscle weakness due to deficiency of CuZn-superoxide dismutase is associated with loss of functional innervation. *Am J Physiol Regul Integr Comp Physiol* 2011;**301**:R1400-1407.

10. Shi Y, Ivannikov MV, Walsh ME, Liu Y, Zhang Y, Jaramillo CA *et al.* The lack of CuZnSOD leads to impaired neurotransmitter release, neuromuscular junction destabilization and reduced muscle strength in mice. *PLoS ONE* 2014;**9**:e100834.

11. Jang YC, Liu Y, Hayworth CR, Bhattacharya A, Lustgarten MS, Muller FL *et al.* Dietary restriction attenuates age-associated muscle atrophy by lowering oxidative stress in mice even in complete absence of CuZnSOD. *Aging Cell* 2012;**11**:770–782.

12. Sakellariou GK, Davis CS, Shi Y, Ivannikov MV, Zhang Y, Vasilaki A *et al.* Neuron-specific expression of CuZnSOD prevents the loss of muscle mass and function that occurs in homozygous CuZnSOD-knockout mice. *FASEB J* 2014;**28**:1666–1681.

13. Zhang Y, Davis C, Sakellariou GK, Shi Y, Kayani AC, Pulliam D *et al.* CuZnSOD gene deletion targeted to skeletal muscle leads to loss of contractile force but does not cause muscle atrophy in adult mice. *FASEB J* 2013;**27**:3536–3548.

14. Vasilaki A, Richardson A, Van Remmen H, Brooks SV, Larkin L, McArdle A *et al.* Role of nerve-muscle interactions and reactive oxygen species in regulation of muscle proteostasis with ageing. *J Physiol (Lond)* 2017;**595**:6409–6415.

15. Lebovitz RM, Zhang H, Vogel H, Cartwright J, Dionne L, Lu N *et al.* Neurodegeneration, myocardial injury, and perinatal death in mitochondrial superoxide dismutase-deficient mice. *Proc Natl Acad Sci USA* 1996;**93**:9782–9787.

16. Li Y, Huang TT, Carlson EJ, Melov S, Ursell PC, Olson JL *et al.* Dilated cardiomyopathy and neonatal lethality in mutant mice lacking manganese superoxide dismutase. *Nat Genet* 1995;**11**:376–381.

17. Van Remmen H, Ikeno Y, Hamilton M, Pahlavani M, Wolf N, Thorpe SR *et al.* Life-long reduction in MnSOD activity results in increased DNA damage and higher incidence of cancer but does not accelerate aging. *Physiol Genomics* 2003;**16**:29–37.

18. Mansouri A, Muller FL, Liu Y, Ng R, Faulkner J, Hamilton M *et al.* Alterations in mitochondrial function, hydrogen peroxide release and oxidative damage in mouse hind-limb skeletal muscle during aging. *Mech Ageing Dev* 2006;**127**:298–306.

19. Lustgarten MS, Jang YC, Liu Y, Muller FL, Qi W, Steinhelper M *et al.* Conditional knockout of Mn-SOD targeted to type IIB skeletal muscle fibers increases oxidative stress and is sufficient to alter aerobic exercise capacity. *Am J Physiol, Cell Physiol* 2009;**297**:C1520-1532.

20. Lustgarten MS, Jang YC, Liu Y, Qi W, Qin Y, Dahia PL *et al.* MnSOD deficiency results in elevated oxidative stress and decreased mitochondrial function but does not lead to muscle atrophy during aging. *Aging Cell* 2011;**10**:493–505.

21. Kuwahara H, Horie T, Ishikawa S, Tsuda C, Kawakami S, Noda Y *et al.* Oxidative stress in skeletal muscle causes severe disturbance of exercise activity without muscle atrophy. *Free Radic Biol Med* 2010;**48**:1252–1262.

22. Ikegami T, Suzuki Y, Shimizu T, Isono K, Koseki H, Shirasawa T. Model mice for tissue-specific deletion of the manganese superoxide dismutase (MnSOD) gene. *Biochem Biophys Res Commun* 2002;**296**:729–736.

23. Muller FL, Liu Y, Abdul-Ghani MA, Lustgarten MS, Bhattacharya A, Jang YC *et al.* High rates of superoxide production in skeletal-muscle mitochondria respiring on both complex I- and complex II-linked substrates. *Biochem J* 2008;**409**:491–499.

24. Picard M, Csukly K, Robillard M-E, Godin R, Ascah A, Bourcier-Lucas C *et al.* Resistance to Ca2+-induced opening of the permeability transition pore differs in mitochondria from glycolytic and oxidative muscles. *Am J Physiol Regul Integr Comp Physiol* 2008;**295**:R659-668.

25. Kuznetsov AV, Veksler V, Gellerich FN, Saks V, Margreiter R, Kunz WS. Analysis of mitochondrial function in situ in permeabilized muscle fibers, tissues and cells. *Nat Protoc* 2008;**3**:965–976.

26. Krumschnabel G, Fontana-Ayoub M, Sumbalova Z, Heidler J, Gauper K, Fasching M *et al.* Simultaneous high-resolution measurement of mitochondrial respiration and hydrogen peroxide production. *Methods Mol Biol* 2015;**1264**:245–261.

27. Matsuzaki S, Kotake Y, Humphries KM. Identification of mitochondrial electron transport chain-mediated NADH radical formation by EPR spin-trapping techniques. *Biochemistry* 2011;**50**:10792–10803.

28. Roberts LJ, Morrow JD. Measurement of F(2)-isoprostanes as an index of oxidative stress in vivo. *Free Radic Biol Med* 2000;**28**:505–513.

29. McLain AL, Cormier PJ, Kinter M, Szweda LI. Glutathionylation of α-ketoglutarate dehydrogenase: the chemical nature and relative susceptibility of the cofactor lipoic acid to modification. *Free Radic Biol Med* 2013;**61**:161–169.

30. Avner BS, Hinken AC, Yuan C, Solaro RJ. H2O2 alters rat cardiac sarcomere function and protein phosphorylation through redox signaling. *Am J Physiol Heart Circ Physiol* 2010;**299**:H723-730.

31. Chaudhuri AR, de Waal EM, Pierce A, Van Remmen H, Ward WF, Richardson A. Detection of protein carbonyls in aging liver tissue: A fluorescence-based proteomic approach. *Mech Ageing Dev* 2006;**127**:849–861.

32. Lane RS, Fu Y, Matsuzaki S, Kinter M, Humphries KM, Griffin TM. Mitochondrial respiration and redox coupling in articular chondrocytes. *Arthritis Res Ther* 2015;**17**:54.

33. Claflin DR, Brooks SV. Direct observation of failing fibers in muscles of dystrophic mice provides mechanistic insight into muscular dystrophy. *Am J Physiol, Cell Physiol* 2008;**294**:C651-658.

34. Qaisar R, Bhaskaran S, Premkumar P, Ranjit R, Natarajan KS, Ahn B *et al.* Oxidative stress-induced dysregulation of excitation-contraction coupling contributes to muscle weakness: Oxidative stress causes muscle defect via calcium imbalance. *Journal of Cachexia, Sarcopenia and Muscle* 2018 doi:10.1002/jcsm.12339.

35. Fu MH, Tupling AR. Protective effects of Hsp70 on the structure and function of SERCA2a expressed in HEK-293 cells during heat stress. *Am J Physiol Heart Circ Physiol* 2009;**296**:H1175-1183.

36. Falk DJ, Todd AG, Lee S, Soustek MS, ElMallah MK, Fuller DD *et al.* Peripheral nerve and neuromuscular junction pathology in Pompe disease. *Hum Mol Genet* 2015;**24**:625–636.

37. Faber RM, Hall JK, Chamberlain JS, Banks GB. Myofiber branching rather than myofiber hyperplasia contributes to muscle hypertrophy in mdx mice. *Skelet Muscle* 2014;**4**:10.

38. Roberts BM, Ahn B, Smuder AJ, Al-Rajhi M, Gill LC, Beharry AW *et al.* Diaphragm and ventilatory dysfunction during cancer cachexia. *FASEB J* 2013;**27**:2600–2610.

39. Ahn B, Pharaoh G, Premkumar P, Huseman K, Ranjit R, Kinter M *et al.* Nrf2 deficiency exacerbates age-related contractile dysfunction and loss of skeletal muscle mass. *Redox Biol* 2018;**17**:47–58.

40. Masser DR, Clark NW, Van Remmen H, Freeman WM. Loss of the antioxidant enzyme CuZnSOD (Sod1) mimics an age-related increase in absolute mitochondrial DNA copy number in the skeletal muscle. *Age (Dordr)* 2016;**38**:323–333.

41. Masser DR, Otalora L, Clark NW, Kinter MT, Elliott MH, Freeman WM. Functional changes in the neural retina occur in the absence of mitochondrial dysfunction in a rodent model of diabetic retinopathy. *J Neurochem* 2017;**143**:595–608.

42. Kuwahara H, Horie T, Ishikawa S, Tsuda C, Kawakami S, Noda Y *et al.* Oxidative stress in skeletal muscle causes severe disturbance of exercise activity without muscle atrophy. *Free Radic Biol Med* 2010;**48**:1252–1262.

43. Williams MD, Van Remmen H, Conrad CC, Huang TT, Epstein CJ, Richardson A. Increased oxidative damage is correlated to altered mitochondrial function in heterozygous manganese superoxide dismutase knockout mice. *J Biol Chem* 1998;**273**:28510–28515.

44. Picard M, Ritchie D, Wright KJ, Romestaing C, Thomas MM, Rowan SL *et al.* Mitochondrial functional impairment with aging is exaggerated in isolated mitochondria compared to permeabilized myofibers. *Aging Cell* 2010;**9**:1032–1046.

45. Webster RP, Roberts VHJ, Myatt L. Protein nitration in placenta - functional significance. *Placenta* 2008;**29**:985–994.

46. Sakellariou GK, Lightfoot AP, Earl KE, Stofanko M, McDonagh B. Redox homeostasis and age-related deficits in neuromuscular integrity and function. *J Cachexia Sarcopenia Muscle* 2017;**8**:881–906.

47. McLain AL, Szweda PA, Szweda LI. α-Ketoglutarate dehydrogenase: a mitochondrial redox sensor. *Free Radic Res* 2011;**45**:29–36.

48. Gordon AM, Homsher E, Regnier M. Regulation of contraction in striated muscle. *Physiol Rev* 2000;**80**:853–924.

49. Morrow RM, Picard M, Derbeneva O, Leipzig J, McManus MJ, Gouspillou G *et al.* Mitochondrial energy deficiency leads to hyperproliferation of skeletal muscle mitochondria and enhanced insulin sensitivity. *Proc Natl Acad Sci USA* 2017;**114**:2705–2710.

50. Lin J, Wu H, Tarr PT, Zhang C-Y, Wu Z, Boss O *et al.* Transcriptional co-activator PGC-1α drives the formation of slow-twitch muscle fibres. *Nature* 2002;**418**:797–801.

51. Weiss ES, Wang KKW, Allen JG, Blue ME, Nwakanma LU, Liu MC *et al.* Alpha II-spectrin breakdown products serve as novel markers of brain injury severity in a canine model of hypothermic circulatory arrest. *Ann Thorac Surg* 2009;**88**:543–550.

52. Haller RG, Henriksson KG, Jorfeldt L, Hultman E, Wibom R, Sahlin K *et al.* Deficiency of skeletal muscle succinate dehydrogenase and aconitase. Pathophysiology of exercise in a novel human muscle oxidative defect. *J Clin Invest* 1991;**88**:1197–1206.

53. Larsson LE, Linderholm H, Mueller R, Ringqvist T, Soernaes R. HEREDITARY METABOLIC MYOPATHY WITH PAROXYSMAL MYOGLOBINURIA DUE TO ABNORMAL GLYCOLYSIS. *J Neurol Neurosurg Psychiatry* 1964;**27**:361–380.

54. Quirós PM, Langer T, López-Otín C. New roles for mitochondrial proteases in health, ageing and disease. *Nat Rev Mol Cell Biol* 2015;**16**:345–359.

55. Nojiri H, Shimizu T, Funakoshi M, Yamaguchi O, Zhou H, Kawakami S *et al.* Oxidative stress causes heart failure with impaired mitochondrial respiration. *J Biol Chem* 2006;**281**:33789–33801.

56. Tsuda M, Fukushima A, Matsumoto J, Takada S, Kakutani N, Nambu H *et al.* Protein acetylation in skeletal muscle mitochondria is involved in impaired fatty acid oxidation and exercise intolerance in heart failure. *J Cachexia Sarcopenia Muscle* 2018 doi:10.1002/jcsm.12322.

57. Powers SK, Jackson MJ. Exercise-induced oxidative stress: cellular mechanisms and impact on muscle force production. *Physiol Rev* 2008;**88**:1243–1276.

58. Gonzalez-Freire M, Adelnia F, Moaddel R, Ferrucci L. Searching for a mitochondrial root to the decline in muscle function with ageing. *J Cachexia Sarcopenia Muscle* 2018;**9**:435–440.

59. Jang YC, Lustgarten MS, Liu Y, Muller FL, Bhattacharya A, Liang H *et al.* Increased superoxide in vivo accelerates age-associated muscle atrophy through mitochondrial dysfunction and neuromuscular junction degeneration. *FASEB J* 2010;**24**:1376–1390.

60. Giniatullin AR, Giniatullin RA. Dual action of hydrogen peroxide on synaptic transmission at the frog neuromuscular junction. *J Physiol (Lond)* 2003;**552**:283–293.

61. Kornegay JN, Childers MK, Bogan DJ, Bogan JR, Nghiem P, Wang J *et al.* The Paradox of Muscle Hypertrophy in Muscular Dystrophy. *Phys Med Rehabil Clin N Am* 2012;**23**:149–xii.

62. Webster C, Silberstein L, Hays AP, Blau HM. Fast muscle fibers are preferentially affected in Duchenne muscular dystrophy. *Cell* 1988;**52**:503–513.

63. Karpati G, Carpenter S, Prescott S. Small-caliber skeletal muscle fibers do not suffer necrosis in mdx mouse dystrophy. *Muscle Nerve* 1988;**11**:795–803.

64. Mackey AL, Kjaer M. The breaking and making of healthy adult human skeletal muscle in vivo. *Skelet Muscle* 2017;**7**:24.

65. Blaivas M, Carlson BM. Muscle fiber branching--difference between grafts in old and young rats. *Mech Ageing Dev* 1991;**60**:43–53.

66. Lovering RM, Michaelson L, Ward CW. Malformed mdx myofibers have normal cytoskeletal architecture yet altered EC coupling and stress-induced Ca2+ signaling. *Am J Physiol, Cell Physiol* 2009;**297**:C571-580.

67. Lynch GS, Hinkle RT, Chamberlain JS, Brooks SV, Faulkner JA. Force and power output of fast and slow skeletal muscles from mdx mice 6-28 months old. *J Physiol (Lond)* 2001;**535**:591–600.

68. von Haehling S, Morley JE, Coats AJS, Anker SD. Ethical guidelines for publishing in the journal of cachexia, sarcopenia and muscle: update 2017. *J Cachexia Sarcopenia Muscle* 2017;**8**:1081–1083.

Mitochondrial oxidative stress impairs contractile function but paradoxically increases muscle mass via fiber branching

Bumsoo Ahn[1], Rojina Ranjit[1], Pavithra Premkumar[1], Gavin Pharaoh[1,2], Katarzyna M. Piekarz[1,3], Satoshi Matsuzaki[1], Dennis R. Claflin[7], Kaitlyn Riddle[1], Jennifer Judge[6], Shylesh Bhaskaran[1], Kavithalakshmi Satara Natarajan[1], Erika Barboza[1], Benjamin Wronowski[2], Michael Kinter[1], Kenneth M. Humphries[1,2,5], Timothy M. Griffin[1,2,3,4,5], Willard M. Freeman[2,5], Arlan Richardson[2,4,5], Susan V. Brooks[6], Holly Van Remmen[1,2,4,5]

[1] Aging and Metabolism Research Program, Oklahoma Medical Research Foundation, Oklahoma City, OK 73104, USA
[2] Department of Physiology, University of Oklahoma Health Sciences Center, Oklahoma City, OK, USA
[3] Oklahoma Center for Neuroscience, University of Oklahoma Health Sciences Center, Oklahoma City, OK, USA
[4] Oklahoma City VA Medical Center, Oklahoma City, OK 73104, USA.
[5] Reynolds Oklahoma Center on Aging, University of Oklahoma Health Sciences Center, Oklahoma City, OK, USA
[6] Department of Molecular and Integrative Physiology, University of Michigan, Ann Arbor, Michigan
[7] Department of Surgery, Section of Plastic Surgery, University of Michigan, Ann Arbor, Michigan

Corresponding author:
Holly Van Remmen, Ph. D.
Aging and Metabolism Research Program
Oklahoma Medical Research Foundation
825 NE 13th Street
Oklahoma City, OK 73104
Phone: 405-271-2520
Fax: 405-271-3470
Email:Holly-VanRemmen@omrf.org

ABSTRACT

Background Excess reactive oxygen species (ROS) and muscle weakness occur in parallel in multiple pathological conditions. However, the causative role of skeletal muscle mitochondrial ROS (mtROS) on neuromuscular junction (NMJ) morphology and function and muscle weakness has not been directly investigated.

Methods We generated mice lacking skeletal muscle-specific MnSOD (m*Sod2*KO) to increase mtROS using a cre-Lox approach driven by human skeletal actin. We determined primary functional parameters of skeletal muscle mitochondrial function (respiration, ROS and calcium retention capacity) using permeabilized muscle fibers and isolated muscle mitochondria. We assessed contractile properties of isolated skeletal muscle using *in situ* and *in vitro* preparations, and whole lumbrical muscles to elucidate the mechanisms of contractile dysfunction.

Results The m*Sod2*KO mice, contrary to our prediction, exhibit a 10-15% increase in muscle mass associated with an ~50% increase in central nuclei and ~35% increase in branched fibers ($p < 0.05$). Despite the increase in muscle mass of gastrocnemius and quadriceps, *in situ* sciatic nerve-stimulated isometric maximum specific force (N/cm^2), force per cross-sectional area, is impaired by ~60% and associated with increased NMJ fragmentation and size by ~40% ($p < 0.05$). Intrinsic alterations of components of the contractile machinery show elevated markers of oxidative stress, e.g., lipid peroxidation is increased by ~100%, oxidized glutathione is elevated by ~50%, and oxidative modifications of myofibrillar proteins are increased by ~30% ($p < 0.05$). We also find an approximate 20% decrease in the intracellular calcium transient that is associated with specific force deficit. Excess superoxide generation from the mitochondrial complexes causes a deficiency of succinate dehydrogenase and reduced complex-II mediated respiration and ATP generation rates leading to severe exercise intolerance (~10 mins vs ~2 hrs in WT, $p < 0.05$).

Conclusions Increased skeletal muscle mtROS is sufficient to elicit NMJ disruption and contractile abnormalities, but not muscle atrophy, suggesting new roles for mitochondrial oxidative stress in maintenance of muscle mass through increased fiber branching.

Keywords Skeletal muscle, mitochondria, MnSOD, reactive oxygen species, fiber branching, hyperplasia

Introduction

Oxidative stress, the imbalance between pro-oxidant generation and antioxidant defense, has been implicated in pathological conditions of skeletal muscle, including sarcopenia[1–3], denervation[4,5], and cancer cachexia[6]. Excess levels of reactive oxygen species (ROS) impair contractile function of skeletal muscle[7] and activate proteases that are associated with degradation of contractile machinery[2,8]. A primary source of oxidative stress is superoxide anions generated from a number of cellular sources, including the mitochondrial electron transport chain (ETC) and NADPH oxidase. Superoxide can be converted to other radical and non-radical species including hydroxyl radicals, peroxynitate, and hydrogen peroxide. Because superoxide and its derivatives can generate oxidative damage to cellular lipids, proteins, and DNA, controlling superoxide levels is a first and primary line of defense against oxidative stress and damage. Superoxide is primarily scavenged by copper zinc-superoxide dismutase (CuZnSOD) in the cytosol, and manganese-superoxide dismutase (MnSOD) in the mitochondrial matrix.

Our laboratory and others have provided insights into potential mechanisms of skeletal muscle weakness associated with oxidative stress during aging (i.e. sarcopenia) using mice lacking CuZnSOD (*Sod1*KO), the cytoplasmic superoxide scavenger[1,9,10]. *Sod1*KO mice reveal a number of phenotypes that mimic features of sarcopenia in old wildtype mice, including loss of innervation, mitochondrial dysfunction, and increased generation of mitochondrial ROS (mtROS)[2,11–13]. We have also shown that loss of innervation is associated with increased mtROS and downstream activation of muscle atrophy and weakness[4,11,14]. In this study, we asked whether increased skeletal muscle mtROS induced by skeletal muscle-specific deletion of the mitochondrial form of SOD (MnSOD), independent of loss of innervation, is sufficient to induce muscle atrophy and weakness.

Previous studies have shown that global deletion of the *Sod2* gene ($Sod2^{-/-}$) leads to neonatal lethality supporting the importance of controlling superoxide levels[15,16]. We demonstrated that heterozygous deletion of MnSOD ($Sod2^{+/-}$) does not affect survival but leads to mitochondrial dysfunction[17]. Muscle mass is not altered in heterozygous MnSOD knockout mice; however, skeletal muscle mitochondrial ATP production is reduced and hydrogen peroxide generation is significantly increased in skeletal muscle[18]. Using a model of *Sod2* deficiency targeted specifically to fast twitch (type IIB) skeletal muscle fibers, we reported an increase in ROS generation and oxidative modifications in fast twitch fibers that was not associated with skeletal muscle atrophy or contractile dysfunction in young and old mice[19,20]. The impact of skeletal muscle specific *Sod2* deletion on exercise intolerance has also been reported[21], but its role on NMJ disruption and skeletal muscle mass and contractile properties have not been directly tested.

Here we tested whether mitochondrial oxidative stress within skeletal muscle, in the absence of neuronal oxidative stress and denervation, contributes to muscle atrophy and weakness using a mouse model in which MnSOD (*Sod2)* is deleted specifically in skeletal muscle using a cre-Lox approach driven by human skeletal actin. Contrary to our expectation, m*Sod2*KO mice exhibit a significant increase in muscle mass associated with dramatic increases in central nuclei, hyperplasia and fiber branching. Despite the increase in muscle mass, contractile function is impaired due to NMJ fragmentation and intrinsic alterations within myofibers, presumably elicited by excess hydrogen peroxide in cytoplasm. Excess superoxide in mitochondrial matrix induces a dramatic loss of succinate dehydrogenase (SDH) and severe functional defects of the mitochondria. Our findings demonstrate, for the first time, that mtROS from skeletal muscle is sufficient to induce NMJ disruption and contractile dysfunction. We also report our novel findings that elevated skeletal muscle mtROS leads to increases in muscle mass through hyperplasia and fiber branching.

Methods

Detailed methods are available in **Supporting Information** section at the end of the article.

Generation of Muscle-specific Sod2 Knockout (m*Sod2* KO) Mice

Tissue-specific *Sod2* KO ($Sod2^{fl/fl}$) mice were described previously and provided to Dr. Van Remmen by Dr. Takahiko Shimizu[19,22]. Briefly, $Sod2^{f/fl}$ mice were generated using mouse *Sod2* genomic DNA, in which the neomycin resistance gene and exon 3 were flanked by two loxP sites. $Sod2^{f/fl}$ mice were then bred to mice containing cre recombinase (Cre) driven by human skeletal actin (HSA) promotor (HSA Cre). PCR was used to identify mice carrying the Cre and Flox constructs by previously described primer sequences and methods[19].

Animals

Approximately 6-8 month old female and male m*Sod2*KO and wildtype (WT) mice were used for all experiments with an exception of mice used for calcium kinetics assays (these mice were 9-13 months). $Sod2^{fl/fl}$ mice were considered WT in the absence of HSA Cre and m*Sod2*KO in the presence of $Sod2^{fl/fl}$. All mice were housed under pathogen-free barrier conditions where water and foods were provided ad libitum. The Institutional Animal Care and Use Committee at Oklahoma Medical Research Foundation (Oklahoma City, OK, USA) approved all procedures.

Enzyme Activity

Activities of CuZnSOD and MnSOD were determined using native gels with negative staining as a method previously described[13]. For histological assessment of SDH activity in muscle sections, mid-belly of gastrocnemius was cut in cross-section and stained with a buffer containing, 50 mM sodium phosphate (pH7.4), 84 mM succinic acid, 0.2 mM phenazine methasulfate, 2 mg/ml nitroblue tetrazolium and 4.5 mM EDTA. For succinate dehydrogenase (SDH) activity in isolated mitochondria (see below for mitochondrial isolation), we diluted 0.25 mg/mL of mitochondria in a buffer containing 210 mM mannitol, 70 mM sucrose, 5.0 MM KH_2PO_4 and 10 mM MOPS, pH 7.4.

Isolation of Skeletal Muscle Mitochondria

Mitochondria were isolated from gastrocnemius muscle following a previously established method [18].

Rate of hydrogen peroxide generation, ATP production and calcium retention capacity

The rate of mitochondrial H_2O_2 production was measured using Amplex Red (77.8 µM), horseradish peroxidase (HRP, 1 U/ml) and SOD (37.5 U/ml) based on a previously described method with minor modifications[13]. Mitochondrial complex I was activated by glutamate (5 mM) and malate (5 mM), while complex II-specific activation was achieved by succinate (10 mM) and rotenone (1 µM). Antimycin A (1 µM) was added to determine maximum rate of H_2O_2 generation. Fluorescence was measured at an excitation wavelength of 545 nm and emission wavelength of 590 nm. The slope of increase in fluorescence was converted to the rate of H_2O_2 generation using a standard curve. The rate of ATP synthesis was measured using the luciferin/luciferase assay following a previously described method[23]. Mitochondrial calcium retention capacity (CRC) was determined using the membrane impermeable dye, Calcium Green-5N, based on a previously described method with modifications[24].

Fiber Permeabilization

Preparation for skeletal muscle fiber permeabilization was previously described[25]. Briefly, a small piece (~3-5 mg) of red gastrocnemius muscle was carefully dissected, and we separated fibers along their striations using fine forceps in ice-cold *buffer X* containing (in mM) 7.23 K_2EGTA, 2.77 CaK_2EGTA, 20 imidazole, 0.5 DTT, 20 taurine, 5.7 ATP, 14.3 PCr, 6.56 $MgCl_2$-$6H_2O$, 50 K-MES (pH 7.1). The muscle bundle was permeabilized in saponin solution (30 µg/mL) for 30 minutes, followed by 3 x 5 minute washes in ice-cold wash buffer containing (in mM) 105 K-MES, 30 KCl, 10 K_2HPO_4, 5 $MgCl_2$-$6H_2O$, 0.5 mg/ml BSA, 0.1 EGTA (pH 7.1).

Measurement of Respiration and Hydrogen Peroxide Production
Oxygen consumption rate (OCR) and the rate of mitochondrial hydrogen peroxide production were measured using the Oxygraph-2k (O2k, OROBOROS Instruments, Innsbruck, Austria) by a previously described method [26] with minor modifications. OCR was determined using an oxygen probe, while rates of hydrogen peroxide generation were determined using O2k-Fluo LED2-Module Fluorescence-Sensor Green. Data for both OCR and rates of hydrogen peroxide generation were normalized by milligrams of muscle bundle wet weights.

Measurements of mitochondrial superoxide release
Mitochondrial superoxide release was determined by using electron paramagnetic resonance (EPR) spin-trap, 5-(2,2-dimethyl-1,3-propoxycyclophosphoryl)-5-methyl-1-pyrroline *N*-oxide (CYPMPO) by a previously described method with minor modifications[27].

Markers of Oxidative Modifications
Levels of F_2-isoprostanes in gastrocnemius were determined by a previously described method [28] with minor modifications. The levels of GSH and GSSG were determined using reverse-phase HPLC and electrochemical detection[29]. GSH and GSSG were extracted from tissue homogenate by treatment with 5% metaphosphoric acid. Myofibrillar (MF) proteins were isolated based on a previously reported method[30]. Abundance of carbonyl groups in muscle homogenate and MF proteins was determined by FTC based on a previously described method[31].

Energy Charge
Ratio of energy charge in gastrocnemius muscles was determined by using a previously published method[32]. All analytes were extracted from tissue homogenate by treatment with 150 mM potassium hydroxide. Concentrations of ATP, ADP, AMP, NAD+ and NADP+ were detected by absorption at 254 nm. Concentrations of NADH and NADPH were detected by fluorescence at excitation 340 nm and emission 430 nm. All analytes were quantified on the basis of the integrated area of standards.

Contractile Properties of Skeletal Muscle
Isometric contractile properties for *in situ* and *in vitro* gastrocnemius muscles were measured based on previously established methods[9].

Assessment of Calcium Kinetics using Skeletal Muscle
Experiments to determine the dynamic calcium responses to twitch stimuli were performed on lumbrical muscles from WT and m*Sod2*KO mice (age 9-13 months). Details on the techniques and apparatus used to measure lumbrical muscle contractile properties and fluorescence have been described previously[33,34].

SERCA activity
The measurement of SERCA ATPase activity was performed at 37°C by using a spectrophotometric assay as described elsewhere[35].

NMJ staining
Neuromuscular junctions were stained following a previously established method with minor modifications[36].

Histology
Gastrocnemius muscle tissues were frozen in liquid nitrogen-cooled isopentane. 10 µm cross-sections were made using a microcryotome (-20°C), dried and used for immunohistochemistry staining.

Quantification of Myofiber Branching
Myofiber branching was determined based on a previously established method with modifications[37,38].

Quantification of Protein Abundances by Selected Reaction Monitoring
We used targeted quantitative mass spectrometry to measure protein abundance as previously described[39].

Determination of mtDNA Copy Number
Absolute copy number of mtDNA was quantified (copies per ng input DNA) by digital PCR based on a previously reported method[40,41].

Immunoblot and qPCR
Standard procedures were used for western blots and qPCR. Antibodies and primers used are detailed in Table S2.

Statistical analyses
Data were analyzed using unpaired two-tailed t tests. Levels of significance were set at $p < 0.05$ in all cases. Data are presented as mean ±SEM.

Results
Defects of Mitochondrial Respiration and Increased H_2O_2 Generation in mSod2KO Mice
To test the causality of excess mtROS on skeletal muscle weakness, we generated a muscle-specific *Sod2* knockout mouse line (m*Sod2*KO mice). We confirmed the extent and specificity of the MnSOD deletion by measuring the activity (Figures S1A) and protein abundance (Figures S1B) of MnSOD in gastrocnemius muscle and heart. Our PCR data also confirms *Sod2* deletion specifically in skeletal muscle (not in heart) of Acta cre positive *Sod2*$^{fl/fl}$ mice. Cre negative *Sod2*$^{fl/fl}$ mice show no deletion as expected (Figure S1C). CuZnSOD activity is not altered in response to the loss of MnSOD. We measured mitochondrial function using isolated skeletal muscle mitochondria. We found that mitochondrial H_2O_2 generation with complex I substrates is significantly higher in isolated skeletal muscle mitochondria from m*Sod2*KO compared to wildtype mitochondria while H_2O_2 generation is dramatically lower with complex II substrates. Antimycin A-induced H_2O_2 generation rate is significantly higher in mitochondria from the m*Sod2*KO mice (Figure 1A). The between-group differences in all conditions disappeared after catalase addition confirming that the signal is generated by H_2O_2 (data not shown). Consistent with the reduced H_2O_2 generation from complex II substrates, mitochondria from the m*Sod2*KO mice have a dramatically lower SDH activity than wildtype mitochondria (Figure S1D-F). The mRNA levels of complex II subunits A and B are not decreased in muscle from m*Sod2*KO (Figure S1G, H), suggesting that the decrease in complex II may be due to post-translational modifications and protein degradation, consistent with previous findings from our laboratory and others[19,42].

Excess mitochondrial ROS, in particular superoxide anions, have been shown to alter mitochondrial function[43]. In agreement with the observed decrease in SDH enzyme activity, complex II-induced ATP generation of m*Sod2*KO is dramatically decreased, while complex I induced ATP generation is not altered (Figure 1B). Consequently, the levels of ATP in gastrocnemius muscle are decreased by ~40 % in m*Sod2*KO compared to wildtype mice (Figure 1C). Mitochondria play an important role in cytoplasmic calcium homeostasis by absorbing calcium ions from cytoplasm[24]. To test mitochondrial calcium retention capacity (CRC), we challenged isolated mitochondria by adding 2μM calcium chloride ($CaCl_2$) per minute until the mitochondrial calcium release level overrides calcium uptake due to permeability transition pore opening. CRC in m*Sod2*KO mice is reduced by ~70% compared to WT (Figure 1D).

Preparation of isolated mitochondria can cause damage to the organelle altering mitochondrial morphology and function and induce selection bias during the centrifugation step[44]. Also, mitochondria *in vivo* have the added complexity of interactions with neighboring organelles and proteins. To address these potential limitations, we measured mitochondrial oxygen consumption (OCR) and H_2O_2 generation rates in permeabilized "red" gastrocnemius muscle fibers located in the lateral heads of the gastrocnemius. These fibers are visually more red in color than surrounding fibers. Consistent with our previous results in isolated mitochondria, we observed that complex II-induced OCR is selectively decreased in m*Sod2*KO mice (Figure 1E), and ROS generation is elevated (Figure 1H). The rates of mitochondrial H_2O_2 production are significantly elevated by ~4-5 fold at basal and during complex I and II-activated conditions in m*Sod2*KO mice. These observations are different from the findings in isolated mitochondria (Figure 1B) potentially due to presence of ADP in permeabilized fibers. Thus, we also measured ROS generation in the absence of ADP using permeabilized fibers (Figure 1I). In muscle mitochondria from wildtype mice, we observed a steep rise in H_2O_2 generation in response to succinate, suggesting superoxide generation through reverse electron transfer[23]. The rise in H_2O_2 generation is substantially lower in m*Sod2*KO in response to succinate consistent with complex II deficiency.

To test mitochondrial function *in vivo*, we measured total running time to exhaustion for the mice on a treadmill, which shows a substantial reduction in m*Sod2*KO mice-10 mins compared with ~2 hrs in WT mice (Figure 1F). Voluntary cage activity of the m*Sod2*KO mice trended to decrease ($p < 0.07$) during the active (dark) phase (Figure S2A,B). Lactate build-up caused by decreased pyruvate utilization has been suggested to be the underlying cause of the exercise intolerance in m*Sod2*KO mice[19,42]. To test pyruvate utilization of skeletal muscle fibers from wildtype and m*Sod2*KO mice, we directly added pyruvate as a substrate in the permeabilized fibers while measuring mitochondrial respiration, indicated as red arrow in Figure 1G. Pyruvate effectively shuts down oxidative phosphorylation in m*Sod2*KO mice.

The rate of ROS generation in the isolated mitochondria or permeabilized fibers was determined using Amplex Red or Amplex UltraRed probes respectively, which detect H_2O_2, but not superoxide. Due to the deficiency of MnSOD in the matrix in m*Sod2*KO mice, the superoxide within the matrix will not be detected. To directly determine mitochondrial superoxide release, we used electron paramagnetic resonance (EPR) in conjunction with superoxide–targeted spin trap. Mitochondria isolated from gastrocnemius muscle were used for the measurements. Superoxide levels derived by EPR signals in m*Sod2*KO mice are significantly elevated for complex I- and II-linked substrates and the inhibitor Antimycin A (Figure 1J). Complex I and III inhibitors, rotenone and Antimycin A, increase superoxide generation from mitochondria for wildtype and m*Sod2*KO, but a greater increase is observed in mitochondria from m*Sod2*KO than from wildtype mice. Addition of exogenous CuZnSOD in the buffer effectively abolished the superoxide-derived EPR signals for complex I- and II-linked substrates (Figure S1I). These observations are consistent with previous data from our laboratory in which we measured an increase in superoxide generation in fast-twitch muscle specific deletion of *Sod2*KO mice[19].

Markers of Oxidative Stress and Redox Potential

To test whether a reduction in MnSOD leads to an increase in oxidative modifications, we assessed lipid peroxidation, protein carbonyls, and tyrosine nitration in gastrocnemius muscle. Lipid peroxidation was determined by F_2-isoprostane levels, which are stable products formed by free radical-catalyzed peroxidation of arachidonic acids. F_2-isoprostane levels are elevated by ~80% in the m*Sod2*KO mice (Figure 2A). To measure protein oxidation of skeletal muscles, we determined the level of carbonylation of proteins using muscle homogenate and observed a trend of increase ($p<0.1$) in the m*Sod2*KO mice (Figure 2E). Because skeletal muscle is a heterogeneous tissue and myofibrillar proteins are highly sensitive to oxidative damage, we isolated myofibrillar proteins and determined the levels of carbonylation, which are significantly

elevated by ~30% in m*Sod2*KO mice (Figure 2F). Nitration of protein tyrosine residues represents another important post-translational modification caused by nitrosative and oxidative stress. The formation of 3-nitrotyrosine is the most commonly studied covalent modification of protein nitration, and elevated levels of this product are implicated in many oxidative stress-associated pathologies, including aging[45]. We observed that protein nitration is elevated by ~60% in muscle from m*Sod2*KO mice (Figure 2C).

Changes in redox status have a major impact on cellular and physiological processes and may underlie many functional deficits associated with aging and oxidative stress[3,46]. Removal of H_2O_2 is catalyzed by the antioxidant enzymes catalase, glutathione peroxidase (Gpx), and peroxiredoxins (Prx). Gpx and Prx require oxidation of GSH and thioredoxin, respectively. The ratio of reduced and oxidized GSH (i.e., GSH:GSSG) is used as an index of redox potential[47]. We found a significant increase in the content of GSSG suggesting oxidative stress, although the GSH:GSSG ratio in m*Sod2*KO mice shows only a trend ($p < 0.07$) for a decrease in the ratio (Figure 2B). Reduction of GSH is catalyzed by glutathione reductase (GR), which requires oxidation of NADPH to $NADP^+$. Similarly, reduction of oxidized thioredoxin requires oxidation of NADH to NAD^+. Perhaps surprisingly, the muscle from m*Sod2*KO mice does not show a significant change in NAD^+, NADH or the NAD^+/NADH ratio (Figure 2D). Figure S5 illustrates the role of antioxidant enzymes and their co-factors in redox homeostasis.

Skeletal Muscle Myofibrils and Mitochondrial Proliferation

To evaluate the impact of mitochondrial oxidative stress on skeletal muscle ultrastructure, we obtained transmission electron micrograph (TEM) images of tibialis anterior (TA) muscles. In m*Sod2*KO, myofibrils are shorter and smaller and not as regularly organized as in wildtype skeletal muscle (Figure S6A). Myofilaments appear to be less tightly packed, I-bands around Z disks (shown as 'Z' in Figure S6A) are indistinct in many areas, and the M-lines (shown as 'M' in Figure S6A) are frequently out of alignment and faint. Mitochondria (shown as white arrow head in Figure S6A) in m*Sod2*KO exhibit localized accumulations between myofibrils and appear to be bigger than those of wildtype. The location of mitochondria in wildtype skeletal muscle is near Z-disks, but in m*Sod2*KO mice their cellular locations are irregular. We measured the protein content of isolated mitochondria in gastrocnemius muscle, and found ~30% increase in mitochondrial protein content in muscle from m*Sod2*KO mice compared to wildtype mice (data not shown). The mitochondrial proliferation is consistent with an increased level of mRNA levels of PGC 1-α (Figure 3A).

Mitochondrial proliferation was confirmed by measuring targeted mitochondrial protein abundance using Selected Reaction Monitoring (SRM). We observed that many TCA cycle enzymes are increased in *mSod2KO* with the notable exceptions of aconitase and SDH (Figure 3C), which are known to be highly sensitive to oxidative stress. Similarly, many enzymes in the fatty acid oxidation pathway are increased (Figure S4) consistent with mitochondrial proliferation. Proteins involved in glycolysis are largely unchanged (Table S1). We determined the abundance of antioxidant enzymes, and found that many of the antioxidant enzymes are significantly elevated in m*Sod2*KO except Sod1 and a few others (Figure S5). Upregulation of TCA cycle, fatty acid oxidation and antioxidant enzymes suggests a compensatory mechanism for decreased oxidative phosphorylation and excess oxidants.

Excess oxidants are known to cause oxidative damage to DNA and to increase mtDNA copy number in skeletal muscle[40] and potentially mtDNA sequence variants. Thus, we determined the copy number of mitochondrial and nuclear DNA using gastrocnemius muscles of wildtype and m*Sod2*KO mice. We found a significant increase in mtDNA copy number (Figure 3B) with no change in the copy number of nuclear DNA (data not shown). Our analyses of heteroplasmic single nucleotide variant (SNV) frequency reveal no change in mtDNA mutational load (Figure S3A). A specific nucleotide, thymine, trends to show increased SNV frequency in m*Sod2*KO (Figure S3B), suggesting that thymine might be more subject to oxidative modifications.

Interestingly, occurrence of SNVs higher than 1% frequency is increased in m*Sod2*KO (Figure S3C). These increases in SNVs are localized in D-Loop and Rnr1/2.

Contractile Dysfunction and Calcium Mishandling in mSod2KO Skeletal Muscle

Excess ROS is known to cause contractile dysfunction in skeletal muscles[9]. To test the impact of mitochondrial ROS on skeletal muscle from wildtype and m*Sod2*KO mice, we measured *in situ* and *in vitro* contractile function of skeletal muscle. The *in vitro* contractile properties of soleus and extensor digitorum longus (EDL) muscles reveal a significant decrease in maximum isometric specific force (N/cm^2) for muscles of m*Sod2*KO compared with wild type mice (Figure S6B,C) with unchanged fatiguability (Figures S6D,E). Our *in situ* experiments using direct stimulation on the gastrocnemius similarly demonstrates a ~40% decrease in specific force for m*Sod2*KO. The force deficit is exacerbated in sciatic nerve-stimulated force generation (Figure 4A,B), suggesting disruption and abnormalities of the neuromuscular junction (NMJ). Intrinsic force deficit is highly associated with calcium mishandling, including intracellular calcium transient (ICT), sensitivity, and uptake kinetics[48]. We find a significant reduction in ICT measured in m*Sod2*KO lumbrical muscles (Figure 4C), while specific force and intracellular calcium fall time are unchanged (Figure 4D,E). The drop in peak intracellular free calcium may be affected by a decrease in calcium release, enhanced calcium buffering, or faster calcium uptake in m*Sod2*KO. Arguing against the latter, we find severe defects in mitochondrial buffering (Figure 1D) and sarcoplasmic/endoplasmic reticulum calcium ATPase (SERCA) pump (Figure 4F).

NMJ Disruption and Fragmentation of mSod2KO Skeletal Muscle

Because our contraction data suggest NMJ abnormalities may exist in the muscle from m*Sod2*KO mice, we asked whether the loss of MnSOD and increased mitochondrial ROS alters the mRNA and protein levels of the acetylcholine receptor (AchR). We found ~2-fold increase in the mRNA level for the AchRα-isoform (Figure 5A). Despite the increase in the mRNA level, the protein abundance of AchR is decreased by ~50% in m*Sod2*KO (Figure 5B), which may be due to an increase in protein degradation. To further determine morphological alterations by excess mtROS, we measured the size of NMJ and the number of fragments and found significant increases in m*Sod2*KO (Figure 5C-E), which are typical of denervation and sarcopenia phenotypes[2]. Note that scoring of the percentage of denervated NMJ reveals no effect of MnSOD deficiency (Figure 5F).

Mitochondrial Oxidative Stress Increases Muscle Mass via Hyperplasia

Contrary to our expected results, m*Sod2*KO mice do not exhibit a loss in muscle mass (Figure 6A). Indeed, in gastrocnemius and quadriceps muscles there are ~10-15% increases in muscle mass, while no changes were observed in smaller muscles. The increase in muscle mass observed in female mice is also evident in male mice (Figure S6A). We find that isolated skeletal muscles from m*Sod2*KO are more red in color than wildtype muscles (Figure S1J) as reported previously[42]. To test a potential shift in muscle fiber type, we performed immunohistochemistry using isoform specific antibodies on cross-sections and found a significant increase in Type 2x fibers in m*Sod2*KO gastrocnemius (Figure 6B). We postulate that accumulation of mitochondria is the underlying cause of red pigment of the skeletal muscle. In line with the idea, our m*Sod2*KO mice demonstrated mitochondrial proliferation (Figure 3A-C). An animal model leading to a significant mitochondrial dysfunction (ANT1KO) and compensatory proliferation exhibits redness of the muscle[49]. Another animal model with PGC1-α overexpression demonstrates increased pigment in skeletal muscle tissues[50]. Increase in muscle mass in gastrocnemius is not caused by a change in fiber size (i.e. hypertrophy), but rather by an increase in the number of fibers by ~60% (hyperplasia) (Figure 6C-E). Furthermore, ~50% of the fibers contain central nuclei in m*Sod2*KO (Figure 6F,G), suggesting generation of new fibers. Regardless of the dramatic increase in central nuclei, embryonic myosin heavy chain (eMHC) expression is not increased in m*Sod2*KO mice

(Figure 6H). Histogram analysis of fiber area in m*Sod2*KO reveals highly variable and distorted bell-shape distributions, as opposed to normally distributed wildtype gastrocnemius (Figure 6I).

Fiber Branching as a Mechanism of an Increase in Muscle Mass in mSod2KO

To directly test the mechanism responsible for hyperplasia, we teased out single fibers from gastrocnemius muscles and determined the number of fibers with or without branches (Figure 7A). We find that ~35% of the fibers contain fiber branches in muscle from the m*Sod2*KO mice, while no fibers exhibit branches in muscle from wildtype mice (Figure 7B). In addition to fiber branching, we examined changes of a calcium-mediated protein degradation pathway calpain, a muscle protease. We find protein expression of calpain-1 significantly lower in m*Sod2*KO mice (Figure 7C). To measure the activity of calpain, we determined the abundance of breakdown products from α-II spectrin at ~150 kDa[51], which is significantly decreased in m*Sod2*KO mice (Figure 7D).

Discussion

The goal of this study is to determine whether compromised function of skeletal muscle mitochondria and elevated mtROS generation are sufficient to cause muscle atrophy independent of loss of muscle innervation. Contrary to our prediction, elevated mitochondrial oxidative stress leads to increases in muscle mass and hyperplasia via fiber branching. Despite the compensatory increase in muscle mass, contractile function is impaired associated with NMJ disruption and possibly due to a calcium mishandling within myofibers. Excess superoxide in mitochondrial matrix leads to dramatic loss of SDH and severe exercise intolerance as reported in animals and patients with SDH deficiency[52,53]. Our findings demonstrate, for the first time, that mtROS from skeletal muscle is sufficient to induce NMJ disruption but not denervation. We also report our novel findings that ROS from skeletal muscle mitochondria increase muscle mass through fiber branching.

MnSOD is localized in the mitochondrial matrix where it is poised to protect the ETC subunits and other matrix proteins from oxidative insult induced by ETC generation of superoxide. In the absence of MnSOD, superoxide is unchecked and the mitochondria are susceptible to oxidative damage that can impair function. We measured a number of indicators of mitochondrial function in muscle from m*Sod2*KO mice. One of the most dramatic changes is the substantial decrease in the level of complex II (SDH) protein subunits despite upregulation of the mRNA levels. The mechanisms by which increased superoxide causes SDH-specific deficiency are unclear, but potential causes include deficiency or dysfunction of SDH import proteins, assembly factors, or activation of mitochondrial proteases, including Lon protease[54]. Previous studies have shown that loss of SDH contributes to substantial reductions in ETC activity and ATP generation rate, leading to severe exercise intolerance in animals[19,21] and in patients[52,53]. Mitochondrial respiration in response to complex II substrate is also significantly lower in mitochondria from m*Sod2*KO mice compared to wildtype mice. Complex I activity is partially reduced, but the loss of SDH is much more substantial than other complexes of ETC in agreement with previous reports in mice lacking MnSOD in skeletal and cardiac muscles[21,55]. We confirmed the impaired mitochondrial function *in vivo* using treadmill running time. The m*Sod2*KO mice are more susceptible to exhaustion during treadmill running. Although our data exhibit ETC activity only, mitochondria are also responsible for fatty acid oxidation, defects in which are likely to contribute to exercise intolerance as shown before[56]. Overall, our results confirm that mitochondrial function is significantly compromised by the loss of MnSOD.

In addition to severe defects in respiration, mitochondria from m*Sod2*KO mice have increased generation of ROS. Excess ROS are known to impair contractile function of skeletal muscle[9]. Isolated skeletal muscle incubated with varying hydrogen peroxide concentrations has demonstrated dose-dependent effects on maximum force generation[7,57]. Increased hydrogen peroxide is known to induce lipid peroxidation in the sarcolemma, which was supported by our

data (Figure 2A). Excess oxidants also induce oxidative modifications in proteins associated with the contractile machinery (i.e. thiol oxidation). To test this idea, we isolated myofibrillar proteins using previously established methods[30], and found that carbonylated proteins were significantly elevated in *mSod2*KO mice. These data support the concept that multiple factors can contribute to muscle weakness, including altered signal transmission through the neuromuscular junction and intrinsic changes to the proteins response for carrying out contractile force generation.

Alterations in the NMJ are a critical contributor to sarcopenia[46], but it is not clear whether defective mitochondrial function precede or follow changes in NMJ and skeletal muscle atrophy and contractile dysfunction[58]. Our laboratory and others previously demonstrated that denervation plays a causal role in AchR fragmentation and degeneration, leading to skeletal muscle atrophy[12]. Furthermore, recent studies support an association between skeletal muscle mtROS and NMJ disruption in multiple pathological conditions, including aging and denervation[36,56,58,59]. In this study, we were interested in determining whether the increased mtROS and mitochondrial dysfunction in the skeletal muscle of m*Sod2*KO mice compromises the NMJ in a feedback manner to potentially initiate muscle atrophy. Our results are consistent with alterations in the NMJ in gastrocnemius muscle of the m*Sod2*KO mice. For example, our *in situ* contractile function data reveal that the maximum isometric specific force of the gastrocnemius is decreased by ~40% with stimulation directly on the muscle, but force generation through sciatic nerve stimulation shows a greater reduction (~60%). This result suggests compromised signaling through the neuromuscular junction in the m*Sod2*KO mice. Consistent with these findings, the expression of the acetylcholine receptor alpha subunit (AchR-α) is decreased in gastrocnemius muscle from the m*Sod2*KO despite an upregulation of AchR-α mRNA levels[59]. Further analyses of NMJ morphology reveals that fragmentation and size of the NMJ area are increased in m*Sod2* KO. Together, these changes suggest that elevated mitochondrial ROS and oxidative stress induce morphological changes in the acetylcholine receptor, including a potentially increased degradation of AchR-α or reduced stability of the AchR complex. Notably, however, we did not find any evidence of loss of innervation in gastrocnemius muscle from the m*Sod2*KO mice. Thus, for the first time, we demonstrate a causal role of excess ROS from skeletal muscle mitochondria on NMJ disruption and muscle weakness, supporting a retrograde effect of muscle mtROS *in vivo*[60].

Contrary to our expected results, significant damage to the mitochondria and excess ROS do not cause atrophy in skeletal muscle. Rather, we find an increase in muscle mass in gastrocnemius and quadriceps. Our findings differ from an existing report, which found no change in skeletal muscle mass in m*Sod2*KO mice[21]. Our study includes data collected from 30-35 female mice/group compared with 5 mice/group in the study that did not see a difference in mass. Our findings in female mice were confirmed in male mice (Figure S7A,B). Notably, the impact of mitochondrial oxidative stress causing hypertrophy on large muscle groups (gastrocnemius and quadriceps), but not in small muscles (TA, EDL and soleus), remains unclear. Another redox-dependent pathological condition, Duchenne Muscular Dystrophy, also preferentially affects muscle groups as reported[61–63]. We predict that the preferential calf hypertrophy results from overuse while functioning to stabilize the body against gravity. A case report of a patient with familiar mitochondrial myopathy, who demonstrated deficiencies in SDH and aconitase with lifelong exercise intolerance, reported calf hypertrophy consistent with our report[52,53]. We also previously found a similar increase in muscle mass in mice with a muscle specific deletion of CuZnSOD[13]. Together these data point to a modulation of muscle mass by oxidative stress that leads to increased muscle mass, but not atrophy.

The increase in muscle mass in the m*Sod2*KO mice is associated with increased central nuclei[21] and a dramatic increase in the number of fibers appearing in a cross section. The increase in fiber number results from fiber branches rather than independently separated fibers. The cause of fiber branching is unknown, but one explanation is incomplete lateral fusion of myotubes during regeneration elicited by injury-induced necrosis[64], which is dramatically elevated in m*Sod2*KO

mice[21]. The increased fiber branching has previously been shown in EDL muscle from old compared to young rats[65]. Fiber branching is also the basis for the increase in fiber numbers in *mdx* mice, where there is also an increase in oxidative stress leading to skeletal muscle hypertrophy and decreased specific force[37] as in m*Sod2*KO skeletal muscle. Although branched fibers compensate for skeletal muscle cell death via necrosis in m*Sod2*KO mice[21], excitation-contraction coupling is disturbed in the branched myofibers[37], and calcium-activated force production has been shown to be reduced[66]. The *mdx* mice have shown an increase in muscle mass, but exhibited decreases in calcium transients in branched fibers compared with unbranched fibers[67]. The calcium transient is indeed decreased in m*Sod2*KO skeletal muscle. Considering that there is no matching increase in synapse number with fiber branching[37], branched fibers may also contribute to neuromuscular dysfunction.

Conclusions

In summary, our results demonstrate that loss of MnSOD increases superoxide in mitochondrial matrix, leading to SDH deficiency, mitochondrial defects, and severe exercise intolerance. Excess hydrogen peroxide produced from the mitochondria induces NMJ alterations through a retrograde effect on neuromuscular junction proteins, contributing to neuromuscular dysfunction-induced skeletal muscle weakness. Despite reports of neurogenic atrophy in multiple pathological conditions (i.e. aging, inactivity, chronic inflammatory diseases), skeletal muscle mass of large muscle groups, including gastrocnemius and quadriceps, is increased due to hyperplasia via fiber branching that may also contribute to NMJ dysfunction.

ACKNOWLEDGEMENTS

This work was supported by the National Institute of Health and National Institute of Aging [P01AG051442, R01-AG047879, R01-AG055395, P30AG050911, T32AG052363], National Institute of General Medical Sciences [5P30GM114731], and the United States Department of Veterans Affairs. The authors would like to thank the Targeted DNA Methylation & Mitochondrial Heteroplasmy, Integrative Redox Biology and Multiplex Protein Quantification Cores at Nathan Shock Center for sharing their expertise. The authors certify that they comply with the ethical guidelines for authorship and publishing of the *Journal of Cachexia, Sarcopenia and Muscle* [68].

ONLINE SUPPLEMENTARY MATERIAL

Additional Supporting Information may be found online in the Supporting Information section.

Supplemental Figure 1. The m*Sod2*KO mice exhibit skeletal muscle specific loss of MnSOD activity and dramatic loss of complex II activity in electron transport chain (ETC). (A) A representative image showing activities of MnSOD and CuZnSOD in skeletal and cardiac muscle homogenates. (B) Immunoblot analysis using gastrocnemius muscle homogenates shows protein abundance of MnSOD in WT, but not in m*Sod2*KO (n = 7-8/group). (C) A representative PCR results showing deletion of floxed site by human skeletal actin (HAS) cre recombinase. (D) Representative SDH activity performed on sections of gastrocnemius muscle. (E) Representative profile of spectrophotometric SDH activity using isolated mitochondria (25 µg/mL) from gastrocnemius. Activation of the SDH enzyme was achieved by 2 min incubation with succinate. (F) Quantification of the succinate consumption rate at active conditions (n = 2). (G) mRNA levels of SDH subunits (n = 7-8). (H) Protein expression of SDH subunits determined by mass spectrometry (n = 6). (I) Representative EPR spectra for measurement of mitochondrial superoxide release rate using isolated skeletal muscle mitochondria with or without superoxide dismutase. Abbreviations (concentrations): glu, glutamate (25 mM); mal, malate (2.5 mM); suc, succinate (25 mM); rot, rotenone (1 µM); SOD, superoxide dismutase (250U/mL). (J) Representative images of isolated gastrocnemius (top) and TA (bottom) muscles that demonstrate redness of the m*Sod2*KO muscle. Values are mean ±SEM. *$p < 0.05$.

Supplemental Figure S2. Spontaneous home cage activity. Mice were individually housed in cages with motion and activity detector units. (A) Hourly activity during 24 hours divided by lights on or off. (B) Average hourly activity during Light Phase and Dark Phase. n = 6. Values are mean ±SEM.

Supplemental Figure S3. Mitochondrial DNA variants. (A) Total frequency of mitochondrial DNA variants from gastrocnemius (n = 8-9). (B) Nucleotide-specific variant frequencies of mitochondrial DNA (n = 4-9). (C) A circos plot image demonstrating single nucleotide variants higher than 1% from WT (black) and m*Sod2*KO (red).

Supplemental Figure S4. Isoform and subunit expression of the enzymes involved in beta-oxidation. Gastrocnemius muscle homogenate was used to determine protein abundance (n = 6). Data are shown as pmol per 100 µg protein. Values are mean ±SEM. *$p < 0.05$. Abbreviation: Cpt, carnitine palmitoyltransferase. See Table 2 for gene id and protein names.

Supplemental Figure S5. Isoform and subunit expression of antioxidant enzymes. Gastrocnemius muscle homogenate was used for the data (n = 6). Data are shown as pmol per 100 µg protein. Values are mean ±SEM. *$p < 0.05$. Abbreviations: Sod, superoxide dismutase; Prx, peroxiredoxin; Trx, thioredoxin; TR, thioredoxin reductase; GSH, glutathione; Gpx, glutathione peroxidase; GR, glutathione reductase; Cat, catalase. See Table 2 for gene id and protein names.

Supplemental Figure S6. *In vitro* contractile properties of isolated fast (EDL) and slow (soleus) twitch muscles. (A) Transmission electron microscopic (TEM) images showing sarcomeric proteins and two subpopulations of mitochondria, subsarcollemal (SS) and intermyofibrillar (IMF) mitochondria. M; M-line, Z; Z-disk. White arrow heads, mitochondria. Isometric maximum specific force (sFo, N/cm^2), force per cross-sectional area in EDL (B) and soleus (C). Relative force (percent of initial) during fatigue protocol in EDL (C) and soleus (D). n = 6. Values are mean ±SEM. *$p < 0.05$.

Supplemental Figure S7. Muscle mass and mitochondrial ATP generation rate in 6-8 months old male mice. (A) Isolated skeletal muscle mass. Abbreviations: Gast, gastrocnemius; Sol, soleus; TA, tibialis anterior; EDL, extensor digitorum longus; Quad, quadriceps. (B) Rate of ATP generation from isolated skeletal muscle mitochondria from male mice (n = 3). Values are mean ±SEM. *$p < 0.05$. Abbreviations: GM, glutamate and malate; Suc, succinate; Rot, Rotenone.

Table S1. Enzymes in glycolysis and gluconeogenesis. Gastrocnemius muscle homogenate was used determine protein abundance (n = 6). Data are shown as pmol per 100 µg protein. Values are mean ±SEM. *$p < 0.05$. See Table 2 for gene id and protein names.

Table S2. Gene IDs and protein names in TCA cycle (A), beta-oxidation (B), antioxidant enzymes (C) and glucose metabolism (D).

Table S3. List of antibody catalog numbers and qRT-PCR primer sequences.

CONFLICT OF INTEREST

Bumsoo Ahn, Rojina Ranjit, Pavithra Premkumar, Gavin Pharaoh, Katarzyna M. Piekarz, Satoshi Matsuzaki, Dennis R. Claflin, Kaitlyn Riddle, Jennifer Judge, Shylesh Bhaskaran, Kavithalakshmi Satara Natarajan, Erika Barboza, Benjamin Wronowski, Mike Kinter, Kenneth M. Humphries, Timothy M. Griffin, Willard M. Freeman, Arlan Richardson, Susan V. Brooks, Holly Van Remmen declare that they have no conflict of interest.

FIGURE LEGENDS.

Figure 1. Defects of Mitochondrial Respiration and Increased H_2O_2 Generation in m*Sod2*KO Mice. (A) Rates of hydrogen peroxide generation determined in isolated mitochondria from gastrocnemius muscle using Amplex Red (n = 3-6). Substrates and inhibitors were added to determine ROS generation in response to substrates and inhibitors of mitochondrial ETC. (B) Rates of ATP production determined in isolated mitochondria from complex I and II (n = 4-5). (C) Contents of cellular nucleotides determined in gastrocnemius tissue homogenate (n = 7-8). (D) Left: A sample observation of calcium retention capacity (CRC) of isolated mitochondria (WT vs. m*Sod2* KO). Calcium levels were determined using membrane-impermeable calcium indicator, Calcium-Green 5N. Right: Quantified calcium retention capacity (n = 4-5). (E) Mitochondrial oxygen consumption rate (OCR) in response to sequential addition of substrates and inhibitors in permeabilized gastrocnemius fibers (n = 4-5). (F) Running time on a treadmill (n = 6). (G) Mitochondrial oxygen consumption rate (OCR) in response to sequential addition of substrates and inhibitors in permeabilized gastrocnemius fibers-testing the impact of pyruvate on mitochondrial OCR (n = 3). (H) Rate of hydrogen peroxide generation determined in response to sequential addition of substrates and inhibitors in permeabilized gastrocnemius fibers using Amplex UltraRed (n = 4-5). (I) Hydrogen peroxide generation rate assessed from permeabilized gastrocnemius fibers in the absence of ADP (n = 4). (J) Mitochondrial superoxide release measured by spin trap CYPMPO using isolated mitochondria. Data are quantification of EPR spectra (n = 5). Values are mean ±SEM. *$p < 0.05$. Abbreviations. ETC, electron transport chain; GM, glutamate and malate; Suc, succinate; Rot, Rotenone; AA, Antimycin A; Asc, Ascorbate; TMPD, N,N,N',N'-tetramethyl-p-phenylenediamine.

Figure 2. Markers of Oxidative Stress and Redox Potential. (A) Lipid peroxidation determined by F_2-isoprostane in gastrocnemius muscles. Values are ng F_2-isoprostane/g muscle tissue (n = 7-8). (B) Reduced GSH, oxidized GSH (GSSG), and the ratio (GSH: GSSG) in gastrocnemius muscles (n = 8-9). (C) Immunoblot images and quantified data showing the proteins conjugated with tyrosine nitration from WT and m*Sod2* KO (n = 7). (D) NAD^+, NADH, and the ratio (NAD^+/NADH) was determined using HPLC in gastrocnemius muscles (n = 9-10). (E) Left: Quantified data for carbonylated proteins from total gastrocnemius homogenate (n = 4-5). Right: Representative images showing carbonylated proteins (Top) and Coomassie-stained total proteins (Bottom). (F) Left: Quantified data for carbonylated proteins from isolated myofibrillar (MF) proteins (n = 4). Right: Representative images showing carbonylated MF proteins (Top) and Coomassie-stained total MF proteins (Bottom). Values are mean ±SEM. *$p < 0.05$.

Figure 3. Skeletal Muscle Myofibrils and Mitochondrial Proliferation. (A) Levels of PGC1-α mRNA in WT and m*Sod2*KO mice (n = 7-8). (B) Mitochondrial DNA (mtDNA) copy numbers per ng genomic DNA (gDNA) from gastrocnemius muscle (n = 9-10). (C) Protein expression of isoforms and subunits in Krebs cycle enzymes (n = 6). Values are mean ±SEM. *$p < 0.05$.

Figure 4. Contractile Dysfunction and Calcium Mishandling in *mSod2KO* Skeletal Muscle. (A) Isometric contractile function of gastrocnemius muscles were determined using *in situ* preparation. Maximum isometric specific force (sFo), force per cross-sectional area (n = 5-7). (B)

Force deficit induced by muscle- or nerve-stimulation (n = 5-7). (C) Intracellular calcium transient (ICT, n = 6). (D) Specific force generation (kPa) (n = 6-7), (E) ICT fall time (n = 6). Isolated lumbrical muscles are used for C-E. (F) Activity of sarcoplasmic/endoplasmic reticulum calcium ATPase (SERCA pump) in response to varying calcium concentrations from gastrocnemius (n = 6). Values are mean ±SEM. *$p < 0.05$.

Figure 5. NMJ Disruption and Fragmentation of m*Sod2*KO Skeletal Muscle. (A) Levels of acetylcholine receptors (AchR) mRNAs. mRNA levels of three AchR isoforms (α, δ, and ε) were determined by qRT-PCR using gastrocnemius muscles (n = 7-8). (B) Protein abundance of AchR-α was determined using immunoblot analysis (n = 8). (C) Representative neuromuscular junction (NMJ) immunofluorescence images from gastrocnemius muscle from WT (Left) and m*Sod2* KO (Right). Acetylcholine receptors (AchR) are stained with Alexa-488 conjugated α-bungarotoxin (n = 5). (D) Quantification of NMJ area. (E) Categorization of NMJs by the number of fragments. (F) Percent of denervated NMJ. Averages of 30-50 NMJs were used as each data point from each mouse. Values are mean ±SEM. *$p < 0.05$.

Figure 6. Mitochondrial Oxidative Stress Increases Muscle Mass via Hyperplasia. (A) Relative muscle weights were determined by skeletal muscle mass (mg) normalized by body weight (g) (n = 30-35). (B) Left: Representative images of fiber typing from WT (top) and m*Sod2*KO (bottom). Type 1 fibers were peuso-colored blue, type 2a fibers red, type 2b fibers green, and extracellular matrix was colored white. Right: Quantified fiber type distribution by percent of total. (C) Mean fiber cross-sectional area (CSA), (D) Total number of fibers, (E) Gross area of gastrocnemius muscle (n = 3), (F) H&E-stained cross-sectional images of gastrocnemius from WT (top) and mSod2 KO (bottom). Dark brown dots indicate nuclei. (G) Percent of fibers with central nuclei (n = 5). (H) Immuno-fluorescent images showing expression of eMHC by barium chrolide injection (Right), but not in WT and m*Sod2*KO gastrocnemius (Left, Middle). (I) A histogram demonstrating fiber sizes from WT and m*Sod2*KO gastrocnemius (~80-100 fibers / mouse) were used for size measurements (n = 5). Values are mean ±SEM. *$p < 0.05$.

Figure 7. Fiber Branching as a Mechanism for an Increase in Muscle Mass in m*Sod2*KO. (A) Representative images of gastrocnemius single fibers that are unbranched (left) and branched (right). (B) Quantifications by percent of branched fibers from WT and m*Sod2* KO mice. (C) Protein contents of calpain-1 determined by immunoblot (n = 4-7). (D) Calpain-cleaved products of αII-spectrin at ~145 kDa (n = 6-7).

REFERENCES

1. Muller FL, Song W, Liu Y, Chaudhuri A, Pieke-Dahl S, Strong R *et al.* Absence of CuZn superoxide dismutase leads to elevated oxidative stress and acceleration of age-dependent skeletal muscle atrophy. *Free Radic Biol Med* 2006;**40**:1993–2004.

2. Jang YC, Lustgarten MS, Liu Y, Muller FL, Bhattacharya A, Liang H *et al.* Increased superoxide in vivo accelerates age-associated muscle atrophy through mitochondrial dysfunction and neuromuscular junction degeneration. *FASEB J* 2010;**24**:1376–1390.

3. Boengler K, Kosiol M, Mayr M, Schulz R, Rohrbach S. Mitochondria and ageing: role in heart, skeletal muscle and adipose tissue. *J Cachexia Sarcopenia Muscle* 2017;**8**:349–369.

4. Muller FL, Song W, Jang YC, Liu Y, Sabia M, Richardson A *et al.* Denervation-induced skeletal muscle atrophy is associated with increased mitochondrial ROS production. *Am J Physiol Regul Integr Comp Physiol* 2007;**293**:R1159-1168.

5. Csukly K, Ascah A, Matas J, Gardiner PF, Fontaine E, Burelle Y. Muscle denervation promotes opening of the permeability transition pore and increases the expression of cyclophilin D. *J Physiol (Lond)* 2006;**574**:319–327.

6. Brown JL, Rosa-Caldwell ME, Lee DE, Blackwell TA, Brown LA, Perry RA *et al.* Mitochondrial degeneration precedes the development of muscle atrophy in progression of cancer cachexia in tumour-bearing mice. *J Cachexia Sarcopenia Muscle* 2017;**8**:926–938.

7. Plant DR, Gregorevic P, Williams DA, Lynch GS. Redox modulation of maximum force production of fast-and slow-twitch skeletal muscles of rats and mice. *J Appl Physiol* 2001;**90**:832–838.

8. McClung JM, Judge AR, Talbert EE, Powers SK. Calpain-1 is required for hydrogen peroxide-induced myotube atrophy. *Am J Physiol, Cell Physiol* 2009;**296**:C363-371.

9. Larkin LM, Davis CS, Sims-Robinson C, Kostrominova TY, Van Remmen H, Richardson A *et al.* Skeletal muscle weakness due to deficiency of CuZn-superoxide dismutase is associated with loss of functional innervation. *Am J Physiol Regul Integr Comp Physiol* 2011;**301**:R1400-1407.

10. Shi Y, Ivannikov MV, Walsh ME, Liu Y, Zhang Y, Jaramillo CA *et al.* The lack of CuZnSOD leads to impaired neurotransmitter release, neuromuscular junction destabilization and reduced muscle strength in mice. *PLoS ONE* 2014;**9**:e100834.

11. Jang YC, Liu Y, Hayworth CR, Bhattacharya A, Lustgarten MS, Muller FL *et al.* Dietary restriction attenuates age-associated muscle atrophy by lowering oxidative stress in mice even in complete absence of CuZnSOD. *Aging Cell* 2012;**11**:770–782.

12. Sakellariou GK, Davis CS, Shi Y, Ivannikov MV, Zhang Y, Vasilaki A *et al.* Neuron-specific expression of CuZnSOD prevents the loss of muscle mass and function that occurs in homozygous CuZnSOD-knockout mice. *FASEB J* 2014;**28**:1666–1681.

13. Zhang Y, Davis C, Sakellariou GK, Shi Y, Kayani AC, Pulliam D *et al.* CuZnSOD gene deletion targeted to skeletal muscle leads to loss of contractile force but does not cause muscle atrophy in adult mice. *FASEB J* 2013;**27**:3536–3548.

14. Vasilaki A, Richardson A, Van Remmen H, Brooks SV, Larkin L, McArdle A *et al.* Role of nerve-muscle interactions and reactive oxygen species in regulation of muscle proteostasis with ageing. *J Physiol (Lond)* 2017;**595**:6409–6415.

15. Lebovitz RM, Zhang H, Vogel H, Cartwright J, Dionne L, Lu N *et al.* Neurodegeneration, myocardial injury, and perinatal death in mitochondrial superoxide dismutase-deficient mice. *Proc Natl Acad Sci USA* 1996;**93**:9782–9787.

16. Li Y, Huang TT, Carlson EJ, Melov S, Ursell PC, Olson JL *et al.* Dilated cardiomyopathy and neonatal lethality in mutant mice lacking manganese superoxide dismutase. *Nat Genet* 1995;**11**:376–381.

17. Van Remmen H, Ikeno Y, Hamilton M, Pahlavani M, Wolf N, Thorpe SR *et al.* Life-long reduction in MnSOD activity results in increased DNA damage and higher incidence of cancer but does not accelerate aging. *Physiol Genomics* 2003;**16**:29–37.

18. Mansouri A, Muller FL, Liu Y, Ng R, Faulkner J, Hamilton M *et al.* Alterations in mitochondrial function, hydrogen peroxide release and oxidative damage in mouse hind-limb skeletal muscle during aging. *Mech Ageing Dev* 2006;**127**:298–306.

19. Lustgarten MS, Jang YC, Liu Y, Muller FL, Qi W, Steinhelper M *et al.* Conditional knockout of Mn-SOD targeted to type IIB skeletal muscle fibers increases oxidative stress and is sufficient to alter aerobic exercise capacity. *Am J Physiol, Cell Physiol* 2009;**297**:C1520-1532.

20. Lustgarten MS, Jang YC, Liu Y, Qi W, Qin Y, Dahia PL *et al.* MnSOD deficiency results in elevated oxidative stress and decreased mitochondrial function but does not lead to muscle atrophy during aging. *Aging Cell* 2011;**10**:493–505.

21. Kuwahara H, Horie T, Ishikawa S, Tsuda C, Kawakami S, Noda Y *et al.* Oxidative stress in skeletal muscle causes severe disturbance of exercise activity without muscle atrophy. *Free Radic Biol Med* 2010;**48**:1252–1262.

22. Ikegami T, Suzuki Y, Shimizu T, Isono K, Koseki H, Shirasawa T. Model mice for tissue-specific deletion of the manganese superoxide dismutase (MnSOD) gene. *Biochem Biophys Res Commun* 2002;**296**:729–736.

23. Muller FL, Liu Y, Abdul-Ghani MA, Lustgarten MS, Bhattacharya A, Jang YC *et al.* High rates of superoxide production in skeletal-muscle mitochondria respiring on both complex I- and complex II-linked substrates. *Biochem J* 2008;**409**:491–499.

24. Picard M, Csukly K, Robillard M-E, Godin R, Ascah A, Bourcier-Lucas C *et al.* Resistance to Ca2+-induced opening of the permeability transition pore differs in mitochondria from glycolytic and oxidative muscles. *Am J Physiol Regul Integr Comp Physiol* 2008;**295**:R659-668.

25. Kuznetsov AV, Veksler V, Gellerich FN, Saks V, Margreiter R, Kunz WS. Analysis of mitochondrial function in situ in permeabilized muscle fibers, tissues and cells. *Nat Protoc* 2008;**3**:965–976.

26. Krumschnabel G, Fontana-Ayoub M, Sumbalova Z, Heidler J, Gauper K, Fasching M *et al.* Simultaneous high-resolution measurement of mitochondrial respiration and hydrogen peroxide production. *Methods Mol Biol* 2015;**1264**:245–261.

27. Matsuzaki S, Kotake Y, Humphries KM. Identification of mitochondrial electron transport chain-mediated NADH radical formation by EPR spin-trapping techniques. *Biochemistry* 2011;**50**:10792–10803.

28. Roberts LJ, Morrow JD. Measurement of F(2)-isoprostanes as an index of oxidative stress in vivo. *Free Radic Biol Med* 2000;**28**:505–513.

29. McLain AL, Cormier PJ, Kinter M, Szweda LI. Glutathionylation of α-ketoglutarate dehydrogenase: the chemical nature and relative susceptibility of the cofactor lipoic acid to modification. *Free Radic Biol Med* 2013;**61**:161–169.

30. Avner BS, Hinken AC, Yuan C, Solaro RJ. H2O2 alters rat cardiac sarcomere function and protein phosphorylation through redox signaling. *Am J Physiol Heart Circ Physiol* 2010;**299**:H723-730.

31. Chaudhuri AR, de Waal EM, Pierce A, Van Remmen H, Ward WF, Richardson A. Detection of protein carbonyls in aging liver tissue: A fluorescence-based proteomic approach. *Mech Ageing Dev* 2006;**127**:849–861.

32. Lane RS, Fu Y, Matsuzaki S, Kinter M, Humphries KM, Griffin TM. Mitochondrial respiration and redox coupling in articular chondrocytes. *Arthritis Res Ther* 2015;**17**:54.

33. Claflin DR, Brooks SV. Direct observation of failing fibers in muscles of dystrophic mice provides mechanistic insight into muscular dystrophy. *Am J Physiol, Cell Physiol* 2008;**294**:C651-658.

34. Qaisar R, Bhaskaran S, Premkumar P, Ranjit R, Natarajan KS, Ahn B *et al.* Oxidative stress-induced dysregulation of excitation-contraction coupling contributes to muscle weakness: Oxidative stress causes muscle defect via calcium imbalance. *Journal of Cachexia, Sarcopenia and Muscle* 2018 doi:10.1002/jcsm.12339.

35. Fu MH, Tupling AR. Protective effects of Hsp70 on the structure and function of SERCA2a expressed in HEK-293 cells during heat stress. *Am J Physiol Heart Circ Physiol* 2009;**296**:H1175-1183.

36. Falk DJ, Todd AG, Lee S, Soustek MS, ElMallah MK, Fuller DD *et al.* Peripheral nerve and neuromuscular junction pathology in Pompe disease. *Hum Mol Genet* 2015;**24**:625–636.

37. Faber RM, Hall JK, Chamberlain JS, Banks GB. Myofiber branching rather than myofiber hyperplasia contributes to muscle hypertrophy in mdx mice. *Skelet Muscle* 2014;**4**:10.

38. Roberts BM, Ahn B, Smuder AJ, Al-Rajhi M, Gill LC, Beharry AW *et al.* Diaphragm and ventilatory dysfunction during cancer cachexia. *FASEB J* 2013;**27**:2600–2610.

39. Ahn B, Pharaoh G, Premkumar P, Huseman K, Ranjit R, Kinter M *et al.* Nrf2 deficiency exacerbates age-related contractile dysfunction and loss of skeletal muscle mass. *Redox Biol* 2018;**17**:47–58.

40. Masser DR, Clark NW, Van Remmen H, Freeman WM. Loss of the antioxidant enzyme CuZnSOD (Sod1) mimics an age-related increase in absolute mitochondrial DNA copy number in the skeletal muscle. *Age (Dordr)* 2016;**38**:323–333.

41. Masser DR, Otalora L, Clark NW, Kinter MT, Elliott MH, Freeman WM. Functional changes in the neural retina occur in the absence of mitochondrial dysfunction in a rodent model of diabetic retinopathy. *J Neurochem* 2017;**143**:595–608.

42. Kuwahara H, Horie T, Ishikawa S, Tsuda C, Kawakami S, Noda Y *et al.* Oxidative stress in skeletal muscle causes severe disturbance of exercise activity without muscle atrophy. *Free Radic Biol Med* 2010;**48**:1252–1262.

43. Williams MD, Van Remmen H, Conrad CC, Huang TT, Epstein CJ, Richardson A. Increased oxidative damage is correlated to altered mitochondrial function in heterozygous manganese superoxide dismutase knockout mice. *J Biol Chem* 1998;**273**:28510–28515.

44. Picard M, Ritchie D, Wright KJ, Romestaing C, Thomas MM, Rowan SL *et al.* Mitochondrial functional impairment with aging is exaggerated in isolated mitochondria compared to permeabilized myofibers. *Aging Cell* 2010;**9**:1032–1046.

45. Webster RP, Roberts VHJ, Myatt L. Protein nitration in placenta - functional significance. *Placenta* 2008;**29**:985–994.

46. Sakellariou GK, Lightfoot AP, Earl KE, Stofanko M, McDonagh B. Redox homeostasis and age-related deficits in neuromuscular integrity and function. *J Cachexia Sarcopenia Muscle* 2017;**8**:881–906.

47. McLain AL, Szweda PA, Szweda LI. α-Ketoglutarate dehydrogenase: a mitochondrial redox sensor. *Free Radic Res* 2011;**45**:29–36.

48. Gordon AM, Homsher E, Regnier M. Regulation of contraction in striated muscle. *Physiol Rev* 2000;**80**:853–924.

49. Morrow RM, Picard M, Derbeneva O, Leipzig J, McManus MJ, Gouspillou G *et al.* Mitochondrial energy deficiency leads to hyperproliferation of skeletal muscle mitochondria and enhanced insulin sensitivity. *Proc Natl Acad Sci USA* 2017;**114**:2705–2710.

50. Lin J, Wu H, Tarr PT, Zhang C-Y, Wu Z, Boss O *et al.* Transcriptional co-activator PGC-1α drives the formation of slow-twitch muscle fibres. *Nature* 2002;**418**:797–801.

51. Weiss ES, Wang KKW, Allen JG, Blue ME, Nwakanma LU, Liu MC *et al.* Alpha II-spectrin breakdown products serve as novel markers of brain injury severity in a canine model of hypothermic circulatory arrest. *Ann Thorac Surg* 2009;**88**:543–550.

52. Haller RG, Henriksson KG, Jorfeldt L, Hultman E, Wibom R, Sahlin K *et al.* Deficiency of skeletal muscle succinate dehydrogenase and aconitase. Pathophysiology of exercise in a novel human muscle oxidative defect. *J Clin Invest* 1991;**88**:1197–1206.

53. Larsson LE, Linderholm H, Mueller R, Ringqvist T, Soernaes R. HEREDITARY METABOLIC MYOPATHY WITH PAROXYSMAL MYOGLOBINURIA DUE TO ABNORMAL GLYCOLYSIS. *J Neurol Neurosurg Psychiatry* 1964;**27**:361–380.

54. Quirós PM, Langer T, López-Otín C. New roles for mitochondrial proteases in health, ageing and disease. *Nat Rev Mol Cell Biol* 2015;**16**:345–359.

55. Nojiri H, Shimizu T, Funakoshi M, Yamaguchi O, Zhou H, Kawakami S *et al.* Oxidative stress causes heart failure with impaired mitochondrial respiration. *J Biol Chem* 2006;**281**:33789–33801.

56. Tsuda M, Fukushima A, Matsumoto J, Takada S, Kakutani N, Nambu H *et al.* Protein acetylation in skeletal muscle mitochondria is involved in impaired fatty acid oxidation and exercise intolerance in heart failure. *J Cachexia Sarcopenia Muscle* 2018 doi:10.1002/jcsm.12322.

57. Powers SK, Jackson MJ. Exercise-induced oxidative stress: cellular mechanisms and impact on muscle force production. *Physiol Rev* 2008;**88**:1243–1276.

58. Gonzalez-Freire M, Adelnia F, Moaddel R, Ferrucci L. Searching for a mitochondrial root to the decline in muscle function with ageing. *J Cachexia Sarcopenia Muscle* 2018;**9**:435–440.

59. Jang YC, Lustgarten MS, Liu Y, Muller FL, Bhattacharya A, Liang H *et al.* Increased superoxide in vivo accelerates age-associated muscle atrophy through mitochondrial dysfunction and neuromuscular junction degeneration. *FASEB J* 2010;**24**:1376–1390.

60. Giniatullin AR, Giniatullin RA. Dual action of hydrogen peroxide on synaptic transmission at the frog neuromuscular junction. *J Physiol (Lond)* 2003;**552**:283–293.

61. Kornegay JN, Childers MK, Bogan DJ, Bogan JR, Nghiem P, Wang J *et al.* The Paradox of Muscle Hypertrophy in Muscular Dystrophy. *Phys Med Rehabil Clin N Am* 2012;**23**:149–xii.

62. Webster C, Silberstein L, Hays AP, Blau HM. Fast muscle fibers are preferentially affected in Duchenne muscular dystrophy. *Cell* 1988;**52**:503–513.

63. Karpati G, Carpenter S, Prescott S. Small-caliber skeletal muscle fibers do not suffer necrosis in mdx mouse dystrophy. *Muscle Nerve* 1988;**11**:795–803.

64. Mackey AL, Kjaer M. The breaking and making of healthy adult human skeletal muscle in vivo. *Skelet Muscle* 2017;**7**:24.

65. Blaivas M, Carlson BM. Muscle fiber branching--difference between grafts in old and young rats. *Mech Ageing Dev* 1991;**60**:43–53.

66. Lovering RM, Michaelson L, Ward CW. Malformed mdx myofibers have normal cytoskeletal architecture yet altered EC coupling and stress-induced Ca2+ signaling. *Am J Physiol, Cell Physiol* 2009;**297**:C571-580.

67. Lynch GS, Hinkle RT, Chamberlain JS, Brooks SV, Faulkner JA. Force and power output of fast and slow skeletal muscles from mdx mice 6-28 months old. *J Physiol (Lond)* 2001;**535**:591–600.

68. von Haehling S, Morley JE, Coats AJS, Anker SD. Ethical guidelines for publishing in the journal of cachexia, sarcopenia and muscle: update 2017. *J Cachexia Sarcopenia Muscle* 2017;**8**:1081–1083.

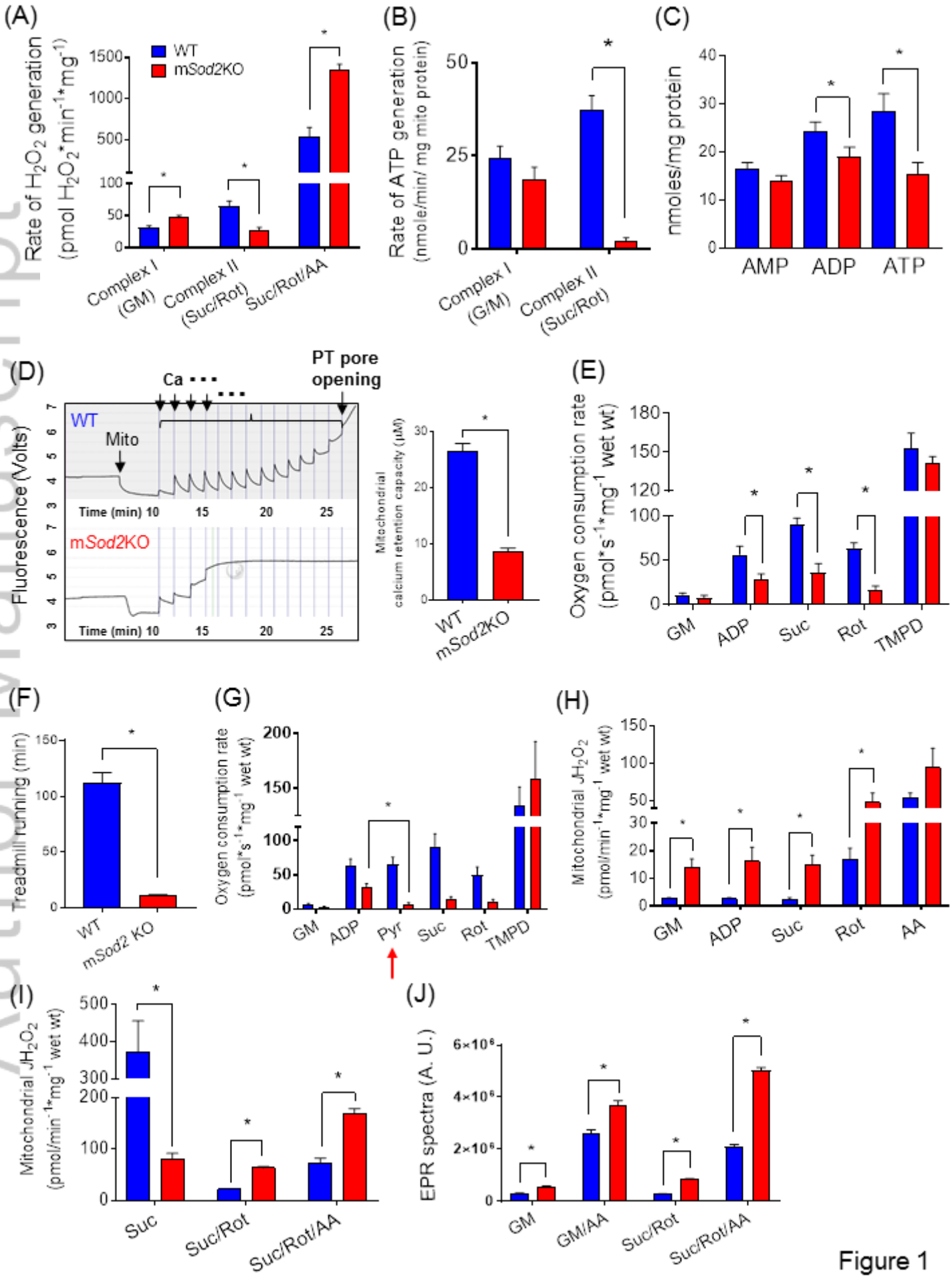

Figure 1

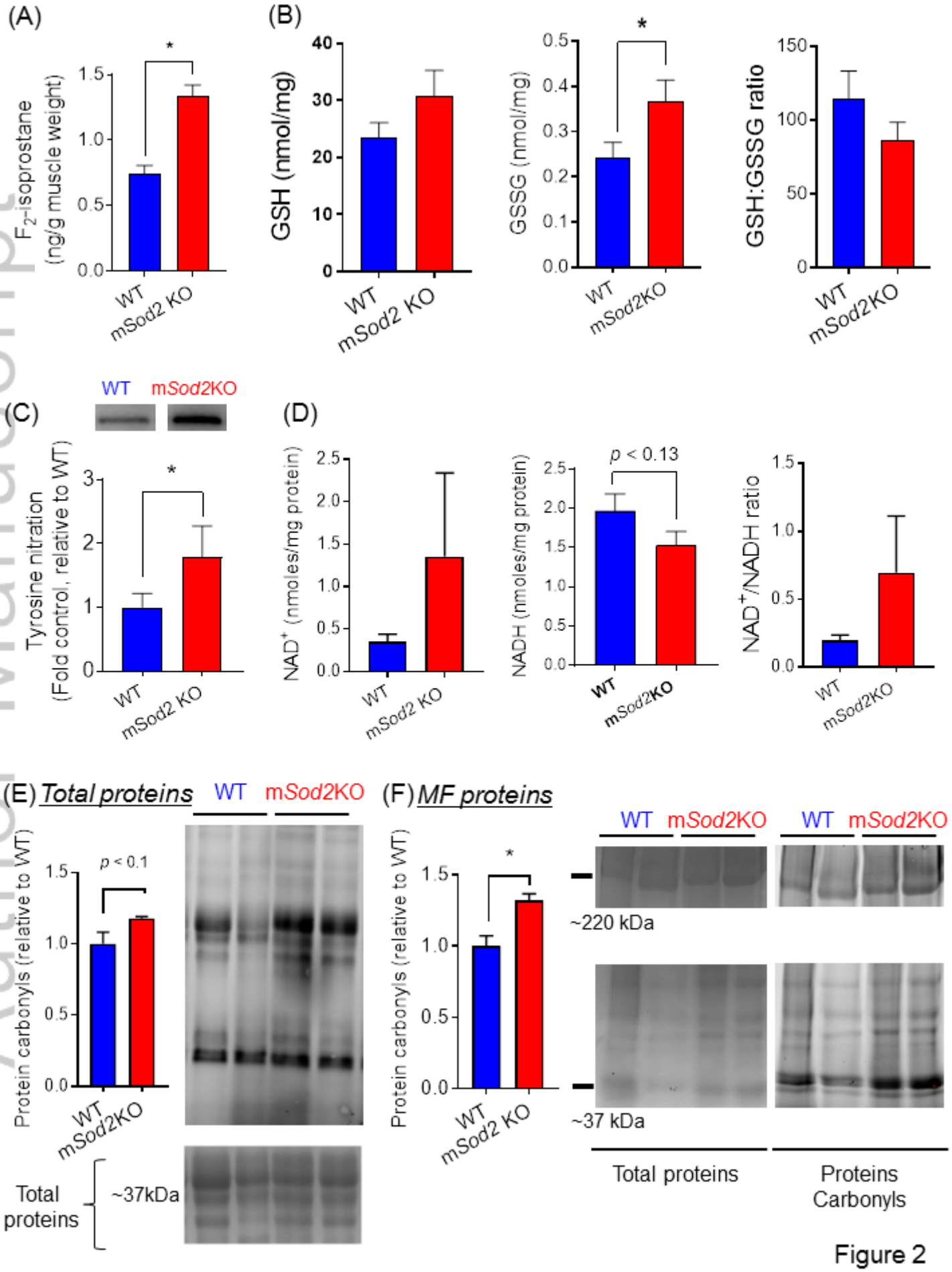

Figure 2

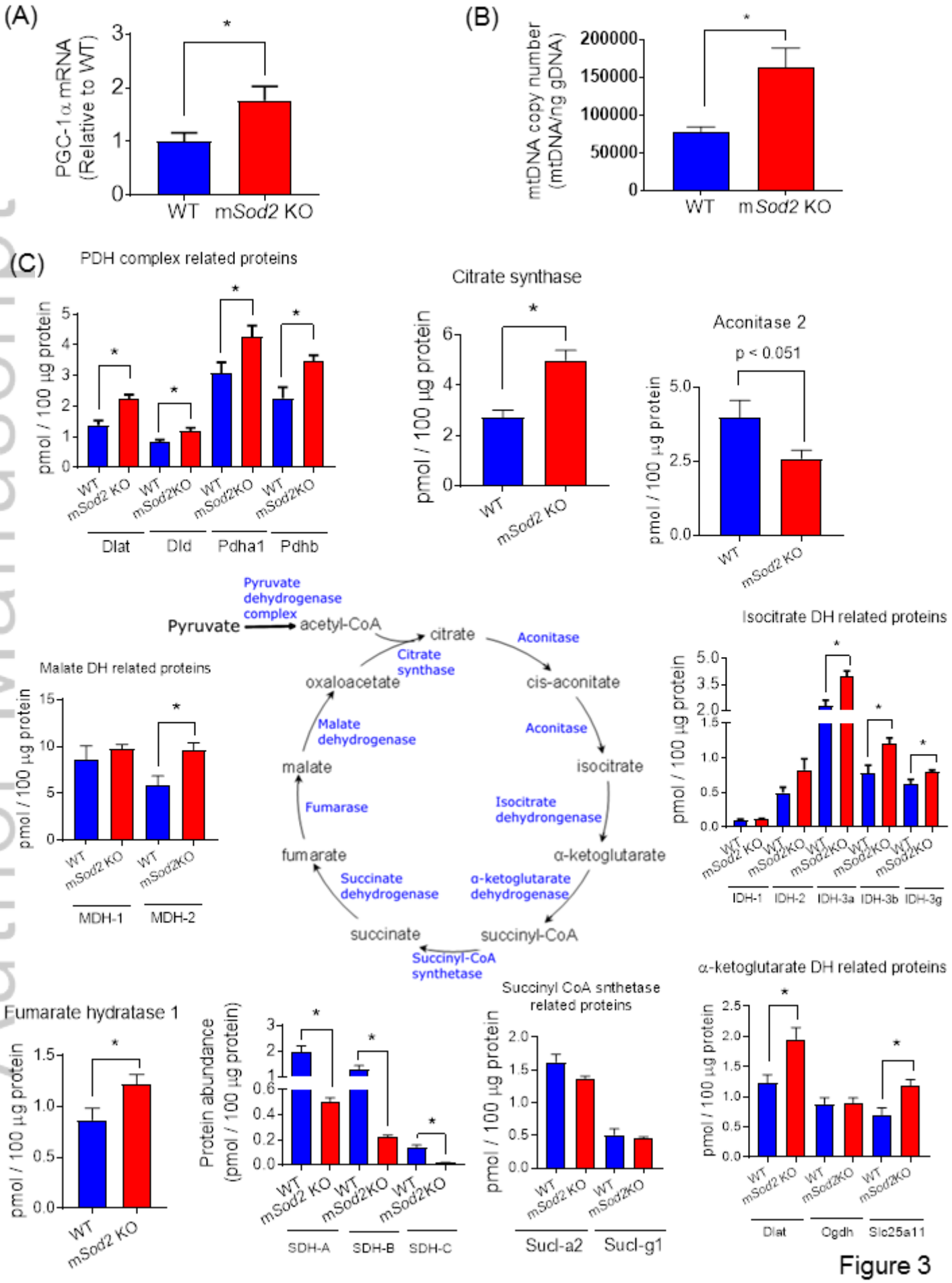

Figure 3

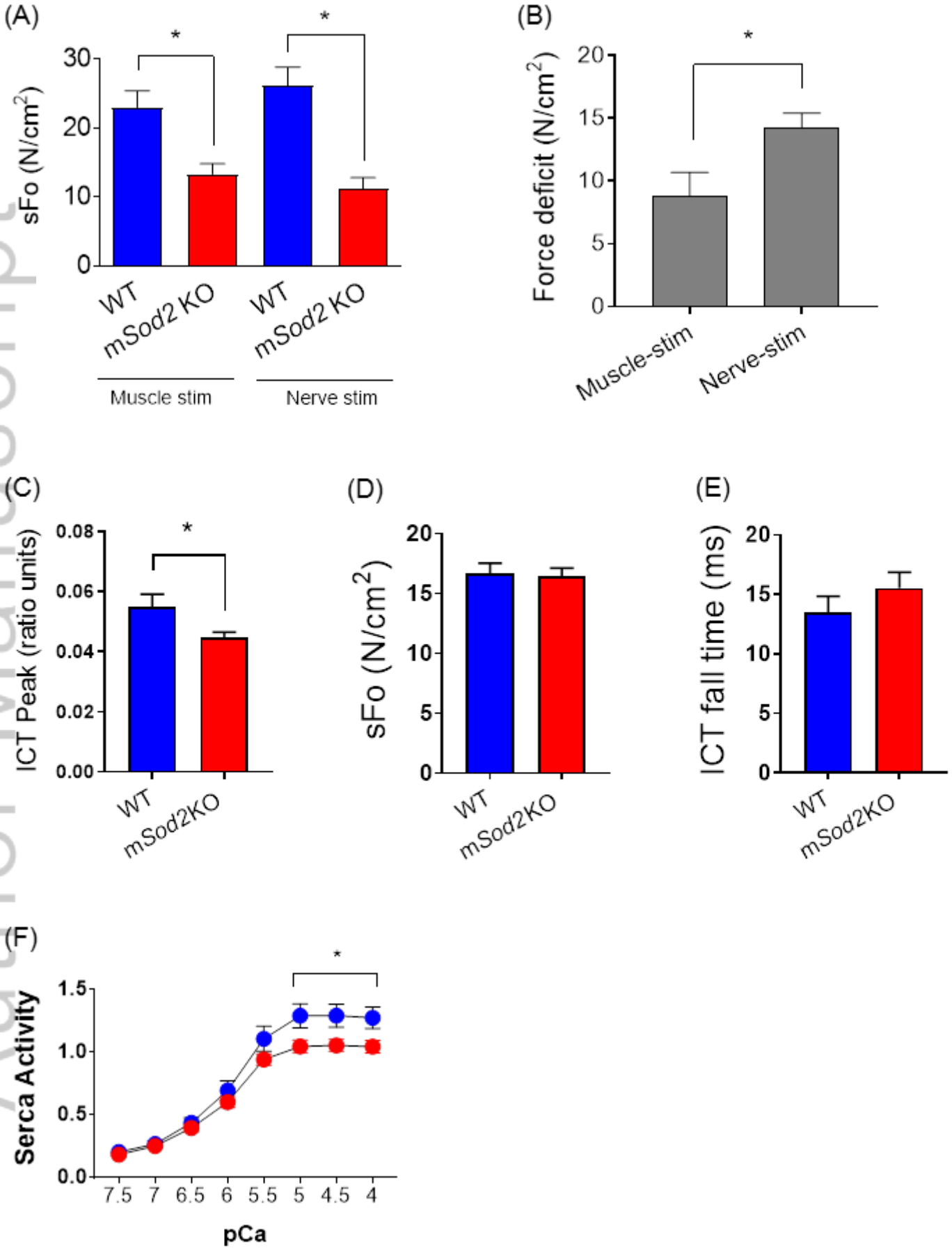

Figure 4

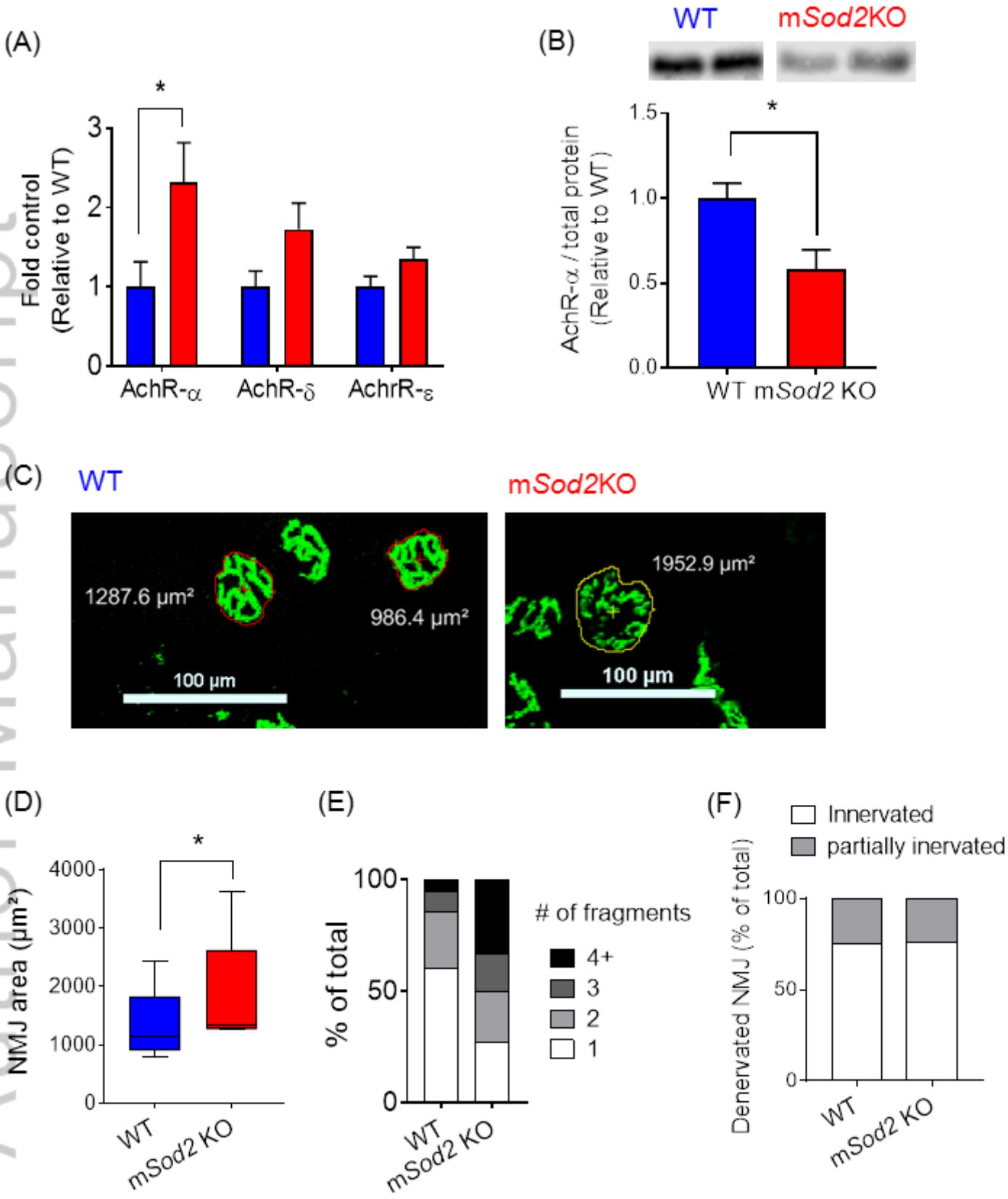

Figure 5

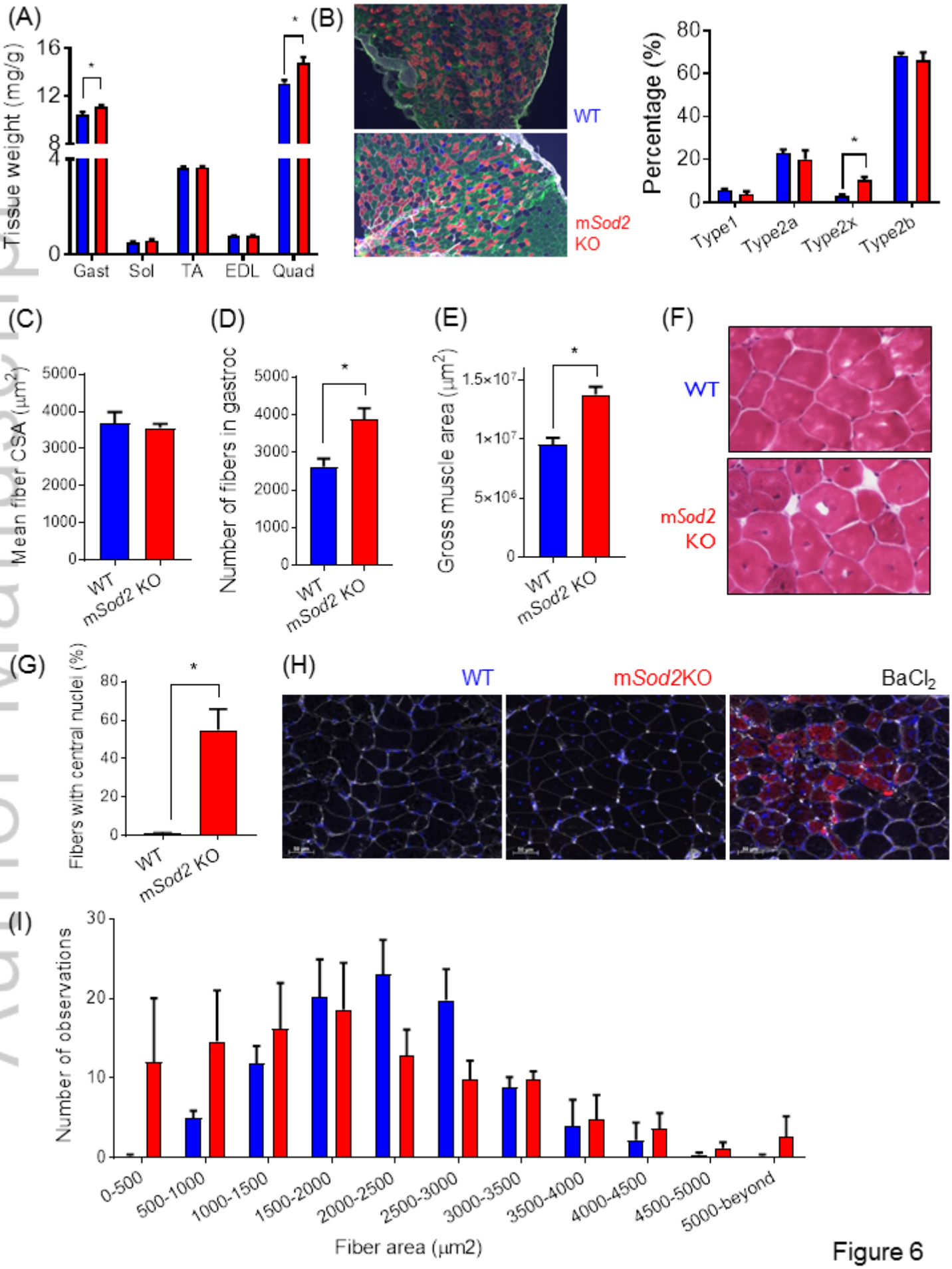

Figure 6

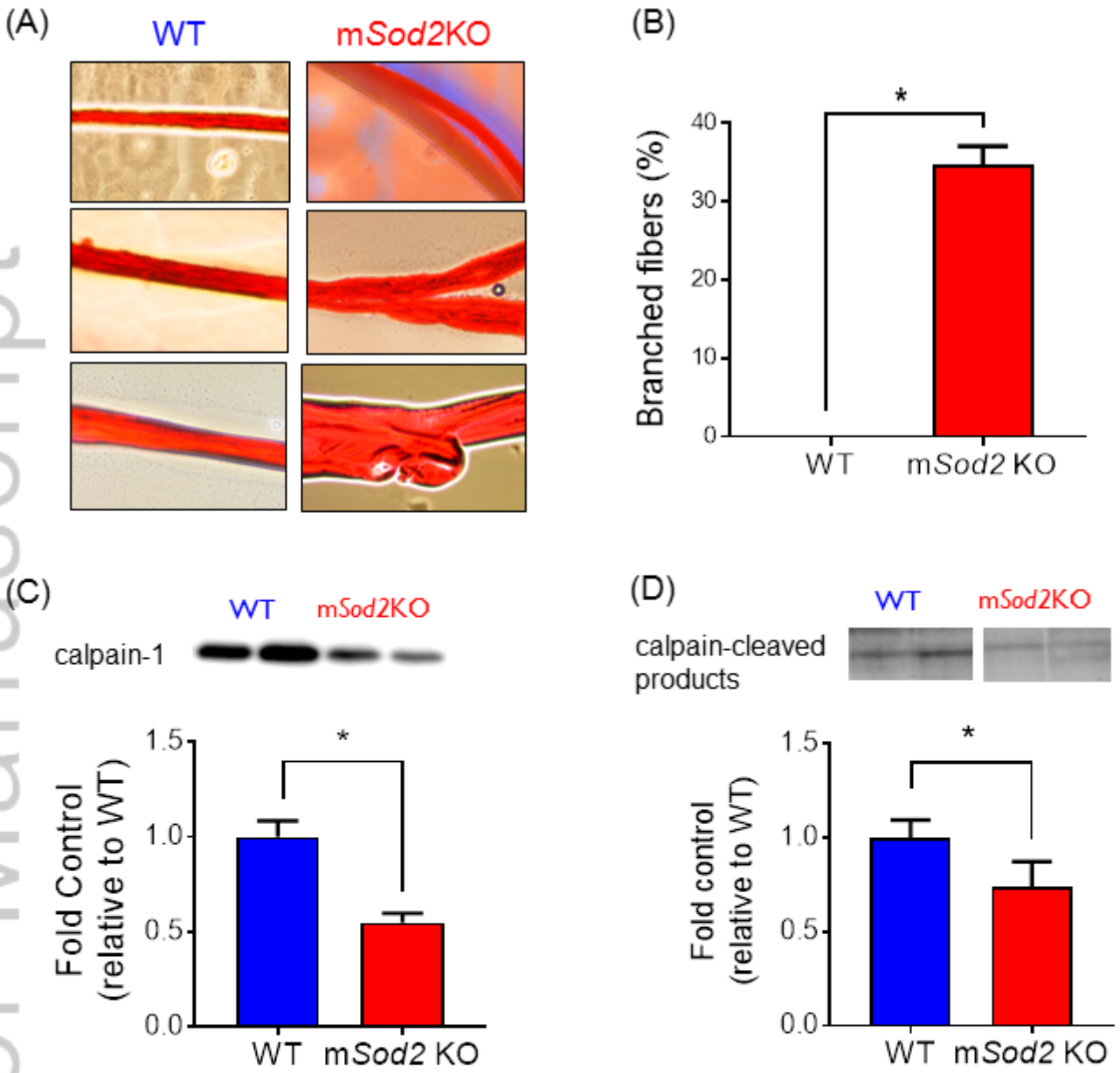

Figure 7

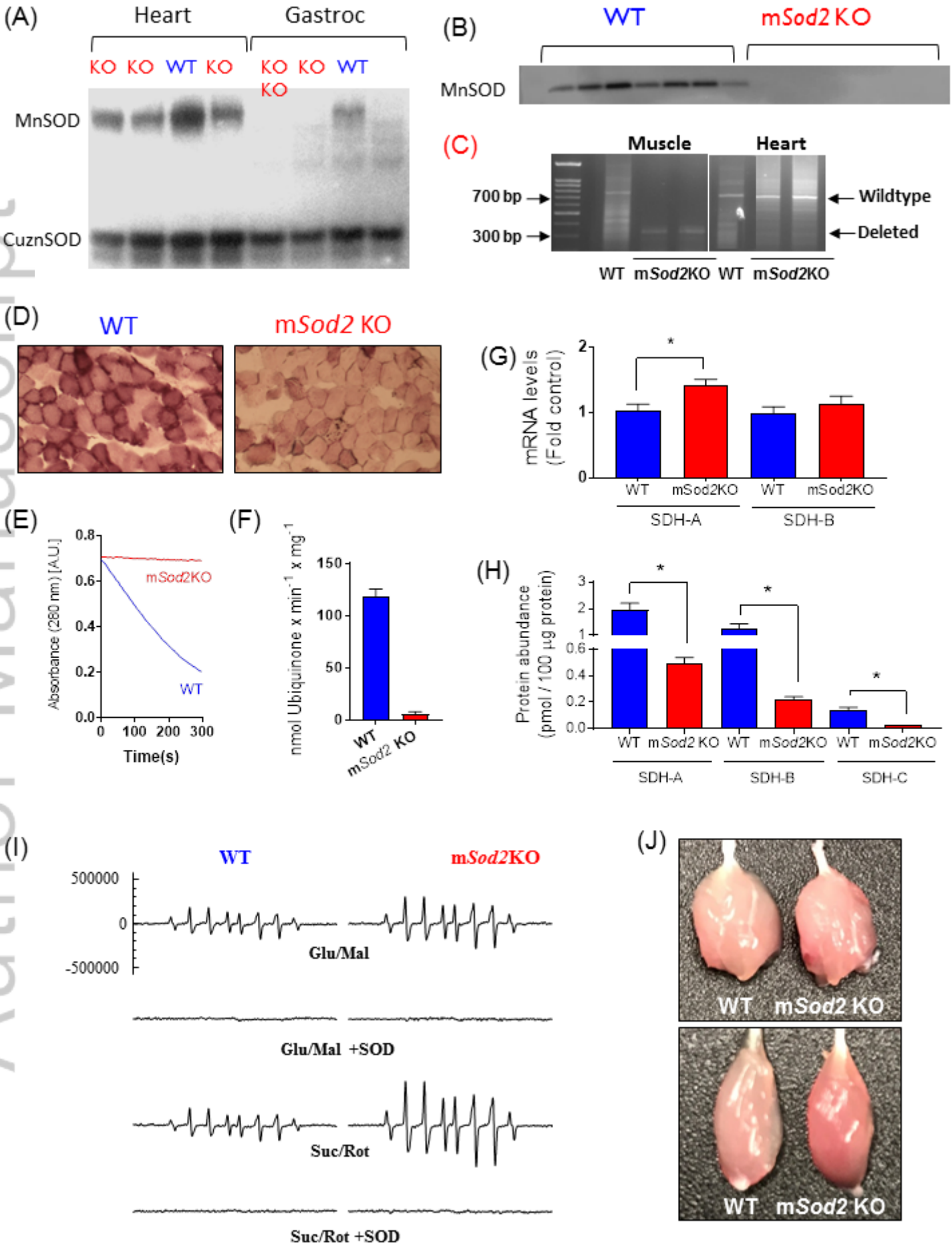

Figure S1

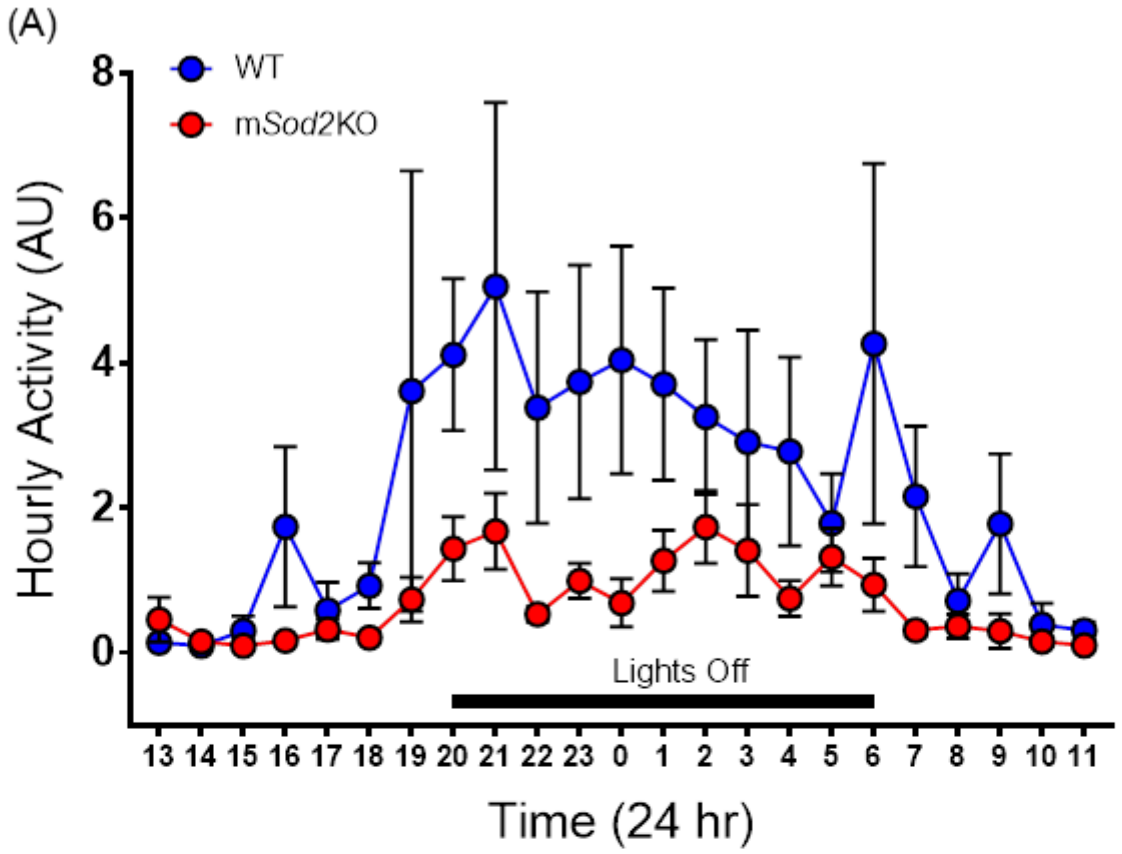

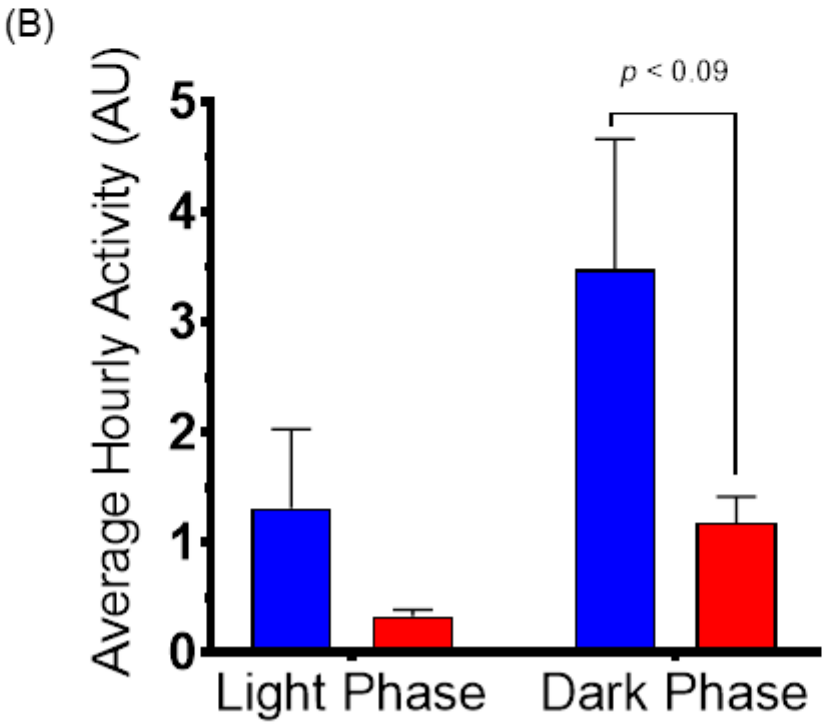

Figure S2

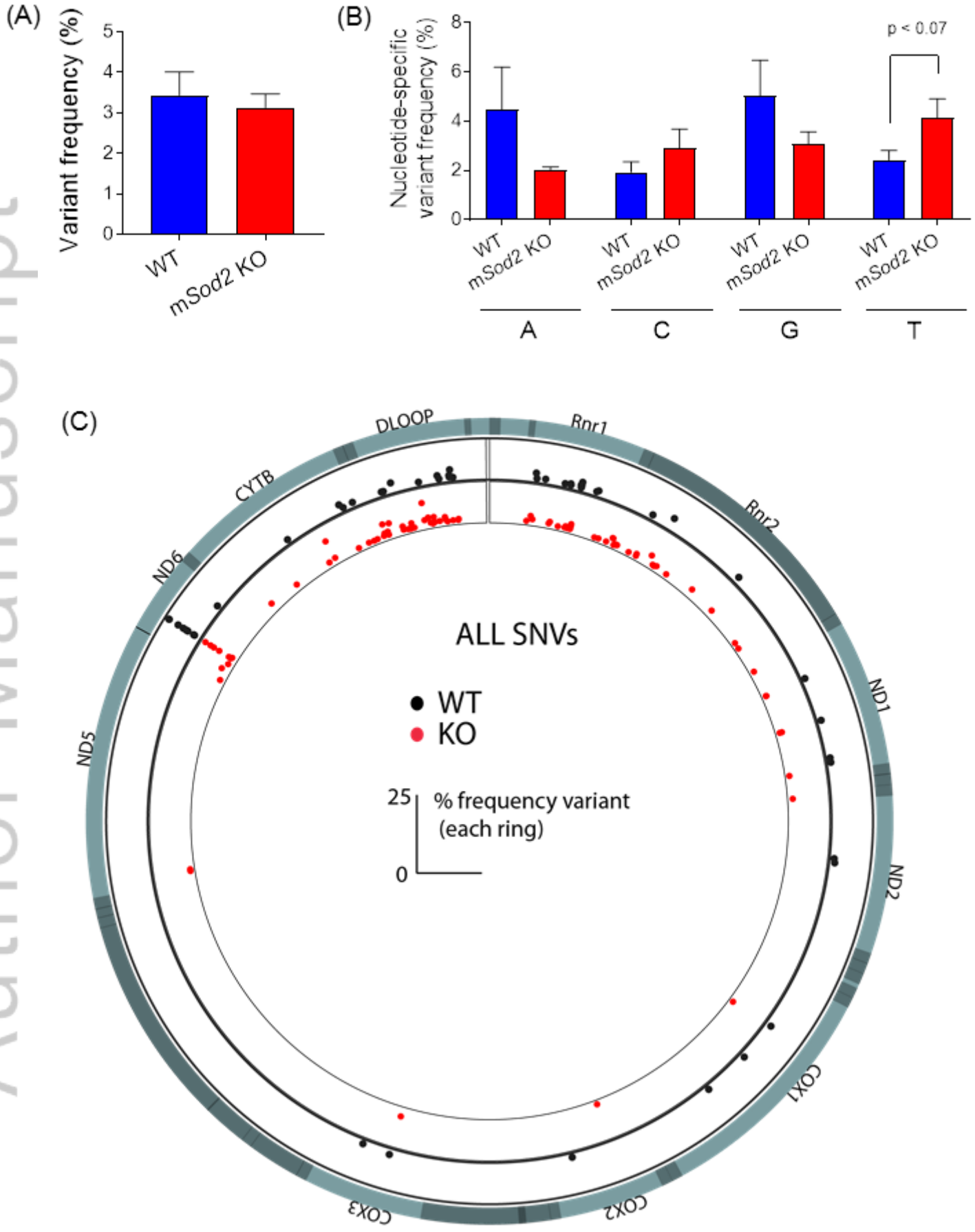

Figure S3

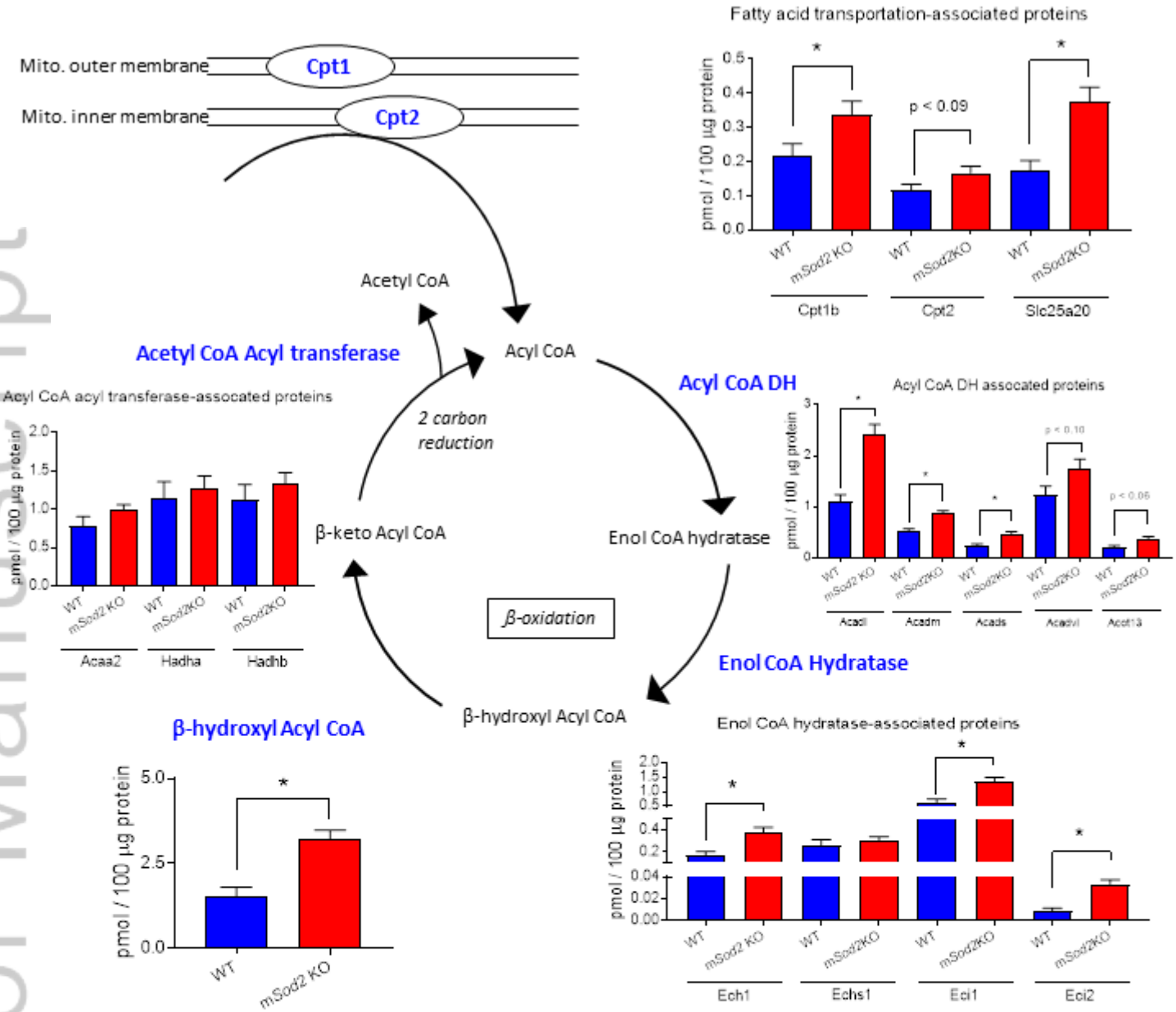

Figure S4

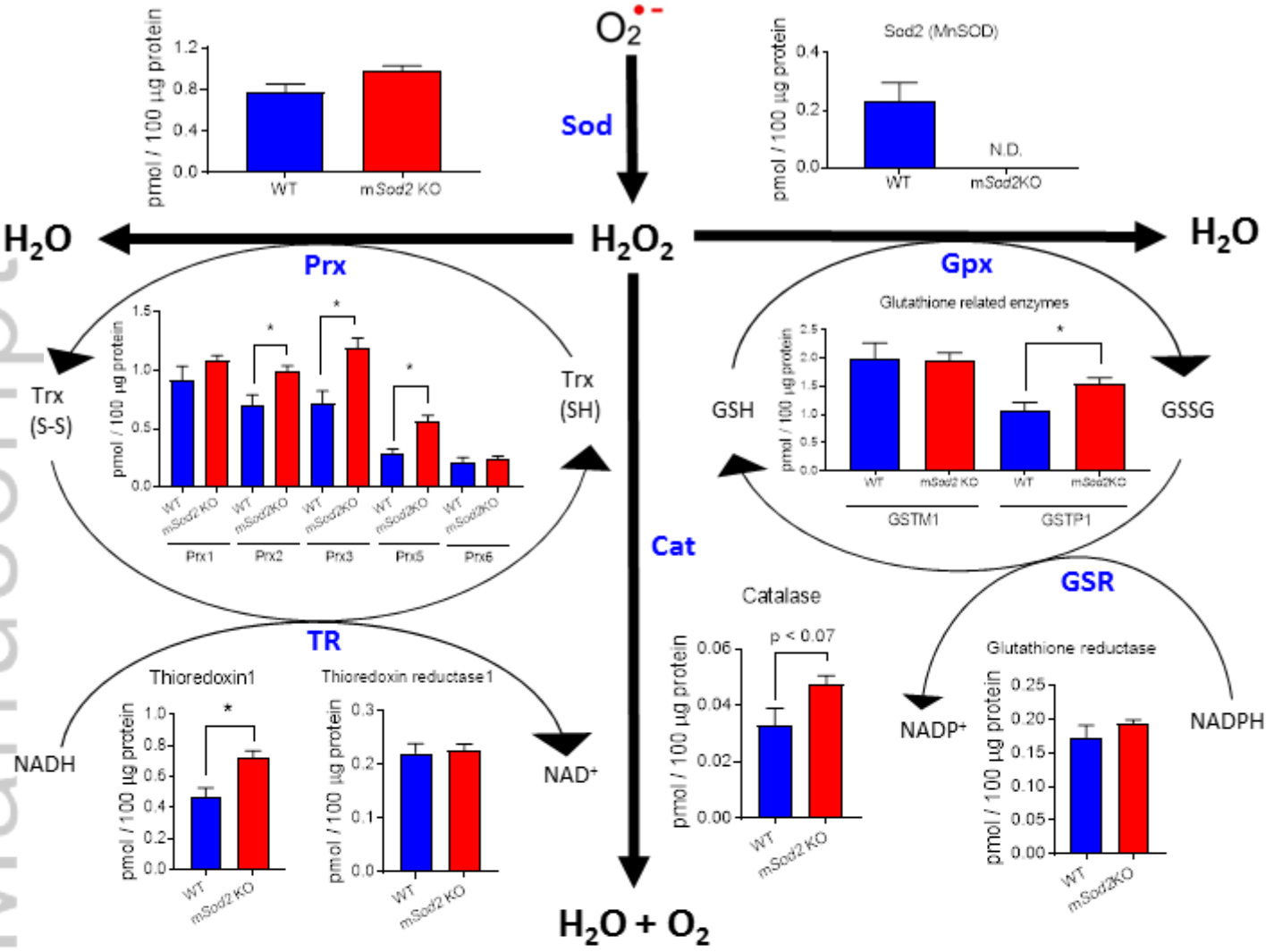

Figure S5

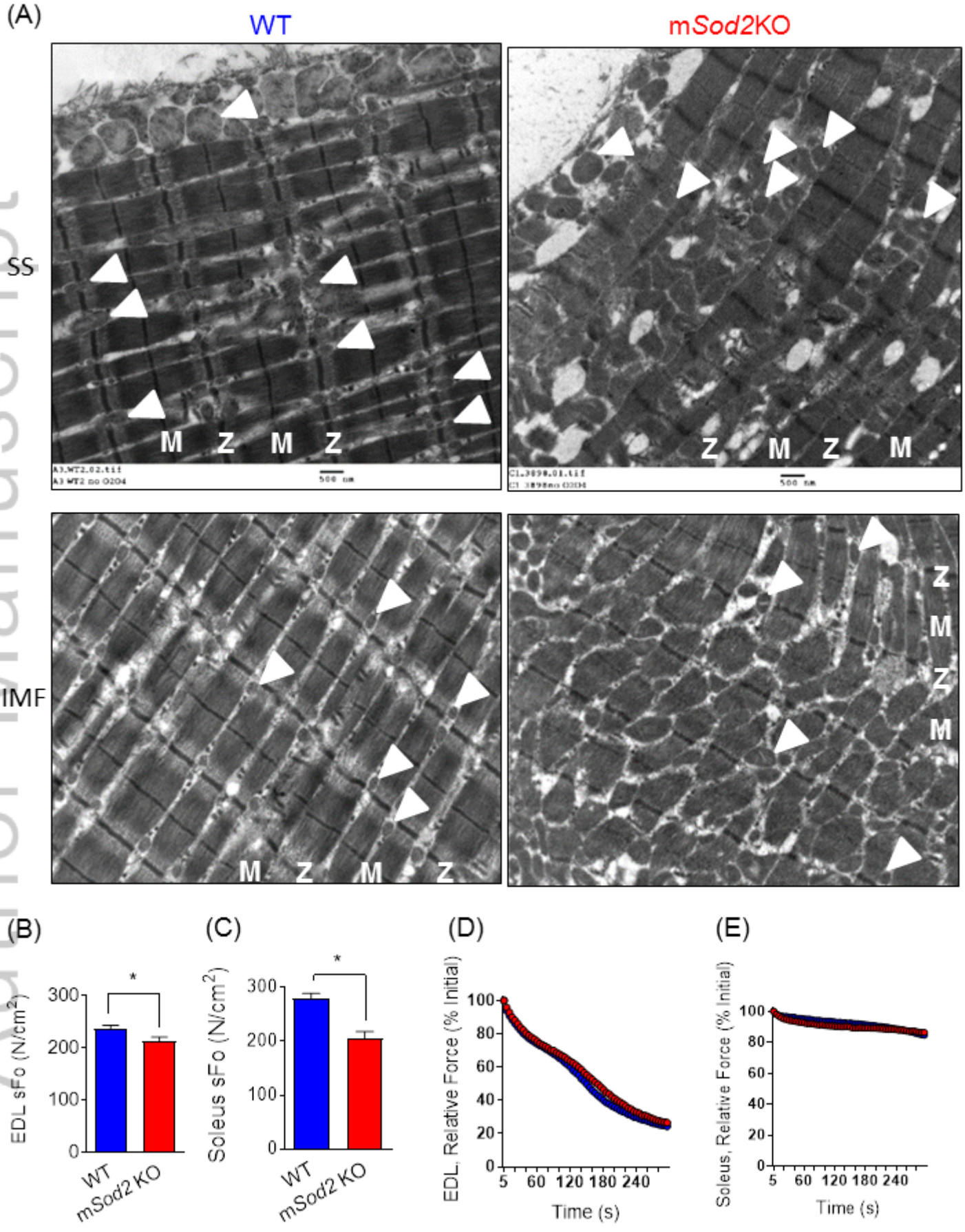

Figure S6

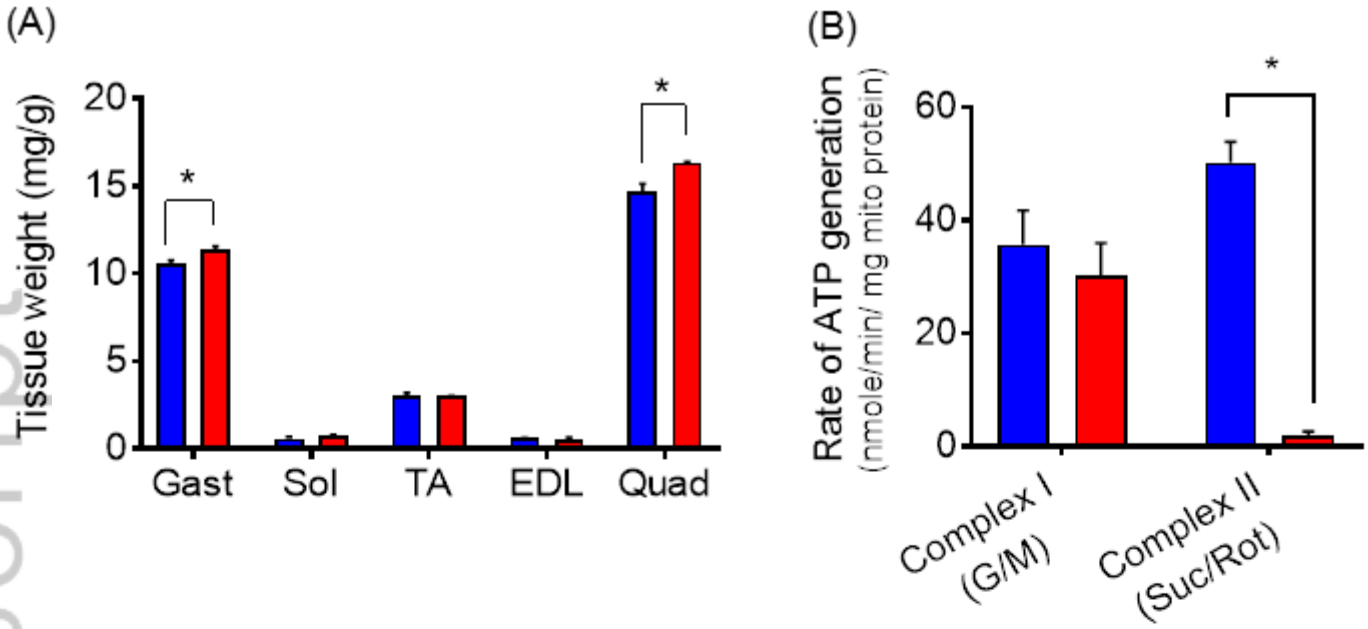

Figure S7

Enzymes in glycolysis and gluconeogenesis

	Mean ±SEM (pmol/100 ug)		
Gene Name	WT	mSod2 KO	*p*-val
AldoA	75.05 ±5.84	83.43 ±6.29	0.35
Eno3	24.61 ±2.92	27.61 ±1.98	0.42
Gapdh	68.62 ±9.14	92.96 ±9.88	0.10
Got1	2.61 ±0.40	3.50 ±0.31	0.11
Got2	2.72 ±0.40	5.66 ±0.38	0.0003*
Gpi1	8.75 ±0.80	10.68 ±0.29	0.06
Hk1	0.46 ±0.06	0.61 ±0.05	0.08
Ldha	41.75 ±5.08	39.01 ±2.14	0.63
Ldhb	2.08 ±0.51	2.49 ±0.26	0.49
Mpc1	0.10 ±0.013	0.15 ±0.013	0.02 *
Mpc2	0.04 ±0.008	0.07 ±0.014	0.09
Pcx	0.18 ±0.022	0.12 ±0.011	0.05
Pfkm	3.96 ±0.41	3.61 ±0.09	0.45
Pgam2	15.06 ±1.73	11.87 ±1.27	0.17
Pgk1	4.39 ±0.26	5.21 ±0.28	0.05
Pfkm	30.87 ±2.51	29.33 ±0.81	0.58
Pygm	15.69 ±1.96	16.09 ±1.58	0.88
Slc2a1	0.032 ±0.006	0.06 ±0.008	0.04
Slc2a4	0.065 ±0.011	0.07 ±0.007	0.54
Tpi1	14.0 ±1.92	13.60 ±1.02	0.87

Table S1

(A) Gene names and IDs in TCA cycles (Figure 3)

Gene name	NCBI Gene id	Protein name
Cs	12974	citrate synthase
Aco2	11429	aconitase 2, mitochondrial
Idh1	15926	isocitrate dehydrogenase 1 (NADP+), soluble
Idh2	269951	isocitrate dehydrogenase 2 (NADP+), mitochondrial
Idh3a	67834	isocitrate dehydrogenase 3 (NAD+) alpha
Idh3b	170718	isocitrate dehydrogenase 3 (NAD+) beta
Idh3g	15929	isocitrate dehydrogenase 3 (NAD+), gamma
Dlat	235339	dihydrolipoamide S-acetyltransferase (E2 component of pyruvate dehydrogenase complex)
Ogdh	18293	oxoglutarate (alpha-ketoglutarate) dehydrogenase (lipoamide)
Slc25a11	67863	solute carrier family 25 (mitochondrial carrier oxoglutarate carrier), member 11
Sucla2	20916	succinate-Coenzyme A ligase, ADP-forming, beta subunit
Suclg1	56451	succinate-CoA ligase, GDP-forming, alpha subunit
Sdha	66945	succinate dehydrogenase complex, subunit A, flavoprotein (Fp)
Sdhb	67680	succinate dehydrogenase complex, subunit B, iron sulfur (Ip)
Sdhc	66052	succinate dehydrogenase complex, subunit C, integral membrane protein
Fh1	14194	fumarate hydratase 1
Mdh1	17449	malate dehydrogenase 1, NAD (soluble)
Mdh2	17448	malate dehydrogenase 2, NAD (mitochondrial)
Dlat	235339	dihydrolipoamide S-acetyltransferase (E2 component of pyruvate dehydrogenase complex)
Dld	13382	dihydrolipoamide dehydrogenase
Pdha1	18597	pyruvate dehydrogenase E1 alpha 1
Pdhb	68263	pyruvate dehydrogenase (lipoamide) beta

(B) Gene names and IDs in beta-oxidation (Figure S3)

Gene name	NCBI Gene ID	Protein name
Cpt1b	12895	carnitine palmitoyltransferase 1b, muscle
Cpt2	12896	carnitine palmitoyltransferase 2
Slc25a20	57279	solute carrier family 25 (mitochondrial carnitine/acylcarnitine translocase), member 20
Acadl	11363	acyl-Coenzyme A dehydrogenase, long-chain
Acadm	11364	acyl-Coenzyme A dehydrogenase, medium chain
Acads	11409	acyl-Coenzyme A dehydrogenase, short chain
Acadvl	11370	acyl-Coenzyme A dehydrogenase, very long chain
Acot13	66834	acyl-CoA thioesterase 13
Ech1	51798	enoyl coenzyme A hydratase 1, peroxisomal
Echs1	93747	enoyl Coenzyme A hydratase, short chain, 1, mitochondrial
Eci1	13177	enoyl-Coenzyme A delta isomerase 1
Eci2	23986	enoyl-Coenzyme A delta isomerase 2
Hadh	15107	hydroxyacyl-Coenzyme A dehydrogenase
Acaa2	52538	acetyl-Coenzyme A acyltransferase 2 (mitochondrial 3-oxoacyl-Coenzyme A thiolase)
Hadha	97212	hydroxyacyl-Coenzyme A dehydrogenase/3-ketoacyl-Coenzyme A thiolase/ enoyl-Coenzyme A hydratase (trifunctional protein), alpha subunit
Hadhb	231086	hydroxyacyl-Coenzyme A dehydrogenase/3-ketoacyl-Coenzyme A thiolase/ enoyl-Coenzyme A hydratase (trifunctional protein), beta subunit

Table S2

(C) Gene names and IDs of antioxidant enzymes (Figure S4)

Gene name	NCBI Gene id	Protein name
Sod1	20655	superoxide dismutase 1, soluble
Sod2	20656	superoxide dismutase 2, mitochondrial
Gstm1	14862	glutathione S-transferase, mu 1
Gstp1	14870	glutathione S-transferase, pi 1
Cat	12359	catalase
Gsr	14782	glutathione reductase
Prdx1	18477	peroxiredoxin 1
Prdx2	21672	peroxiredoxin 2
Prdx3	11757	peroxiredoxin 3
Prdx5	54683	peroxiredoxin 5
Prdx6	11758	peroxiredoxin 6
Txn1	22166	thioredoxin 1
Txnrd1	50493	thioredoxin reductase 1

(D) Gene names and IDs in glycolysis and gluconeo genesis (Table S1)

Gene name	NCBI Gene id	Protein name
AldoA	11674	aldolase A, fructose-bisphosphate
Eno3	13808	enolase 3, beta muscle
Gapdh	14433	glyceraldehyde-3-phosphate dehydrogenase
Got1	14718	glutamic-oxaloacetic transaminase 1, soluble
Got2	14719	glutamatic-oxaloacetic transaminase 2, mitochondrial
Gpi1	14751	glucose phosphate isomerase 1
Hk1	15275	hexokinase 1
Ldha	16828	lactate dehydrogenase A
Ldhb	16832	lactate dehydrogenase B
Mpc1	55951	Mitochondrial pyruvate carrier1
Mpc2	70456	Mitochondrial pyruvate carrier2
Pcx	18563	pyruvate carboxylase
Pfkm	18642	phosphofructokinase, muscle
Pgam2	56012	phosphoglycerate mutase 2
Pgk1	18655	phosphoglycerate kinase 1
Pfkm	18642	phosphofructokinase, muscle
Pygm	19309	muscle glycogen phosphorylase
Slc2a1	20525	solute carrier family 2 (facilitated glucose transporter), member 1
Slc2a4	20528	solute carrier family 2 (facilitated glucose transporter), member 4
Tpi1	21991	triosephosphate isomerase 1

Primary antibodies

	Catalogue #	Ratio (incubation)
Nitrotyrosine	Milipore, 06-284	1 to 1000 (overnight)
AchR-a	Santa Cruz, sc-365479	1 to 1000 (overnight)
Calpain-1	Cell Signaling, #2556	1 to 1000 (overnight)
Spectrin α II	Santa Cruz, sc-48382	1 to 1000 (overnight)

Primer sequences

	Forward	Reverse
AchR-α	ACCTGGACCTATGACGGCTCT	AGTTACTCAGGTCGGGCTGGT
AchR-δ	CATCGAGTGGATCATCATTGAC	CGGCGGATGATAAGGTAGAA
AchR-ε	GATTGGCATTGACTGGCACG	CCACTCCAAACTGCCCATC
Shda	CAGAAGTCGATGCAGAACCA	CGACCCGCACTTTGTAATCT
Sdhb	GGAGGGCAAGCAACAGTATC	GCGTTCCTCTGTGAAGTCGT

Table S3

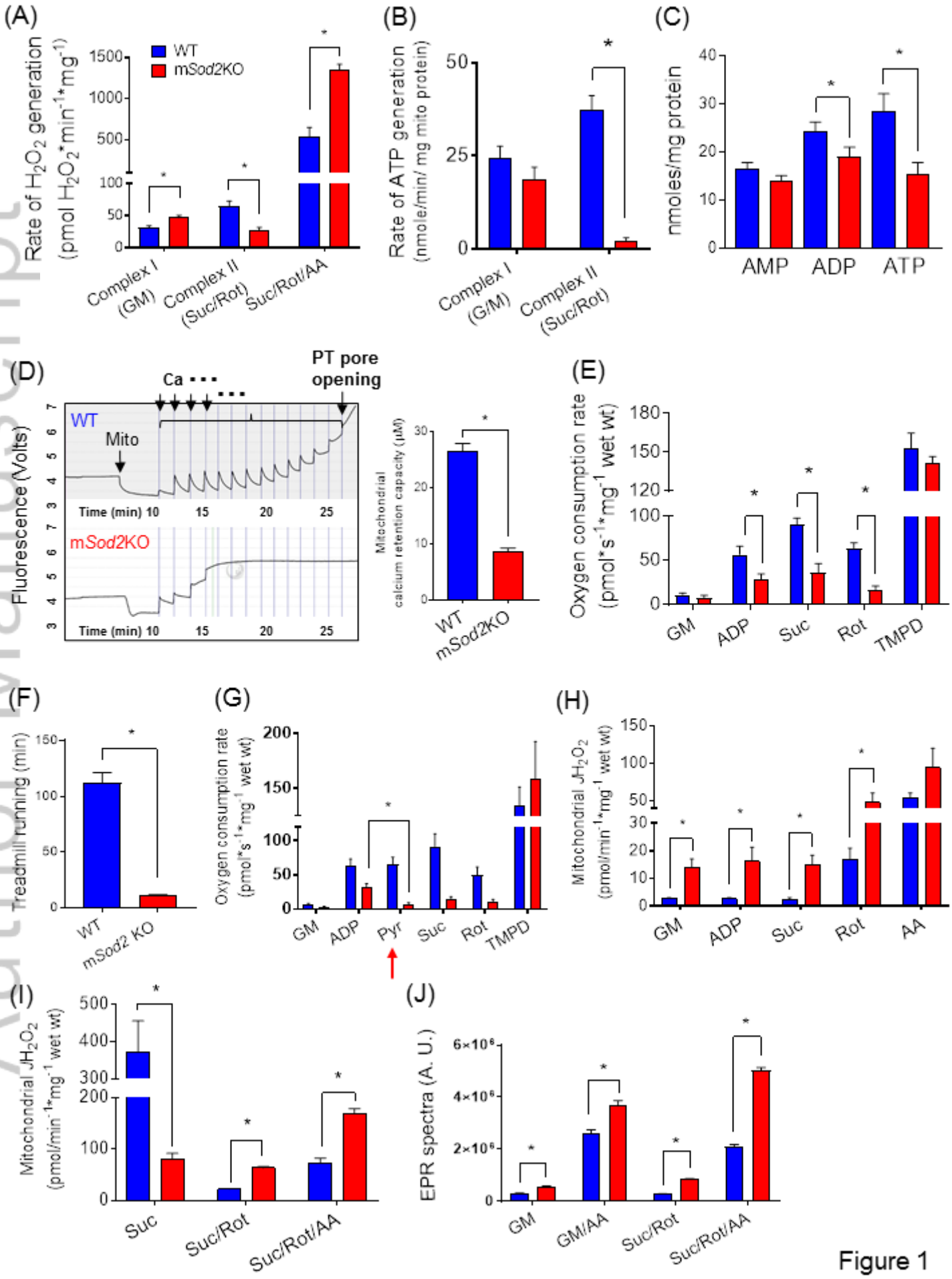

Figure 1

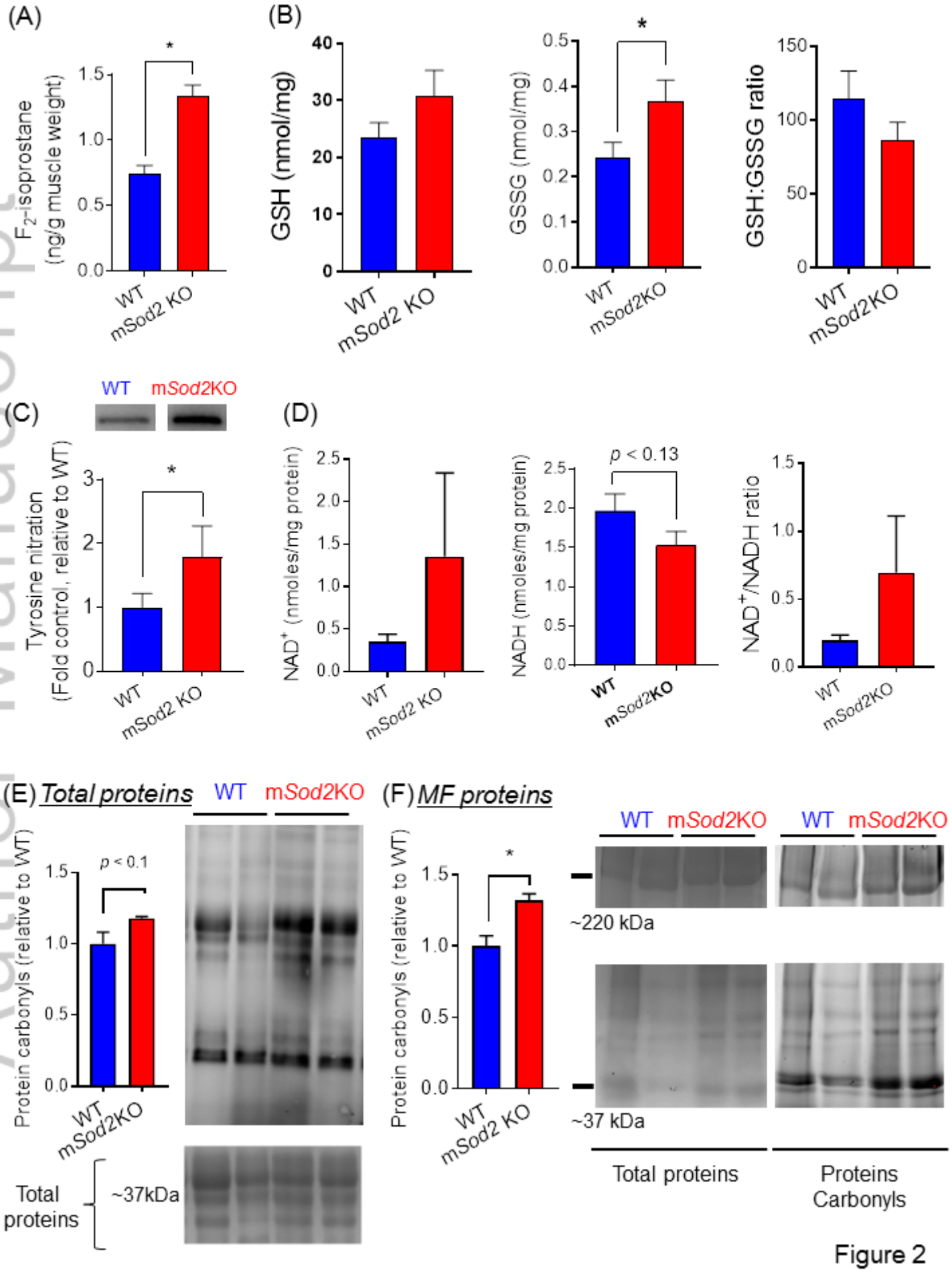

Figure 2

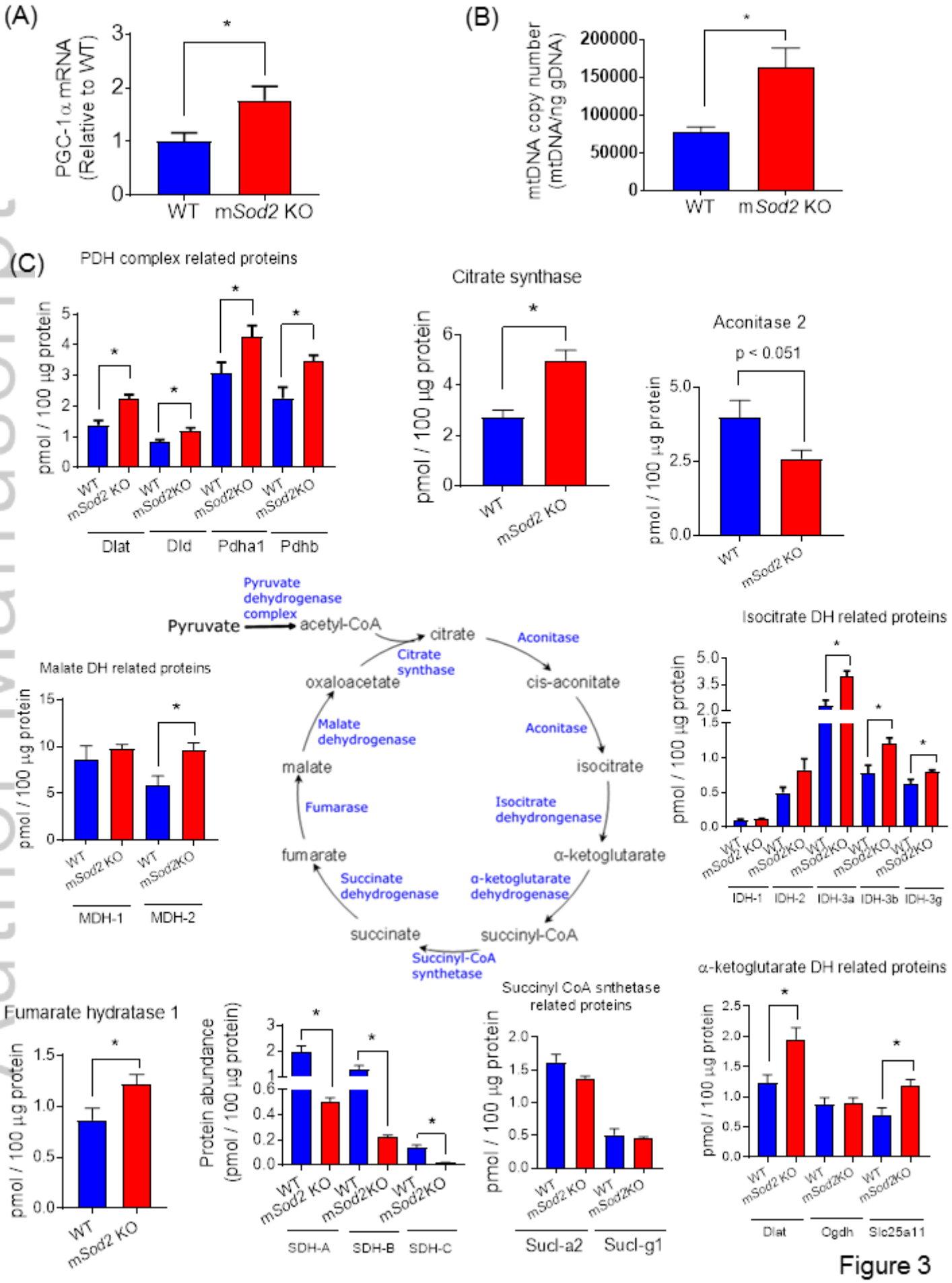

Figure 3

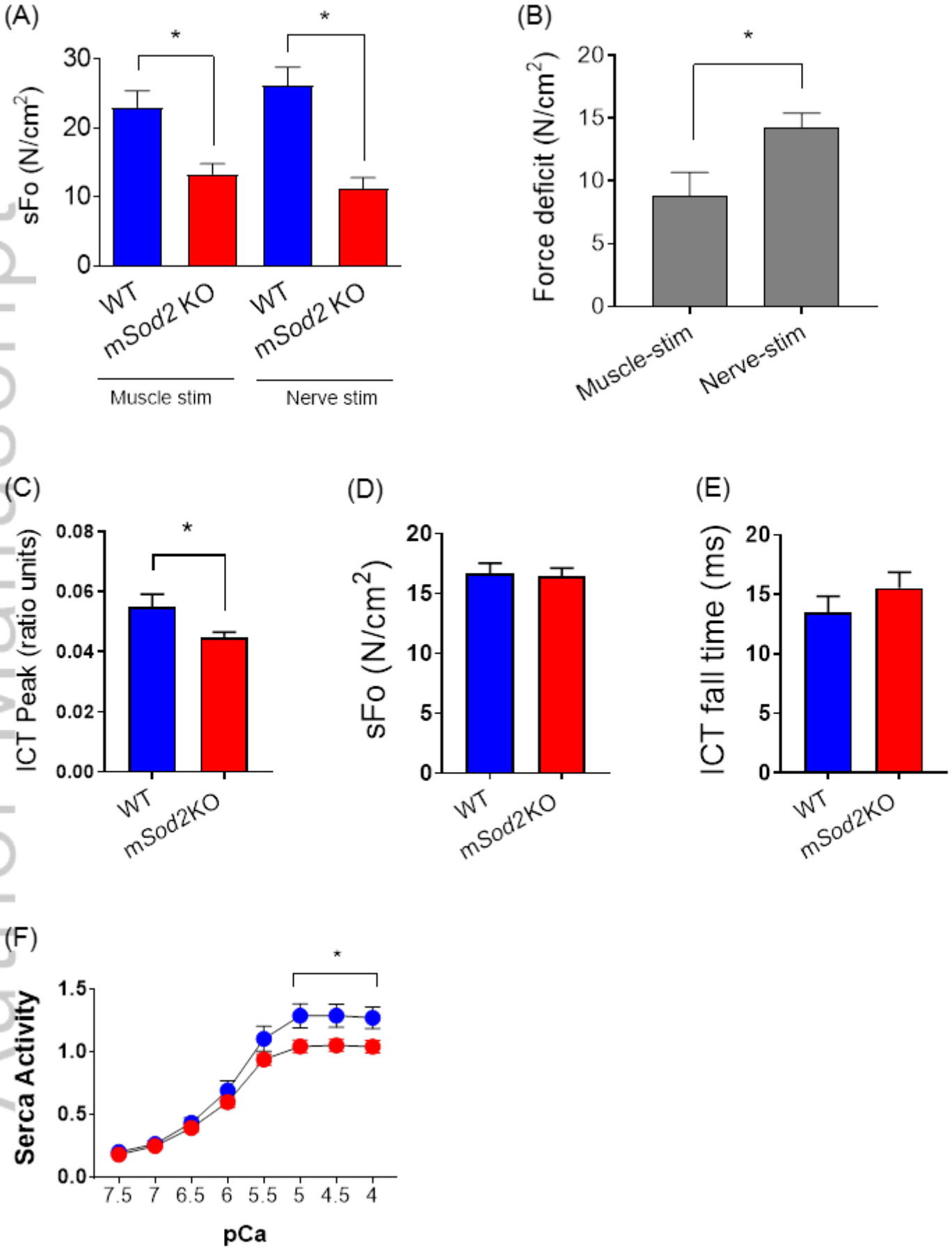

Figure 4

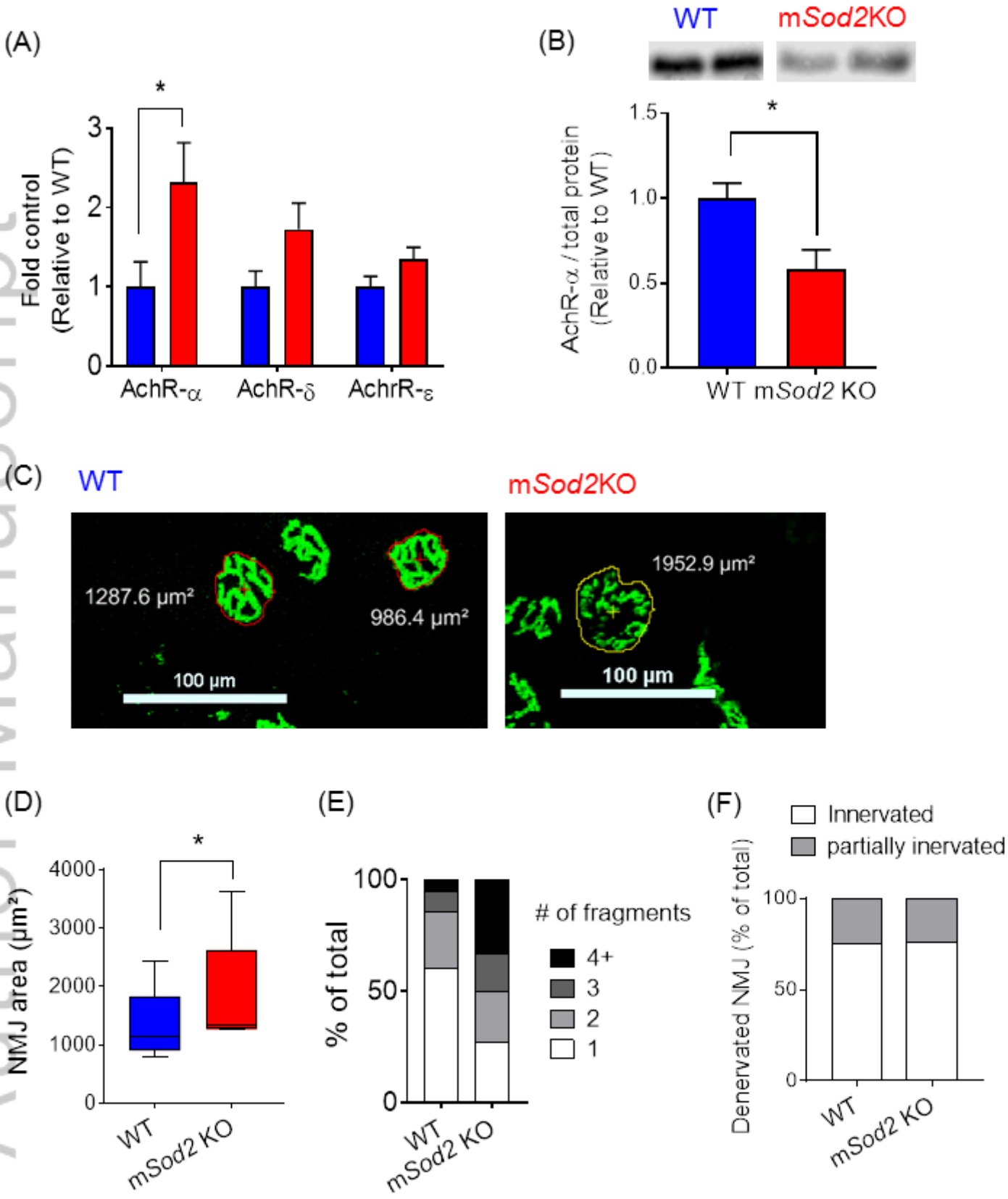

Figure 5

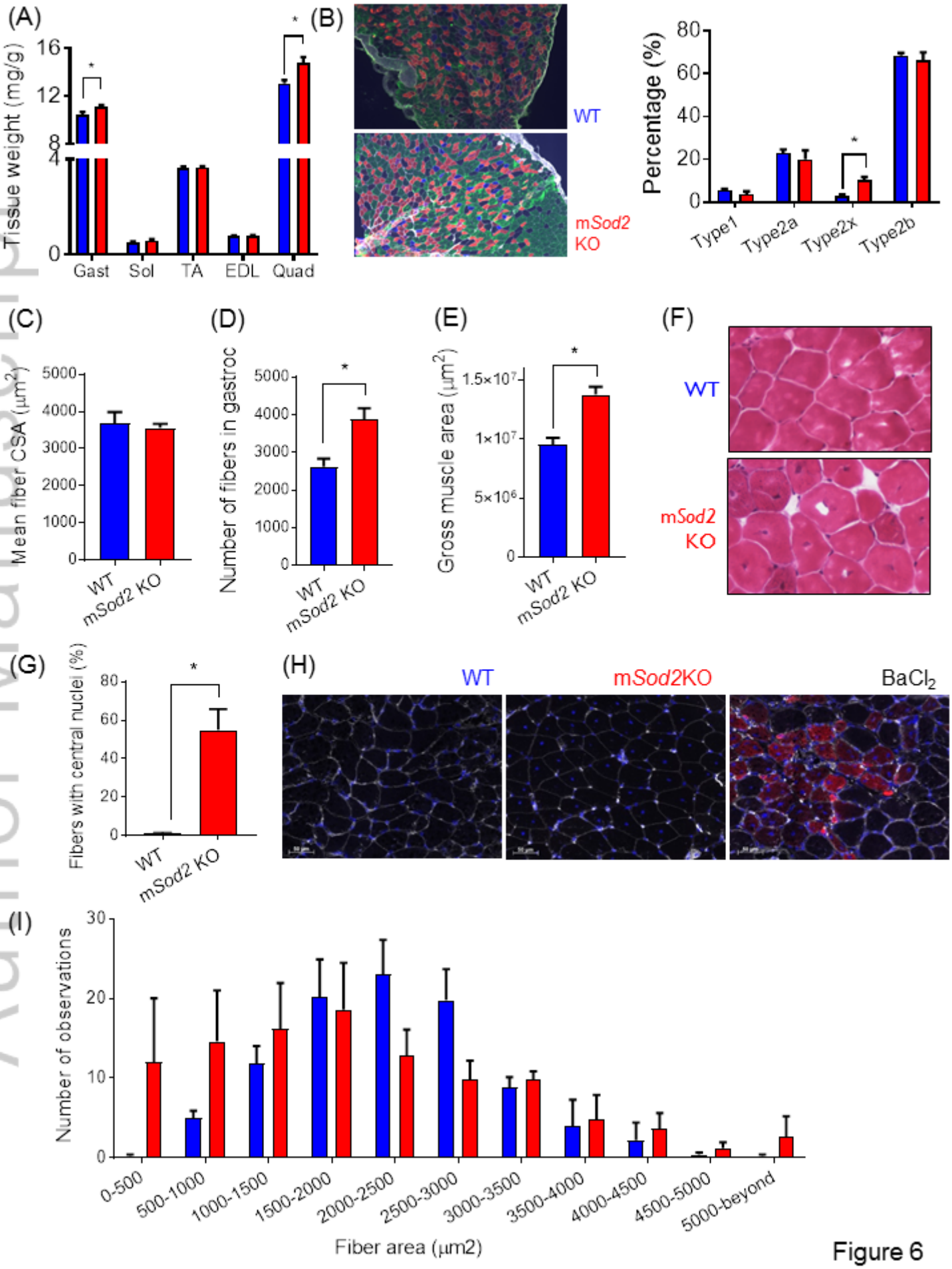

Figure 6

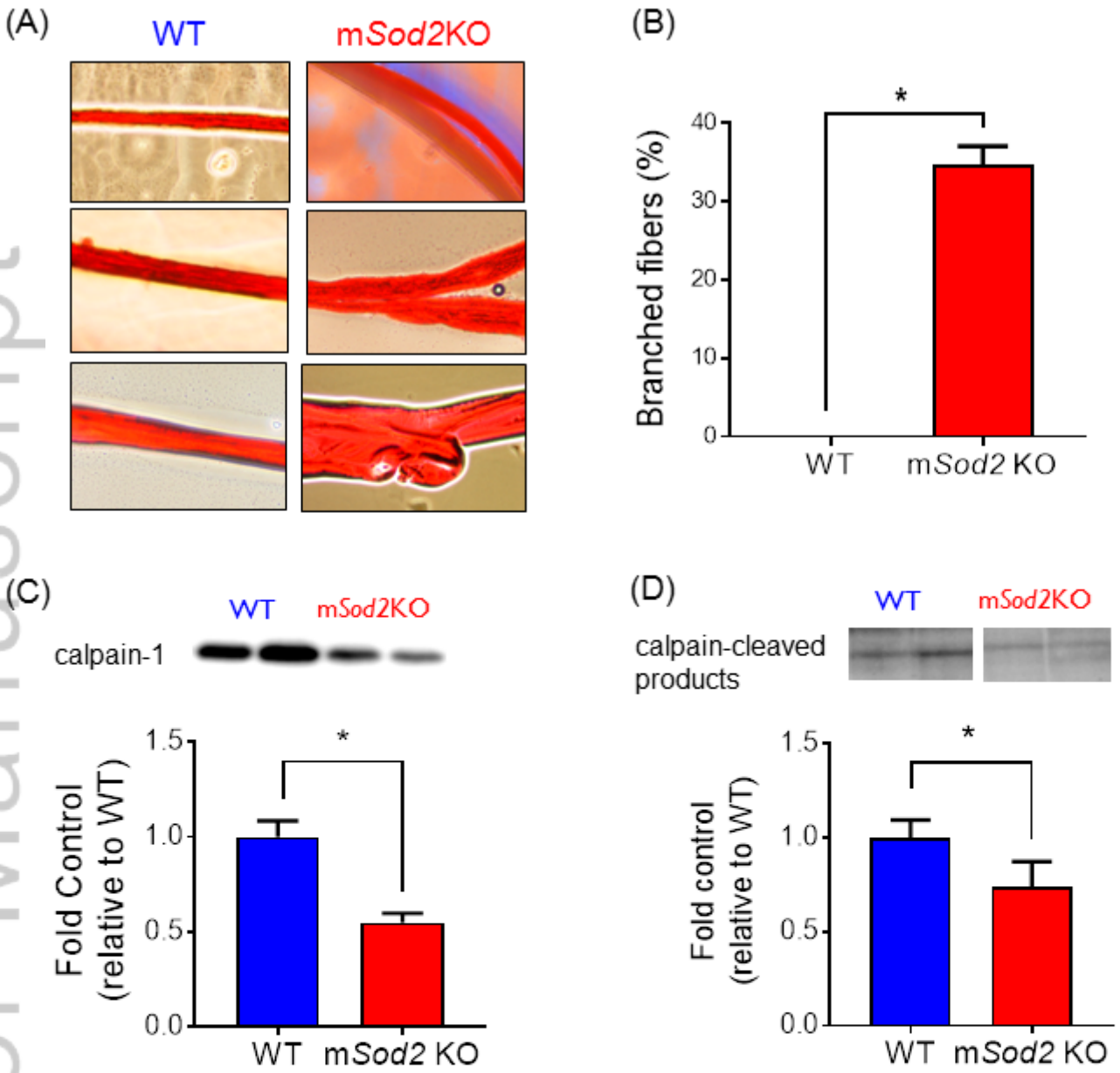

Figure 7

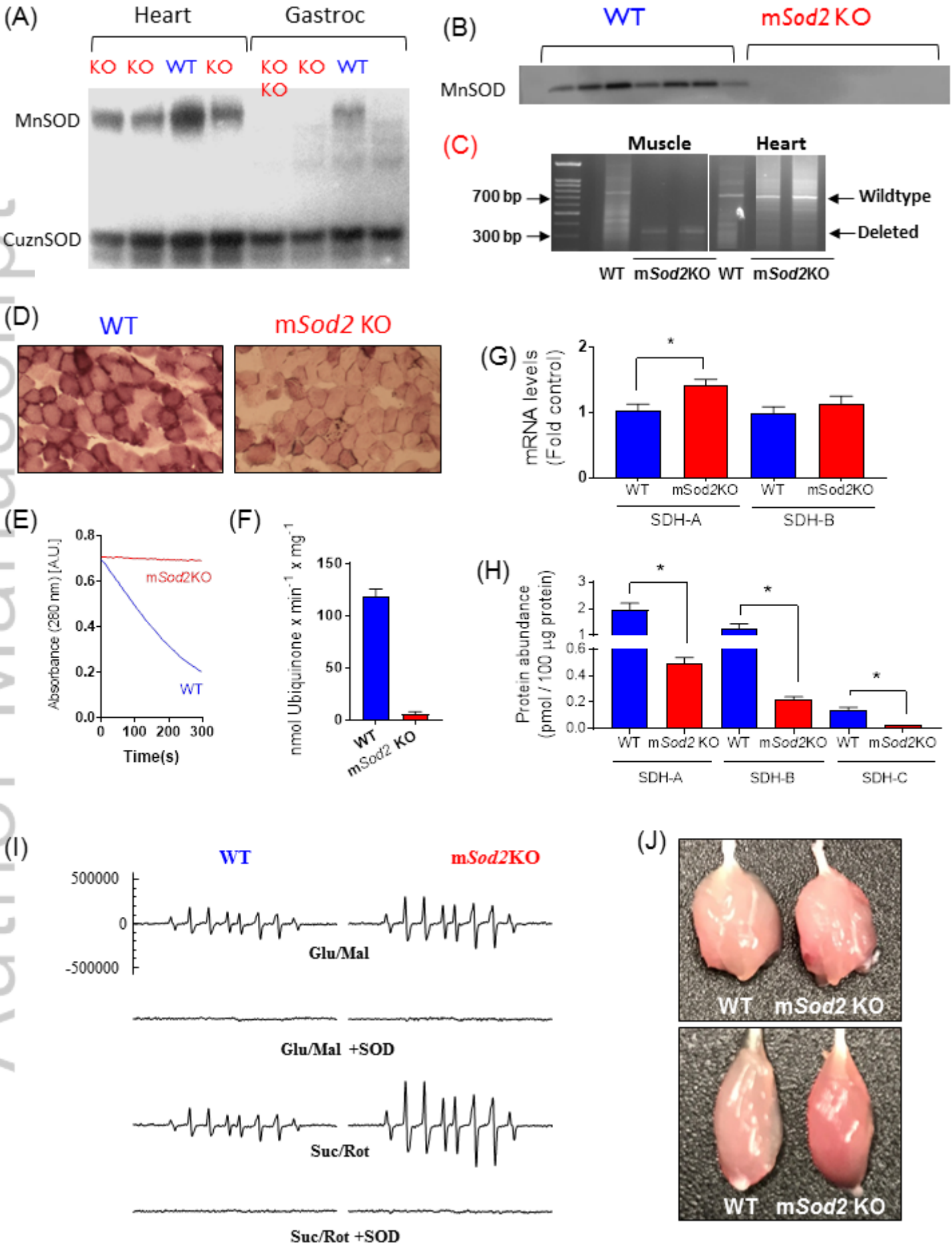

Figure S1

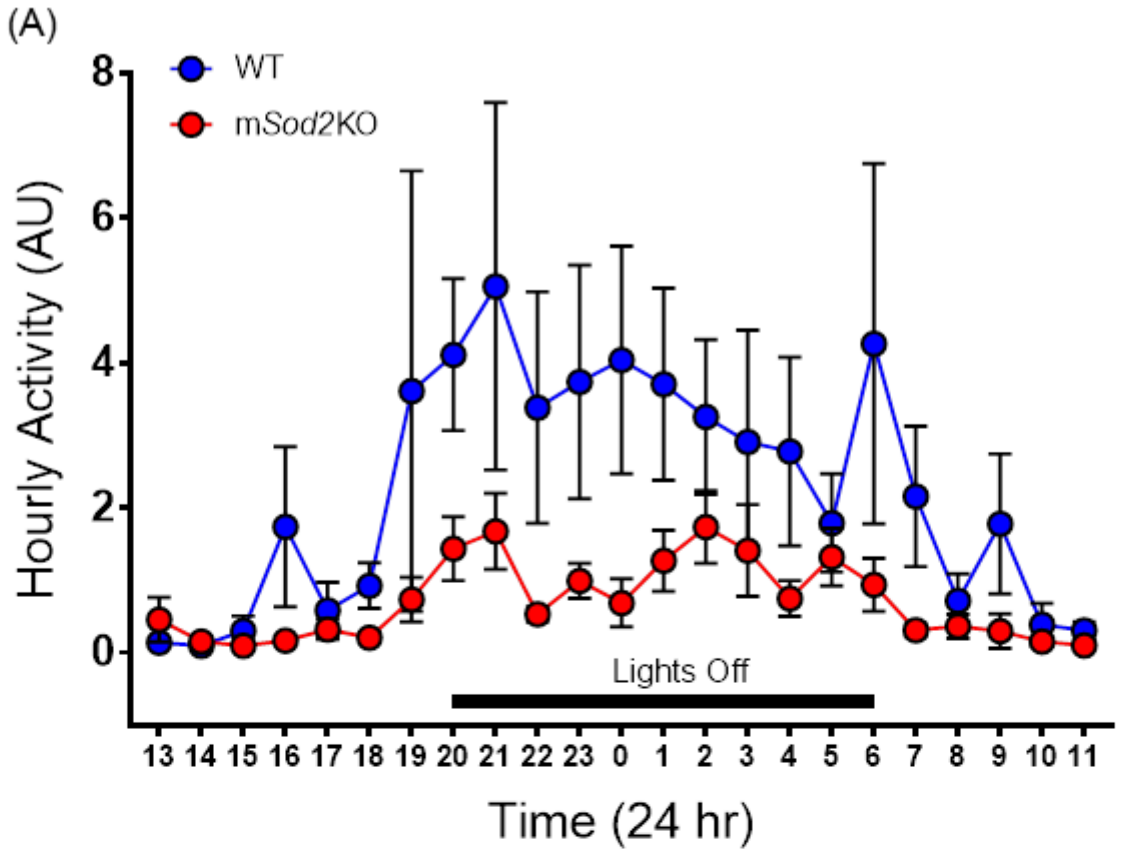

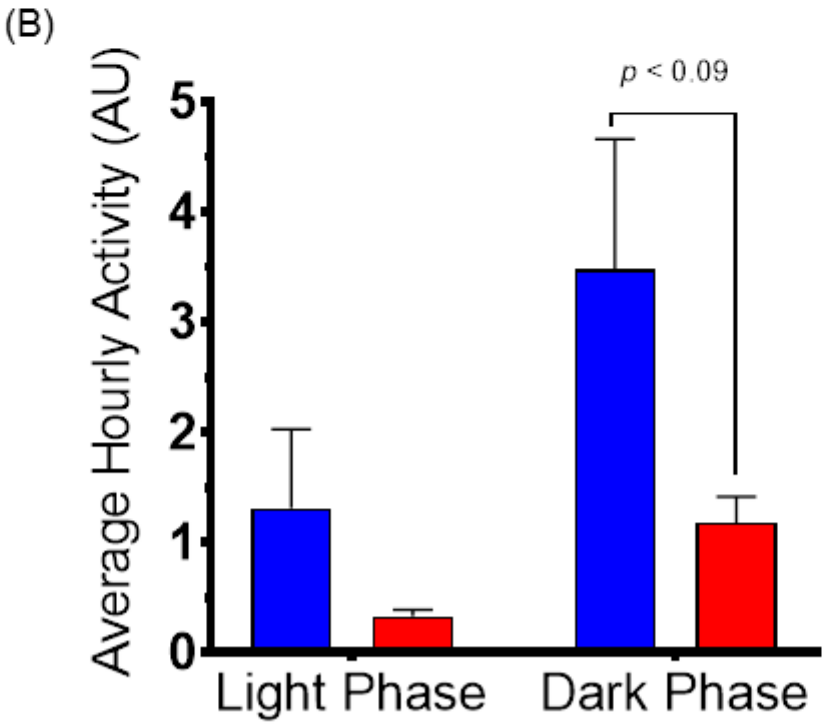

Figure S2

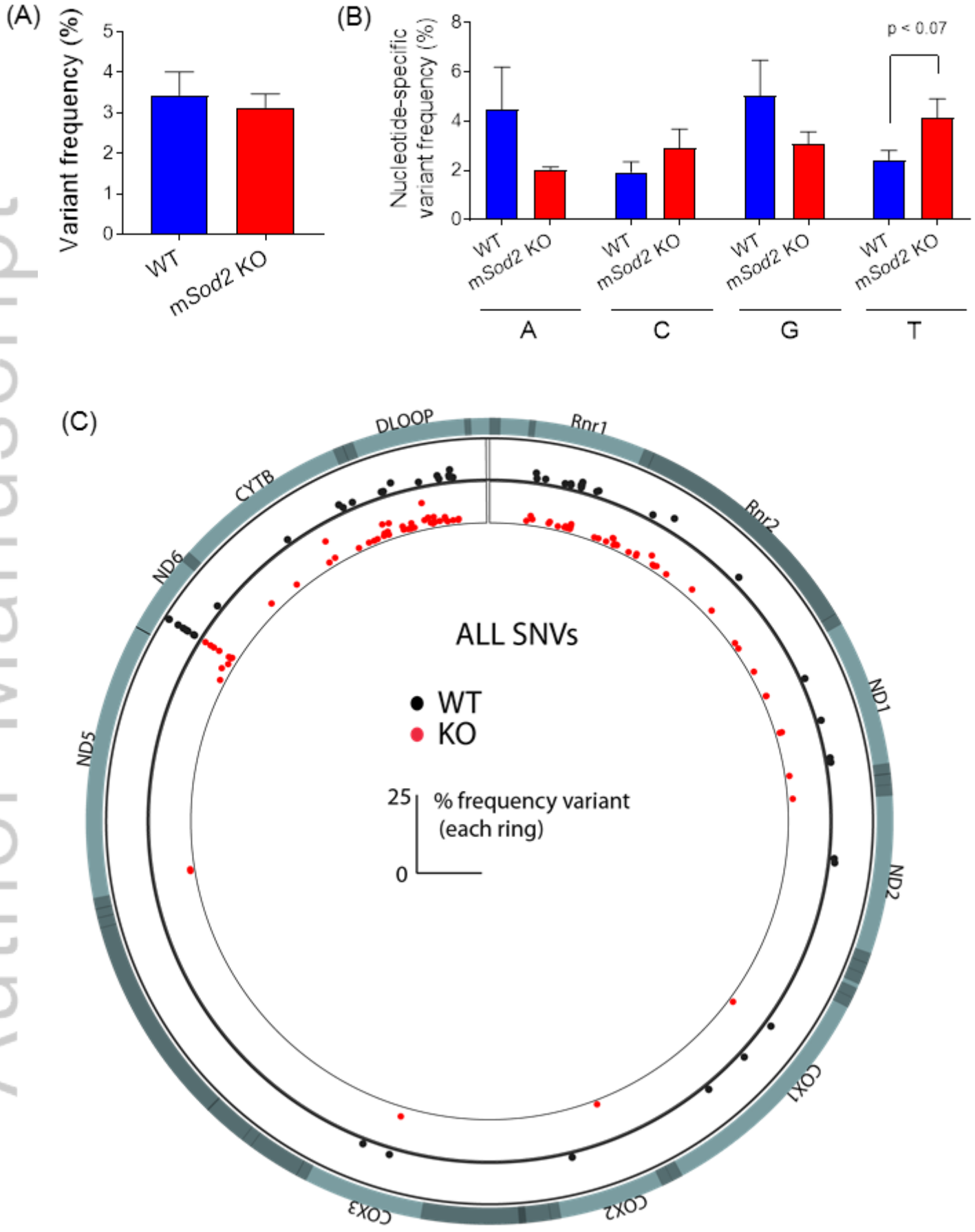

Figure S3

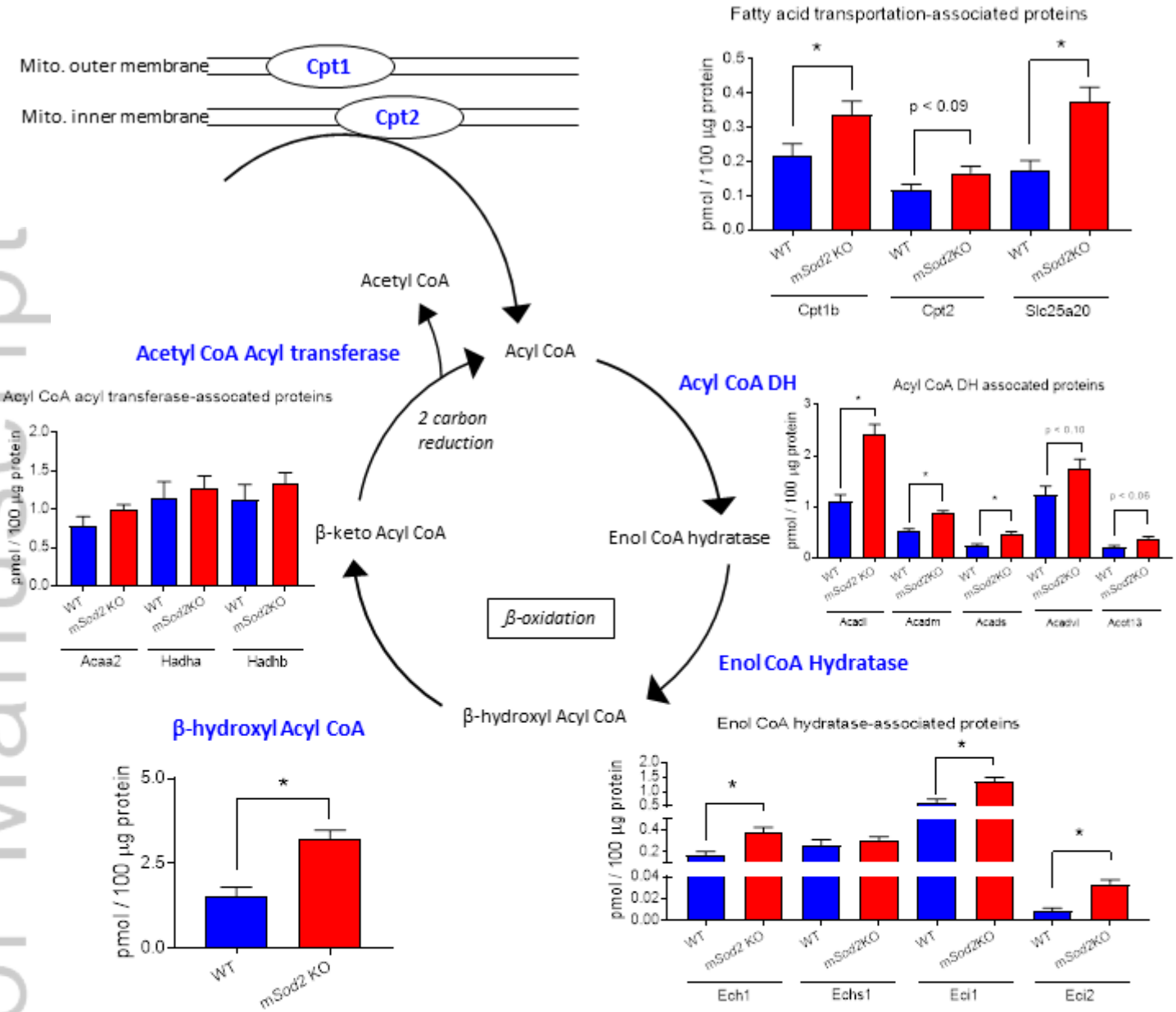

Figure S4

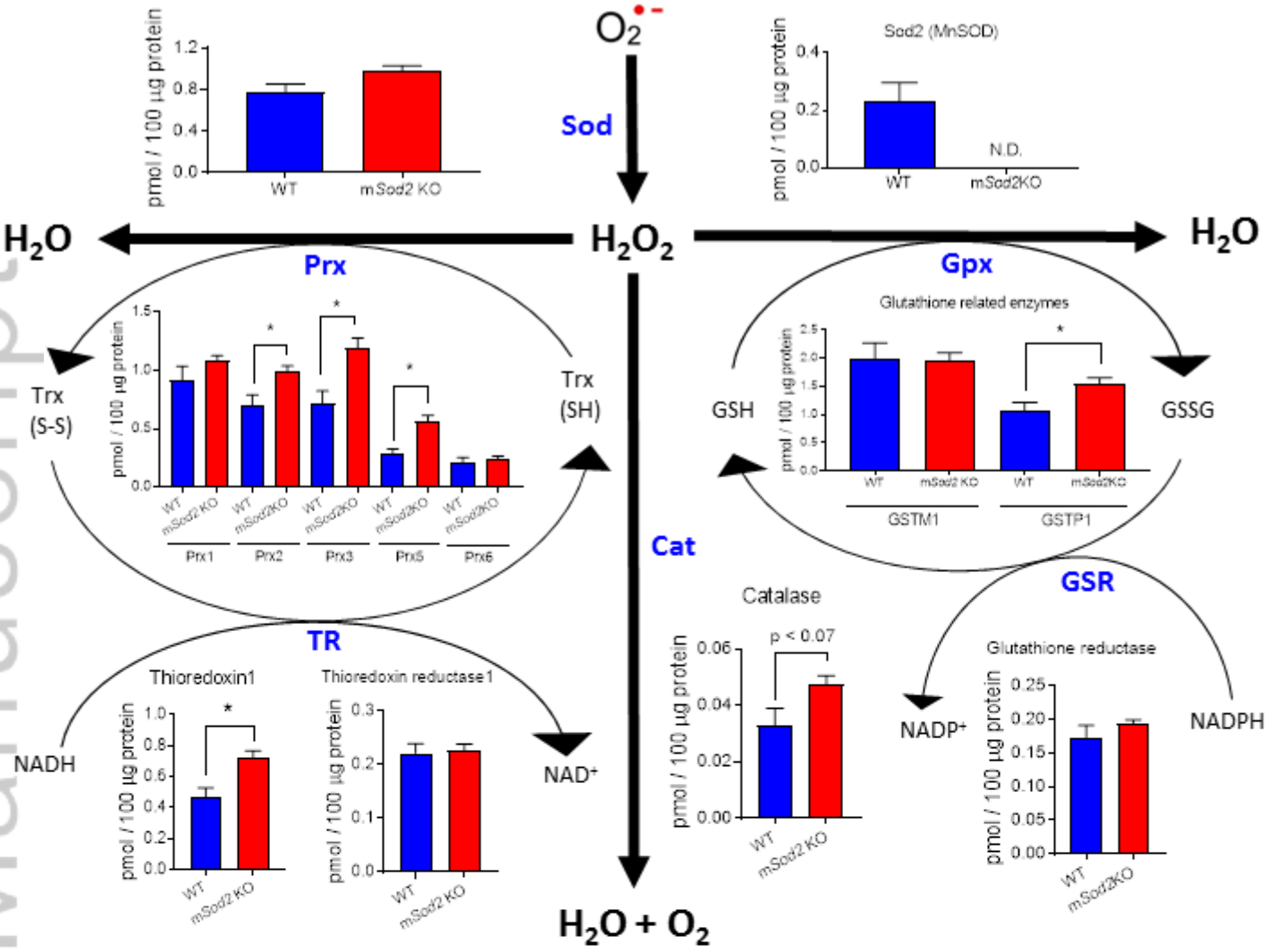

Figure S5

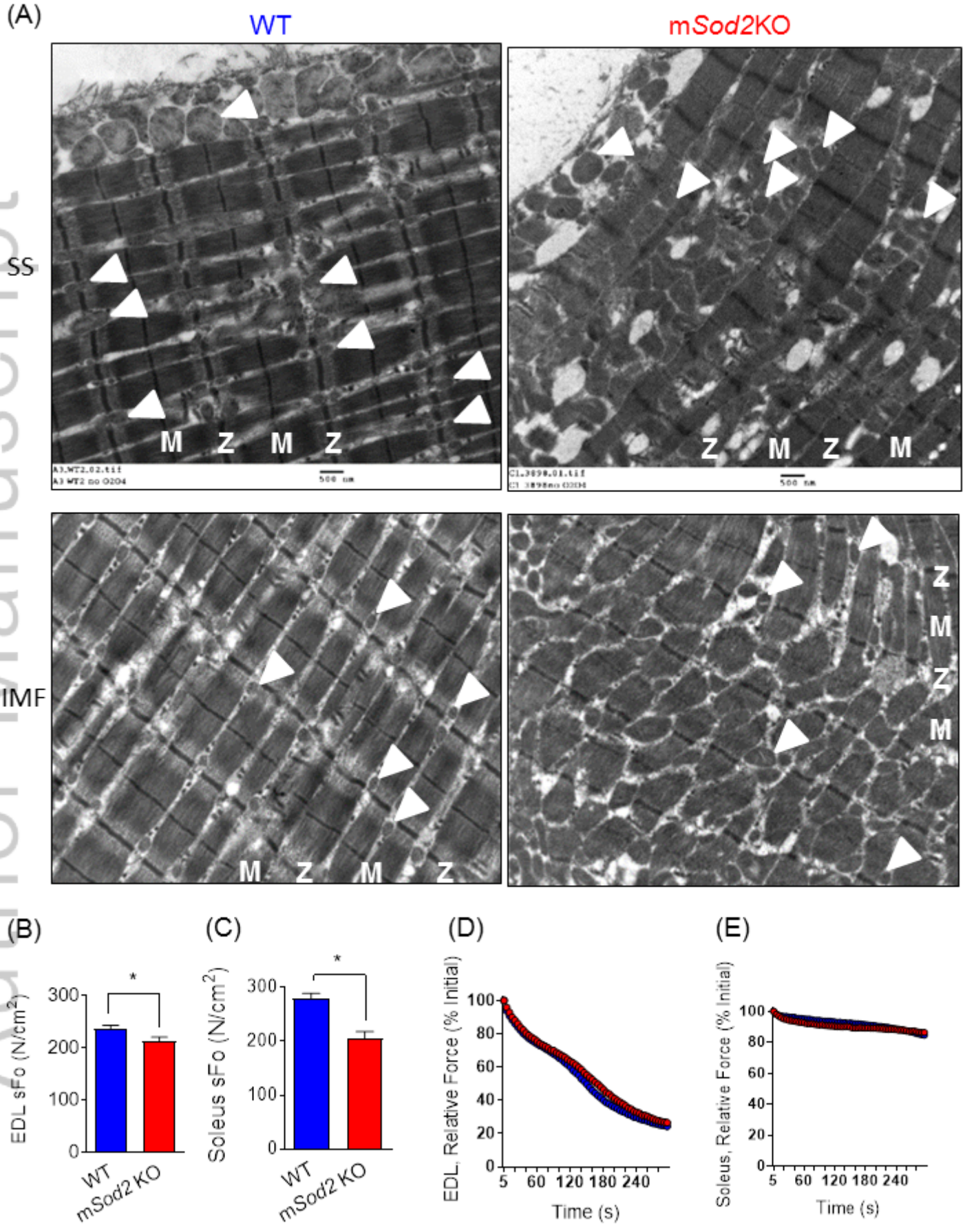

Figure S6

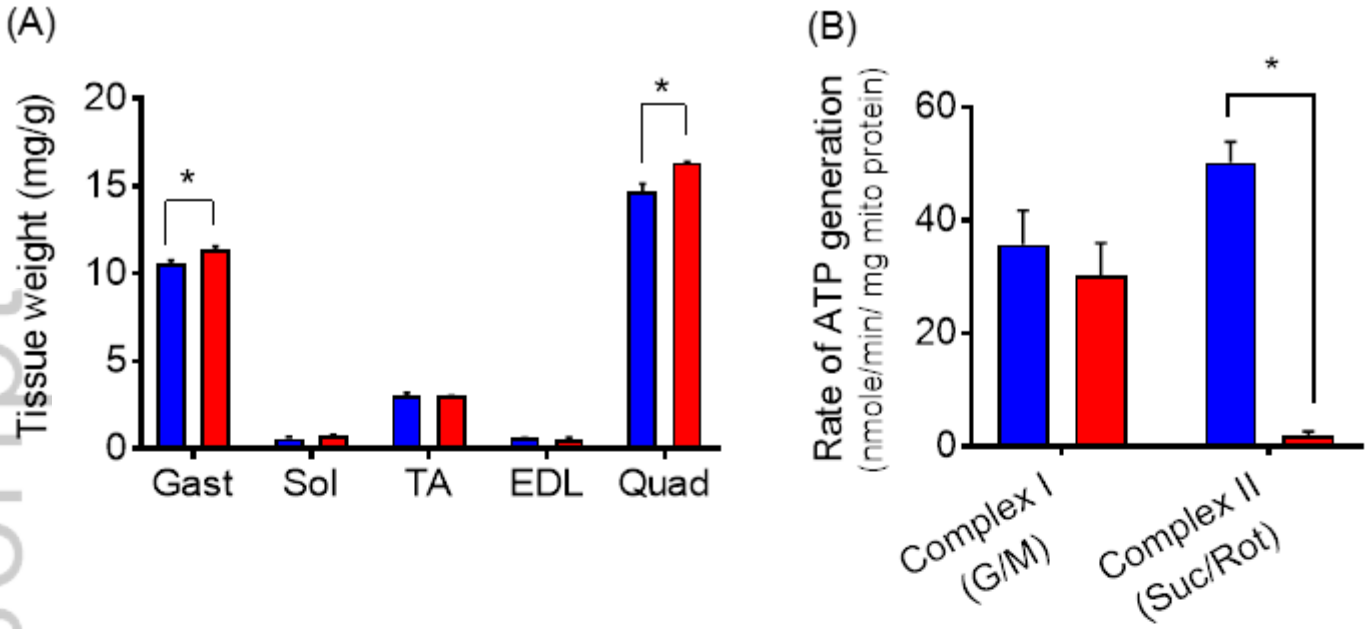

Figure S7

Enzymes in glycolysis and gluconeogenesis

	Mean ±SEM (pmol/100 ug)		
Gene Name	WT	mSod2 KO	*p*-val
AldoA	75.05 ±5.84	83.43 ±6.29	0.35
Eno3	24.61 ±2.92	27.61 ±1.98	0.42
Gapdh	68.62 ±9.14	92.96 ±9.88	0.10
Got1	2.61 ±0.40	3.50 ±0.31	0.11
Got2	2.72 ±0.40	5.66 ±0.38	0.0003*
Gpi1	8.75 ±0.80	10.68 ±0.29	0.06
Hk1	0.46 ±0.06	0.61 ±0.05	0.08
Ldha	41.75 ±5.08	39.01 ±2.14	0.63
Ldhb	2.08 ±0.51	2.49 ±0.26	0.49
Mpc1	0.10 ±0.013	0.15 ±0.013	0.02 *
Mpc2	0.04 ±0.008	0.07 ±0.014	0.09
Pcx	0.18 ±0.022	0.12 ±0.011	0.05
Pfkm	3.96 ±0.41	3.61 ±0.09	0.45
Pgam2	15.06 ±1.73	11.87 ±1.27	0.17
Pgk1	4.39 ±0.26	5.21 ±0.28	0.05
Pfkm	30.87 ±2.51	29.33 ±0.81	0.58
Pygm	15.69 ±1.96	16.09 ±1.58	0.88
Slc2a1	0.032 ±0.006	0.06 ±0.008	0.04
Slc2a4	0.065 ±0.011	0.07 ±0.007	0.54
Tpi1	14.0 ±1.92	13.60 ±1.02	0.87

Table S1

(A) Gene names and IDs in TCA cycles (Figure 3)

Gene name	NCBI Gene id	Protein name
Cs	12974	citrate synthase
Aco2	11429	aconitase 2, mitochondrial
Idh1	15926	isocitrate dehydrogenase 1 (NADP+), soluble
Idh2	269951	isocitrate dehydrogenase 2 (NADP+), mitochondrial
Idh3a	67834	isocitrate dehydrogenase 3 (NAD+) alpha
Idh3b	170718	isocitrate dehydrogenase 3 (NAD+) beta
Idh3g	15929	isocitrate dehydrogenase 3 (NAD+), gamma
Dlat	235339	dihydrolipoamide S-acetyltransferase (E2 component of pyruvate dehydrogenase complex)
Ogdh	18293	oxoglutarate (alpha-ketoglutarate) dehydrogenase (lipoamide)
Slc25a11	67863	solute carrier family 25 (mitochondrial carrier oxoglutarate carrier), member 11
Sucla2	20916	succinate-Coenzyme A ligase, ADP-forming, beta subunit
Suclg1	56451	succinate-CoA ligase, GDP-forming, alpha subunit
Sdha	66945	succinate dehydrogenase complex, subunit A, flavoprotein (Fp)
Sdhb	67680	succinate dehydrogenase complex, subunit B, iron sulfur (Ip)
Sdhc	66052	succinate dehydrogenase complex, subunit C, integral membrane protein
Fh1	14194	fumarate hydratase 1
Mdh1	17449	malate dehydrogenase 1, NAD (soluble)
Mdh2	17448	malate dehydrogenase 2, NAD (mitochondrial)
Dlat	235339	dihydrolipoamide S-acetyltransferase (E2 component of pyruvate dehydrogenase complex)
Dld	13382	dihydrolipoamide dehydrogenase
Pdha1	18597	pyruvate dehydrogenase E1 alpha 1
Pdhb	68263	pyruvate dehydrogenase (lipoamide) beta

(B) Gene names and IDs in beta-oxidation (Figure S3)

Gene name	NCBI Gene ID	Protein name
Cpt1b	12895	carnitine palmitoyltransferase 1b, muscle
Cpt2	12896	carnitine palmitoyltransferase 2
Slc25a20	57279	solute carrier family 25 (mitochondrial carnitine/acylcarnitine translocase), member 20
Acadl	11363	acyl-Coenzyme A dehydrogenase, long-chain
Acadm	11364	acyl-Coenzyme A dehydrogenase, medium chain
Acads	11409	acyl-Coenzyme A dehydrogenase, short chain
Acadvl	11370	acyl-Coenzyme A dehydrogenase, very long chain
Acot13	66834	acyl-CoA thioesterase 13
Ech1	51798	enoyl coenzyme A hydratase 1, peroxisomal
Echs1	93747	enoyl Coenzyme A hydratase, short chain, 1, mitochondrial
Eci1	13177	enoyl-Coenzyme A delta isomerase 1
Eci2	23986	enoyl-Coenzyme A delta isomerase 2
Hadh	15107	hydroxyacyl-Coenzyme A dehydrogenase
Acaa2	52538	acetyl-Coenzyme A acyltransferase 2 (mitochondrial 3-oxoacyl-Coenzyme A thiolase)
Hadha	97212	hydroxyacyl-Coenzyme A dehydrogenase/3-ketoacyl-Coenzyme A thiolase/ enoyl-Coenzyme A hydratase (trifunctional protein), alpha subunit
Hadhb	231086	hydroxyacyl-Coenzyme A dehydrogenase/3-ketoacyl-Coenzyme A thiolase/ enoyl-Coenzyme A hydratase (trifunctional protein), beta subunit

Table S2

(C) Gene names and IDs of antioxidant enzymes (Figure S4)

Gene name	NCBI Gene id	Protein name
Sod1	20655	superoxide dismutase 1, soluble
Sod2	20656	superoxide dismutase 2, mitochondrial
Gstm1	14862	glutathione S-transferase, mu 1
Gstp1	14870	glutathione S-transferase, pi 1
Cat	12359	catalase
Gsr	14782	glutathione reductase
Prdx1	18477	peroxiredoxin 1
Prdx2	21672	peroxiredoxin 2
Prdx3	11757	peroxiredoxin 3
Prdx5	54683	peroxiredoxin 5
Prdx6	11758	peroxiredoxin 6
Txn1	22166	thioredoxin 1
Txnrd1	50493	thioredoxin reductase 1

(D) Gene names and IDs in glycolysis and gluconeo genesis (Table S1)

Gene name	NCBI Gene id	Protein name
AldoA	11674	aldolase A, fructose-bisphosphate
Eno3	13808	enolase 3, beta muscle
Gapdh	14433	glyceraldehyde-3-phosphate dehydrogenase
Got1	14718	glutamic-oxaloacetic transaminase 1, soluble
Got2	14719	glutamatic-oxaloacetic transaminase 2, mitochondrial
Gpi1	14751	glucose phosphate isomerase 1
Hk1	15275	hexokinase 1
Ldha	16828	lactate dehydrogenase A
Ldhb	16832	lactate dehydrogenase B
Mpc1	55951	Mitochondrial pyruvate carrier1
Mpc2	70456	Mitochondrial pyruvate carrier2
Pcx	18563	pyruvate carboxylase
Pfkm	18642	phosphofructokinase, muscle
Pgam2	56012	phosphoglycerate mutase 2
Pgk1	18655	phosphoglycerate kinase 1
Pfkm	18642	phosphofructokinase, muscle
Pygm	19309	muscle glycogen phosphorylase
Slc2a1	20525	solute carrier family 2 (facilitated glucose transporter), member 1
Slc2a4	20528	solute carrier family 2 (facilitated glucose transporter), member 4
Tpi1	21991	triosephosphate isomerase 1

Primary antibodies

	Catalogue #	Ratio (incubation)
Nitrotyrosine	Milipore, 06-284	1 to 1000 (overnight)
AchR-a	Santa Cruz, sc-365479	1 to 1000 (overnight)
Calpain-1	Cell Signaling, #2556	1 to 1000 (overnight)
Spectrin α II	Santa Cruz, sc-48382	1 to 1000 (overnight)

Primer sequences

	Forward	Reverse
AchR-α	ACCTGGACCTATGACGGCTCT	AGTTACTCAGGTCGGGCTGGT
AchR-δ	CATCGAGTGGATCATCATTGAC	CGGCGGATGATAAGGTAGAA
AchR-ε	GATTGGCATTGACTGGCACG	CCACTCCAAACTGCCCATC
Shda	CAGAAGTCGATGCAGAACCA	CGACCCGCACTTTGTAATCT
Sdhb	GGAGGGCAAGCAACAGTATC	GCGTTCCTCTGTGAAGTCGT

Table S3